Mechanical Engineering

Graduation Session March 2026

Assessing the Impact of Occupancy on Indoor Air Quality: An Analysis of Interaction Effects and Occupancy Data Reliability

Supervisors:

Prof. Eliodoro Chiavazzo

Prof. Heidi Salonen

Prof. Xiaoshu Lu

Candidate:

Alberto Todini

Acknowledgments

I am extremely grateful to everyone who has helped and supported me in one way or another during the elaboration of this thesis.

I am very much indebted to my supervisor in Finland, Prof. Heidi Salonen, and to my advisor, Prof. Xiaoshu Lu, for their insight, availability, and continued encouragement. Their expertise and comments were of great value with respect to determining the direction and depth of this work, and their support during my time spent in Finland made this experience an intellectually enriching and personally rewarding one.

I would also like to sincerely thank my academic advisor in Italy, Prof. Eliodoro Chiavazzo, for his valuable guidance and for supporting my decision to undertake this research abroad. His trust and perspective have been instrumental in connecting the international and local dimensions of this thesis.

The financial support of the SustainSchool project, which received funding from the Research Council of Finland under grant number 359189, made this research possible. I am grateful for the funding because it was what enabled the data collection, analysis, and collaborative work forming the basis of the study.

I would also like to thank the schools in Espoo, which took part in the monitoring campaign, and all those involved in facilitating sensor deployments and data access. Your cooperation and openness have made this research both feasible and meaningful.

Abstract

Indoor Air Quality (IAQ) is a key component of a healthy productive learning environment, particularly in primary schools where children are more physiologically sensitive to indoor pollutants. While continuous IAQ monitoring provides valuable information regarding ventilation performance and risk of exposure, high-volume deployments in public buildings are constrained by pragmatic costs of installation, power consumption, and redundancy of data.

This dissertation deals with optimizing IAQ monitoring networks by reducing the number of operational sensors and the sampling frequency to ensure sufficient spatial and temporal representativeness. The study is founded on a 6–8 month measured data set from several classrooms in a Finnish primary school for CO, PM., PM, temperature, and relative humidity. The data were extensively cleaned, synchronized, and normalized before conducting statistical and machine learning analysis. Correlation matrices and cluster analysis were employed to identify redundant nodes, characterize IAQ spatial patterns, and assess network simplification potential.

Results indicate that a large number of sensors can represent the whole class environment with minimal loss of information quality. Optimized sampling intervals were also found to reduce a considerable amount of energy as well as data requirements without accuracy sacrifice. Findings provide practical guidelines for designing more efficient, scalable, and sustainable IAQ monitoring systems for school facilities—trading fidelity for interpretability as well as long-term operation.

Chapter 1

Introduction

Indoor Air Quality (IAQ) is now a critical component of healthy and sustainable building design, particularly in schools. Schools are unique indoor environments: they house large numbers of children in relatively small areas for extended periods with minimal ventilation and variable maintenance practices. A number of studies have established that low IAQ can negatively impact not only physical health but also student attentiveness, concentration, and academic performance. Children are especially vulnerable to indoor pollutants because their lungs are still underdeveloped and they inhale more air per unit of body weight than adults. Prolonged exposure to increased concentrations of pollutants may therefore result in respiratory irritation, asthma, and long-term effects.

Classroom CO levels are often used as an indicator of ventilation adequacy and room loading. With an increase in CO levels beyond 1000 ppm, cognitive functions such as decision-making and problem-solving are impaired, indicating poor fresh air exchange. Particulate matter (PM. and PM), which originates from outdoor air infiltration, indoor activity resuspension, and local traffic emissions, has the ability to penetrate into the body very deeply and trigger allergies and other diseases. Temperature and relative humidity (RH) also control the feeling of comfort as well as the biological stability of microbes. In order to avoid discomfort, smells, mould, and electrostatic impact, moderate thermal and humidity conditions are thus necessary.

Permanent measurement of these parameters assists in untangling

the dynamics of the air quality in classrooms. Daytime processes, mainly regulated by teaching schedules, create repetitive patterns of pollutant growth and deterioration. In general, CO and PM levels increase sharply after the beginning of classes, peak prior to breaks, and decrease upon windows being opened or when rooms are vacated. It requires repeated sampling frequently enough and multiple monitors in various rooms or floors to pick up such trends. However, the expansion of such monitoring to multiple schools or cities poses practical and cost considerations.

1.1 Motivation and Challenges

While newer low-cost sensors have made IAQ monitoring accessible, large-scale deployment is fraught. First, low-cost sensors are unreliable in terms of accuracy, signal drift, and noise sensitivity, especially over long durations or in changing environments. Their data will require high-quality control and calibration before they can be relied upon. Second, large sensor networks across schools can be logistically complex and costly. All the sensor nodes consume power, ideally from batteries that must live for months or years. Too much data transmission also increases network load and power expenditure.

Moreover, the collected data sets may become very redundant. Pollutant profiles in nearby classrooms or floors are likely to be the same, and therefore multiple sensors capture redundant data. Without design, redundancy leads to unnecessary power consumption and maintenance without increasing diagnostic perception. Finally, comprehension of multi-parameter data is problematic for non-expert stakeholders. Facility managers at schools and teachers get maximum value from well-delineated, actionable measures—such as ventilation performance indexes or readily visible visual dashboards—rather than raw or convoluted streams of data.

Under these constraints, there is a strong need for minimization of monitoring strategies that decrease the sensor number and measurement frequency without altering the interpretability and precision of

IAQ estimation. This reduction not only conserves energy and money but also simplifies long-term network upkeep.

1.2 Research Context

This thesis was built on the larger background of IAQ monitoring projects in Finland, where indoor environmental quality consciousness among citizens has grown significantly over the last few years. Several Finnish municipalities have started pilot projects to integrate continuous IAQ monitoring in schools, both for ensuring healthy learning environments as well as for evaluating the performance of new ventilation systems. The information used in this study are from one of these programs and include a very long time frame, fall 2024 through spring 2025, allowing for the possibility to look at seasonal variation.

Every school that was involved was equipped with a set of low-power, compact sensors for measuring environmental parameters of significance: CO_2, $PM_{2.5}$, PM_{10}, temperature, and relative humidity. The data were transmitted to a central location for collection and analysis. While the primary goal of the campaign was to capture trends in air quality, the resulting dataset is also an ideal opportunity to investigate how the sensor network can be rendered rational without compromising information quality.

1.3 Objectives and Scope

The broad objective of this thesis is to explore how IAQ monitoring systems in primary schools can be efficient, scalable, and interpretable. The research work provides answers to two main research questions:

How much spatial and temporal variability exists among classrooms and floors in the monitored school? This is intended to determine whether the current sensor density is capable of capturing large differences or whether there are sensors with redundant data.

How does one reduce energy consumption and data redundancy in the monitoring network and sampling schedule without compromising

diagnostic performance? This is accomplished by finding representative sensor nodes and appropriate sampling intervals through statistical and clustering analysis.

To answer these queries, the thesis combines data-driven tools—correlation matrices, hierarchical clustering, and redundancy analysis—into useful sensor placement and upkeep issues. The result is used in an attempt to recommend an optimized configuration and data collection method that balances accuracy and sustainability.

Chapter 2

State of the art

Indoor air quality in educational settings has become a growing concern in Nordic countries due to specific climatic and architectural challenges. Long, harsh winters and energy-efficient construction with airtight insulation result in buildings that are thermally efficient but often poorly ventilated [1]. With students and staff spending a considerable part of their day indoors, often in the same room for several hours in succession, the potential health and cognitive effects of suboptimal IAQ are magnified. [2][3]

Schools in Finland, Sweden, Norway, and Denmark usually use mechanical ventilation systems to provide the exchange of air. These systems balance fresh air supply with energy efficiency, normally running at reduced rates during unoccupied periods. While these mechanical systems offer predictability and control, their actual performance is not necessarily good enough to provide the required ventilation in densely occupied spaces like classrooms. Additional ventilation is provided by manual airing in many schools; teachers usually open windows periodically to enhance airflow, especially during transitional seasons in spring and autumn. However, this is a very inconsistent strategy, highly dependent on occupant behavior and outdoor weather, with constraints based on thermal comfort.

Several field studies in Nordic schools have reported frequent exceedances of recommended CO_2 thresholds, especially during core teaching hours. CO_2, while not directly harmful at typical indoor concentrations, is a commonly adopted proxy for ventilation effectiveness

and occupancy load; levels above 1000 ppm are usually considered indicative of under-ventilation [4]. A comprehensive Finnish survey showed that many classrooms exhibited average CO_2 concentrations well in excess of this threshold during the school day, indicating insufficient ventilation rates for the number of occupants present [5]. Analogous findings have been reported in Sweden and Norway, where indoor CO_2 levels have been linked to both poor ventilation and reduced cognitive performance amongst students [6][7].

Apart from CO_2, particulate matter (PM), especially $PM.$ and PM, is another key pollutant of concern in Nordic schools. While buildings in these countries are generally well-sealed against outdoor air pollution, PM accumulation indoors may still be generated by human activities such as walking, playing, and cleaning [8]. Several studies have pointed out that in Nordic schools, resuspension of particles from floors and furniture is often a more significant source of PM_{10} than outdoor infiltration, especially in spaces with hard flooring and high occupancy turnover [9]. The highest PM loads usually occur in those locations related to intensive physical activities and foot traffic, such as gymnasiums, cafeterias, and corridors. Furthermore, poor or infrequent cleaning promotes the accumulation of particles over time [10].

Thermal conditions and RH also play a critical role in both the perception of IAQ and the possibility of health effects. During the heating season, indoor environments in Nordic schools may become excessively dry, especially in buildings with older or poorly regulated HVAC systems [11]. Low humidity levels-often below 30% RH-can lead to discomfort, skin dryness, and irritation of the respiratory tract [12]. Furthermore, a reduction in ventilation rates to conserve heat may exacerbate IAQ by allowing a buildup of certain pollutants, odors, and even CO. Balancing thermal comfort and air quality has thus remained one of the challenges in Nordic educational buildings, especially in older facilities with limited control over ventilation [1].

Poor IAQ in schools from a health perspective has been linked to symptoms such as headaches, fatigue, eye and throat irritation, and difficulties in concentrating [2][12]. The symptoms related to indoor

air quality disturb not only comfort but also adversely affect academic performance and increased absenteeism [3]. Although Nordic countries have created building codes and ventilation guidelines to address IAQ (e.g., FiSIAQ, 2017), the enforcement and continuous evaluation remain limited, especially in older buildings.

Despite increasing awareness and policy attention, most IAQ assessments in Nordic schools so far have been limited to short-term measurement campaigns, snapshot inspections, or occupant surveys [5][8]. Most of them rely on fixed-point measurements in one or two rooms over some hours or days, which give a very partial view of actual indoor air dynamics. Some municipalities, such as Espoo and Helsinki, started piloting broader monitoring initiatives, while long-term high-resolution IAQ data for multiple functional spaces, like classrooms, gyms, and communal areas, remains scarce [13]. In this respect, the current study addresses a well-delineated research gap by carrying out a multi-site, multi-month IAQ monitoring campaign in four primary schools in Espoo, Finland. Such a detailed spatiotemporal variation in indoor environmental conditions has been captured with a network of standardized sensors at high frequency. Unlike previous attempts, this would enable the identification of diurnal/seasonal IAQ patterns, comparisons between room types and ventilation configurations, and investigation of sensor redundancy and network efficiency. The work contributes not only to a better understanding of IAQ dynamics in Nordic schools but also provides a methodological framework for efficient and scalable indoor monitoring networks that might support evidence-based building management and public health strategies by integrating rigorous pre-processing, time synchronization, and clustering-based diagnostics.

2.1 Sensor Network Optimization for Indoor Air Quality Monitoring

Indoor air quality monitoring has increasingly become driven by data, and the focus is no longer solely on measuring environmental conditions but rather on designing smart, efficient, and scalable sensor networks. In schools especially, where IAQ varies greatly between rooms and time, budgets and resources to monitor them are usually limited. Hence, sensor placement is crucial in terms of optimizing number/density and configuration-not just for acquiring meaningful spatiotemporal variations but also ensuring cost-effectiveness and data reliability.

2.1.1 The Need for Optimized IAQ Monitoring Networks

Conventional IAQ studies typically rely on single-point or sparse measurements that have been taken over short time periods. Such methods can identify broad trends in indoor exposure, but they cannot capture the dynamic, fine-grained nature of indoor air. They are especially inadequate in complex environments such as schools, where occupancy patterns, ventilation behavior, and room functions change throughout the day.

With the increasing availability of low-cost, compact air quality sensors, the deployment of dense monitoring networks across multiple indoor zones is now feasible. However, more sensors do not necessarily yield better data. Indeed, unplanned deployments often result in informational overlap, excessive redundancy, or the appearance of blind spots—compromising both the interpretability of the dataset and the efficiency of the monitoring system [14][15]. Optimization of sensor networks involves the determination of which sensors are necessary, which are redundant, and how sensor data can be aggregated or clustered to maintain meaningful resolution while minimizing hardware and data-handling complexity.

2.2 Redundancy Analysis and Information Overlap

A key concept in optimization of sensor networks is redundancy, which is defined as the degree to which multiple sensors measure the same information. For indoor IAQ sensor networks, this often occurs when sensors are located in rooms serving similar uses or operating under similar ventilation regimes, such as adjacent classrooms on the same ventilation loop.

Redundancy usually has been tested by:

- Pearson or Spearman correlation coefficients to quantify linear or rank-based similarity.
- Dynamic time warping (DTW) or Euclidean distance to evaluate temporal similarity.
- Mutual information to capture non-linear dependencies and shared signal entropy. [16]

High correlation or low distance between two sensors suggests that one may be unnecessary—or that it could be repositioned to a more informative location. For example, in their study of mobile air pollution sensing, Hasenfratz et al. (2012) demonstrated that spatial and temporal redundancies could be reduced by optimizing both sensor location and sampling strategy. Although their focus was on mobile urban sensing, the methodology is transferable to indoor networks where airflow and occupancy follow repeatable patterns.

In the IAQ studies, this quantification of redundancy enables a downscaling of sensors while conserving the spatial information in schools; this reduces costs and improves data handling, especially during long-term deployment conditions where large volumes of high-frequency data can strain storage and processing capacity.

2.3 Clustering and Zone Representation

Beyond the pairwise redundancy, clustering algorithms are widely applied in order to group sensors or rooms based on their IAQ time-series profiles. This allows identifying spatial zones or categories of usage showing similar behavior and thus enables the selection of representative nodes for each group.

Clustering can be applied using:

- k-means clustering based on time-averaged features or correlation matrices;
- Hierarchical clustering to build dendrograms of similarity,
- Dimensionality reduction using PCA before grouping may be conducted as in Iqbal et al. (2020) and Zimmerman et al. (2019).

For instance, Iqbal et al. (2020) used clustering to optimize sensor placement in a smart building and found that up to 40% could be taken out with very minor loss of spatial resolution, provided representative nodes are chosen within each cluster. Their study concerned commercial buildings, but the idea extends to schools, where rooms may share similar ventilation or occupancy patterns-for example, classrooms along the same hallway or under the same HVAC zone.

In educational buildings, clustering not only aids in optimizing sensor layouts, but also supports data aggregation and zone-level IAQ reporting, which can be more actionable for facility managers.

2.4 Challenges in Low-Cost Sensor Networks

A new wave of inexpensive IAQ sensors, including NDIR (nondispersive infrared) for CO_2 and laser scattering for PM, has recently made high-resolution deployments practical where it was previously not possible. However, trade-offs are also made in accuracy, stability, and drift, particularly over longer-term monitoring campaigns [17][14]. Quality assurance thus represents a critical step in post-deployment evaluation, including drift correction and sensor validation against

reference-grade equipment. In particular, sensor drift or response delays may artificially reduce intersensor correlation, masking redundancy or exaggerating variability [18]. Therefore, the data cleaning, synchronization, and standardization that were applied within this study will form part of any optimization framework. In this sense, the study of Tavernini et al. (2025) is highly relevant. This study, carried out in schools in Finland, has shown how spatiotemporal IAQ data can be used to optimize sensor placement using both statistical clustering and practical constraints related to room function and accessibility. Their findings showed that it is possible to reduce network complexity by identifying spatial patterns and shared ventilation effects without the loss of critical IAQ insights.

Chapter 3

Case Study and methodology

3.1 Case study

3.1.1 Case study 1: Jousenkaari primary School

Jousenkaari School is located at Palloilutie 5, 02120 Espoo, Finland, in a residential area with low housing density and moderate outdoor pollution. The surrounding environment is characterized by light traffic and greenery, and thus it can be considered a relatively clean outdoor air background for IAQ comparison. The school building contains two main floors with a mechanical ventilation system that supplies fresh air to classrooms, corridors, and common areas. Constructed with energy-efficient design principles typical of Finnish school facilities, Jousenkaari offers a representative test bed for the evaluation of IAQ dynamics in mechanically ventilated conditions.

The specific areas of interest in Jousenkaari were selected to provide representation of different occupancy and activity profiles. The deployment included ten monitoring units distributed across both floors, covering a range of environments that include:

The dining and lobby area, with short but intense occupancy peaks during meal breaks.

The gym, a large, intermittently occupied space with vigorous physical activity and extreme short-term fluctuation of CO_2 and $PM_{2.5}$ and PM_{10}.

A number of first- and second-floor classrooms and corridors, i.e.,

C1.24, C2.14a, B2.08a, and B2.20, and connecting corridors. This mix of spaces enabled the identification of contrasts between highly dynamic spaces and stable, instructional environments. The overall spatial design of the sites under observation is found in Figure 2.1, which shows the first- and second-floor layouts of Jousenkaari School and the sensor nodes' approximate location.

Each monitoring unit was connected to the school electrical grid and linked via Wi-Fi, providing power and enabling continuous data recording during the campaign. The sensors were programmed with a sampling interval of approximately two minutes, which provided a good temporal resolution suitable to outline the rapid changes of pollutant concentrations associated with occupancy patterns, window opening, and ventilation cycles.

Although the devices tracked several environmental parameters, this study focuses on six significant IAQ factors:

Carbon dioxide (CO_2) – proxy for ventilation efficiency and occupancy;

$PM_{2.5}$ and PM_{10} – indicators of particulate pollution, influenced by infiltration, resuspension, and occupant activity;

Temperature and relative humidity (RH) – determinants of thermal comfort, moisture control, and thermal balance;

Barometric pressure – useful for normalizing sensor data and detecting pressure gradients due to ventilation.

Sensors located in classrooms were mounted at teacher-desk height (approximately 110 cm) to measure representative exposure conditions in the occupied breathing zone. The measurement campaign lasted from October 2024 to May 2025, thus covering both the heating and spring ventilation seasons in Southern Finland. This period provided valuable information on how external weather, indoor heating, and occupant behavior collectively impact air quality trends.

Mechanical ventilation operated constantly but at varying flow rates throughout the heating season, and occupants supplemented ventilation sporadically by opening windows both during lessons and breaks. Hybrid ventilation periods generated steep, short-term variation in CO_2 and temperature, evident in the high-frequency data. The

gymnasium and canteen exhibited the greatest variation in CO_2 and PM levels due to variable occupancy and activity, whereas classrooms exhibited more gradual diurnal patterns with steep peaks before recess and steady decline during periods of no occupancy.

The Jousenkaari dataset thus makes an excellent case for clustering and spatial redundancy analysis. With the density of sensors and overlap among adjacent measurement zones, this site provides an ideal opportunity to test the hypothesis that fewer, strategically located nodes can still ensure the integrity of IAQ measurements. Additionally, by incorporating quantitative metrics (CO_2, PM) and comfort metrics (temperature, RH), the study allows for a comprehensive investigation of both ventilation effectiveness and occupant comfort.

figure of the layout of the sensors

3.1.2 Case study 2: Monikko school

Monikko School, Veräjäpellonkatu 2–4, 02650 Espoo, is located in a mixed-use suburban area that includes residential blocks, sports facilities, and moderate local traffic. The building is one of Espoo's larger school complexes, capable of accommodating several grade levels with communal facilities such as dining halls, arts rooms, and sports halls. Its three-storey design incorporates mechanical ventilation and modern insulation systems, providing a controlled indoor environment suitable for long-term IAQ analysis.

Campaign at Monikko was intended to quantify conditions of air quality in broad categories of functional areas and levels of use. Ten IAQ sensors were positioned in the following locations of primary interest:

Gym, large, high-activity area with high but short-duration use.

Dining space and stage, with short-duration peak use and intermittent ventilation behavior.

First, second, and third floor classrooms (1100, 2111, 2091b, 3052), with standard teaching areas fully utilized throughout school days.

Second and third floor lobbies and corridors, with air mixing and dispersion impacts within semi-open transition areas.

Teacher's lounge (Room 3001), with adult use patterns significantly different from classroom environments.

Needlework classroom (Room 2139), which is a special space with particular ventilation demands according to material handling and sewing machines.

These surveyed areas encompassed a wide range of indoor microenvironments, which enabled comparison of evaluation between high-activity, common, and everyday-use areas. The sensor locations are marked around Figure 2.2, illustrating the first, second, and third floor plans of Monikko School.

As for the previous case the main variables studied were Pressure, Humidity, Temperature, $PM_{2.5}$, PM_{10} and CO_2.

Classroom ceiling-mounted sensors were located at teacher desk height (approximately 110 cm) in the breathing zone for pupils and staff during operation. The sampling period was October 2024 to May 2025, incorporating both heating and spring ventilation periods. This gave the dataset the impact of cold outside air, dynamic mechanical ventilation rates, and occupant opening window behavior.

Monikko's design concept, with wide halls and large lobbies, achieves large air mixing and pressure balancing between areas. As expected, the surveyed hallways provided useful insight into the manner in which contaminants are distributed vertically across floors. The dining hall and the gym, however, demonstrated significant short-term spikes in CO_2 and PM due to dense occupation and body movement. These fluctuations were useful test cases for the clustering and correlation analysis applied subsequently in this study.

Operationally, the mechanical ventilation system operated continuously throughout the measurement period, supplying baseline airflow to all of the rooms. Airing through manual opening of windows was observed primarily during less severe weather in the spring months, generating detectable transient reductions in CO_2 and particulate concentrations.

The Monikko dataset provides a rich view of IAQ behavior in a complex, multi-level school building. It is particularly well-suited to sensor network optimization validation, as the diversity of zones being moni-

tored generates high variability while also indicating potential redundancies between adjacent sensors. The juxtaposition of classrooms, shared areas, and special spaces contributes to a more general understanding of the ways building design and use patterns affect spatial IAQ heterogeneity.

figures of the school layout and sensor position

3.1.3 Case Study 3: Tiistila school

Tiitsilä School is located at Tiistilänkuja 4, 02230 Espoo, within a quiet, low-density traffic, open green field suburban neighborhood in southern Espoo with single-family detached homes. The comparatively clean outdoor environment of the location provides a solid foundation for indoor air quality (IAQ) studies in that the outdoor contribution of pollutants is low relative to more densely packed urban locations. The building belongs to a new school complex, comprising a daycare center, a standard example of Finland's new energy-efficient school building.

The school building comprises two main floors with central corridors and open common areas. The building is equipped with a mechanical ventilation system operating throughout the year, with positive pressure and adequate air exchange. Designed in accordance with national indoor climate standards, Tiitsilä's ventilation system regulates air flow and temperature to increase thermal comfort and minimize the accumulation of pollutants during occupancy. Architectural design facilitates natural air movement through broad corridors and extensive openings between classrooms and common spaces.

The Tiitsilä IAQ monitoring campaign was designed to evaluate the air quality variation across different activity areas and occupancy densities, while testing the performance and spatial representativeness of a limited number of sensors. A total of ten monitoring units were strategically located within the building. The areas under surveillance comprised the primary lobby and cafeteria, three classrooms (Rooms 1107, 1203, and 2282), three hall/lobby areas (1101, 1201, and 2279), the gymnasium (1328), and the arts classroom (1413). These spaces

were chosen to represent variability across different indoor environments—ranging from high-occupancy teaching spaces to large, intermittently used communal areas.

All sensors were mains-powered and Wi-Fi connected for round-the-clock data logging and remote sync. The sampling rate was set at approximately two minutes, which gave sufficient temporal resolution to record short-term IAQ phenomena associated with class timetables, ventilation cycles, and occupant activities. Like previous cases the main variables studied were Pressure, Humidity, Temperature, $PM_{2.5}$, PM_{10} and CO_2.

Sensors placed in classrooms were mounted at teacher desk height (around 110 cm above floor level) to represent the pupil and staff breathing zone. The use of this normalized installation height made readings comparable from one room and location to another. The measurement campaign took place from October 2024 to May 2025, including both the cold heating season and the spring transition season. During this time, the building's ventilation system operated continuously, but window ventilation was periodically performed during mild conditions or after intensive events. Such manual interventions led to visible short-term excursions of CO and particulate matter, particularly during classroom teaching with high occupancy or in the gym after sports events.

The mechanical ventilation in Tiitsilä supplied steady baseline airflow, yet the IAQ data exhibited daily cycles with close correlation to occupancy. CO concentrations tended to rise during morning classes, peak before lunch, and decrease during breaks or if windows were open. $PM_{2.5}$ and PM_{10} exhibited the identical cyclic trend, and their peaks tended to be linked to occupant movement, cleaning, or class transition. The gym and dining area, which is characterized by short but dense occupancy periods, displayed the highest short-term variability, while the classrooms presented more smoothed diurnal profiles.

The building's architectural design also influenced air pollutant spatial patterns. The lobby and hallway sensors measured intermediate air quality between classrooms, pointing to the mixing role played by mechanically delivered air and human traffic in pollutants across

open-plan hallways. The arts classroom (Room 1413), where creative activities occasionally involve materials that generate fine particulates, offered a fascinating contrast to standard classroom conditions, occasionally experiencing higher PM even under low occupancy conditions.

Overall, the Tiitsilä dataset is a rich and well-balanced data source for the exploration of IAQ variability in a school setting. The data's temporal coverage and spatial distribution enable the performance of correlation and clustering analyses in detail for identifying redundant measurements and determining the representativeness of every sensor. By making comparisons between measurements from functionally disparate spaces, this site supports the overall research goal of identifying how the number and placement of IAQ sensors can be reduced without compromising strong monitoring performance.

The results from Tiitsilä also guide energy-efficient IAQ control. Because all of the sensors were Wi-Fi connected and mains powered, the site's data are particularly apt to evaluate the trade-offs between temporal resolution and energy use, particularly when making plans for possible future changeovers to battery-powered or wireless networks in similar schools.

3.1.4 Case study 4: Tapiola school

Tapiola School, Opintie 1, 02100 Espoo, is located in the original Tapiola area where modernist town planning is combined with an abundance of greenery. Both primary and secondary education are housed in the school complex, with shared facilities for both of them such as a library, gym, and art rooms. Its mechanically ventilated two-story building has a conditioned indoor climate that is optimally suited for the purpose of long-term indoor air quality (IAQ) measurement. It is surrounded by restricted traffic movement and dense plant cover, which provides low outdoor particulate penetration and enables attention to be placed on indoor air flows that are generated by occupants.

The Tapiola campaign targeted a heterogeneous set of activity spaces to retrieve spatial IAQ patterns and to test the sensor network's robustness in mixed-use environments. Ten low-cost IAQ sen-

sors were installed on each floor of the building in the priority areas gym and stage, library D1174, classrooms D1172, D1169, B1080, and B1063, needlework classroom D1129, arts classroom D1143, table-tennis area/lobby, and main dining area/lobby. This was to provide coverage of standard teaching rooms, high-activity common spaces, and specialty areas with standard ventilation and emission profiles.

All devices were mains-powered and connected to the school Wi-Fi, so data collection could run continuously throughout the study. Sensors sampled every two minutes or so, with sufficient temporal resolution to track the dynamics of IAQ change throughout lessons, breaks, and cleaning runs. The same six parameters monitored in the other schools—CO_2, $PM_{2.5}$, PM_{10}, temperature, relative humidity, and barometric pressure—were continuously monitored from October 2024 through May 2025. Classroom units were placed at teacher-desk height ($\approx$ 110 cm), as at the other sites, for consistency between datasets.

The ventilation system in the school delivers air through multiple zones with variable flow rates based on occupancy schedules. During the heating season, there is continuous airflow to maintain constant thermal comfort, and during spring, periodic part-window airing, particularly in art and needlework lessons where odor from materials or dust accumulation is expected, is carried out. Such hybrid ventilation strategies led to sudden short-term variation in CO_2 and particulate concentration, as was uncovered in the high-frequency data set.

Spatially, the highest CO_2 and PM peaks occurred in the gym and cafeteria due to high-density, transient occupancy. The library and art room exhibited more stable diurnal patterns but with small $PM_{2.5}$ peaks due to material handling or cleaning. The sensors in the lobbies and hallways recorded intermediate air quality conditions, with evidence of pollutant transport between clusters of rooms. Interestingly, the needlework class occasionally registered localized PM peaks related to textile dust emission, creating a sharp contrast with regular teaching classrooms.

The Tapiola building design, as a group of linked wings (Blocks A–F), enhances passive air circulation via open corridors and exten-

sive public areas. The design supports mixing among spaces and enhances the contribution of building geometry to IAQ mixing. The field measurements thus achieved provide insightful input for spatial correlation analysis inputs and model validation of clustering algorithms for future use in redundant measurement location determination.

Cumulatively, the Tapiola dataset makes a compelling case for understanding IAQ variability in a compound school environment where scholastic, artistic, and recreational activities share space. It positively substantiates the thesis objective of determining the extent to which low-density sensor networks can accurately represent IAQ conditions in compound structures. That it is a location of permanent mechanical ventilation, variable occupancy, and heterogenous room use renders Tapiola a particularly pertinent test case for temporally and spatially variant air-quality dynamics.

3.2 Methodology

This study employed a high-fidelity analytical platform with the aim of recording indoor air quality spatial and temporal patterns in various settings at schools. Indeed, it had two purposes: to understand the dynamics of air quality within and among educational environments and to explore how sensor networks can be designed for better and more informative monitoring.

The approach was to apply a systematic yet adaptive design, first based on extensive data collection from a variety of sensors mounted in classrooms, corridors, and interior spaces. Once collected, the raw data was put through an extensive pre-processing in order to remove errors, gaps, and inconsistencies between devices and locations.

This involved the combined use of statistical techniques for bringing out the pattern and trend in the data, such as time of day, seasonal, building type, and occupancy level. Also, clustering algorithms were used to determine groupings of comparable sensor readings that helped in highlighting redundancies in the sensor network. This was important to know so that it might be determined where sensors can

report redundant information - and where effective eliminations or relocations can maintain data integrity at minimal cost and simplicity.

By quantifying the level of redundancy and mapping areas of both high and low variability, this study provides critical guidance on developing smarter, leaner IAQ monitoring systems with no compromise in data quality. Beyond improving the capacity for real-time monitoring of indoor spaces, such an approach will be supportive of more responsive decision-making with respect to the management of school facilities and the conduct of public health planning.

3.2.1 Data Aquisition

All schools were equipped with a standard network of ten IAQ sensors (N = 10) strategically located across diverse indoor environments—classrooms, lobbies, dining halls, arts and crafts areas, and gymnasiums. The number and placement of sensors were chosen to offer spatial representative coverage with minimal system complexity and maintenance needs.

An identical sensor model, installation height, and configuration protocol were employed across all locations to ensure consistency. Sensors installed in classrooms were located about 110 cm above floor level, close to the breathing zone of seated occupants. Positioning sensors away from direct ventilation outlet exposure, heaters, or open windows was undertaken with a view to minimizing localized airflow disturbances and avoiding biasing measurements. In larger open spaces like gymnasiums and dining halls, sensors were installed in the middle of the space, off exterior walls and doors, to monitor representative conditions within the occupied zone.

Each school had mechanical ventilation systems that maintained steady airflow year-round. However, during spring, natural ventilation was supplemented periodically through manual window opening—introducing intermittent airflow fluctuations and creating conditions well-suited for high-frequency IAQ analysis.

The whole monitoring campaign relied on the air-Q indoor air quality monitor (Corant GmbH, Germany)—a compact, multi-sensor de-

vice designed for unbroken, high-resolution indoor environment monitoring. All of the devices employed were mains powered and linked via Wi-Fi to the local school network, enabling real-time transfer of data to a central server without operational restrictions of battery-driven devices.

Table 3.1: Summary of measured indoor air quality parameters and their analytical roles.

Parameter	**Unit**	**Analytical Role**
CO_2	ppm	Indicator of ventilation effectiveness and occupancy
$PM_{2.5}$	$\mu g \cdot m^{-3}$	Measure of fine particulate pollution (respirable fraction)
PM_{10}	$\mu g \cdot m^{-3}$	Coarse particulate load; proxy for resuspension
Temperature	°C	Thermal comfort and ventilation control
Relative Humidity (RH)	%	Moisture balance and perceived comfort
Barometric Pressure	hPa	Normalization variable; relevant for pressure-driven airflow

These parameters allowed for a multidimensional analysis of IAQ, considering the actual pollutant concentrations together with thermal and comfort parameters. All the selected variables had a direct relationship with the evaluation of ventilation effectiveness, exposure to particles, and thermal conditions perceived by occupants.

Technically, the air-Q uses a series of sensing technologies:

CO_2 measurement is performed using NDIR detection, offering low cross-sensitivity to other gases and thus being appropriate for occupancy-related ventilation assessment.

$PM_{2.5}$ and PM_{10} concentrations are measured by using an optical laser-scattering method which estimates the size and mass of particles based on intensity of scattered light.

The integrated MEMS sensors record temperature, humidity, and pressure with high responsiveness and stability, along with low power consumption.

Internally, the air-Q samples environmental conditions every 1.8 seconds; for this deployment, data were logged and transmitted every two minutes ($\Delta t = 2min$), which corresponds to the standardized

temporal resolution of the sensor network. No internal averaging or smoothing was performed, such that the full fidelity of short-term variations driven by ventilation cycles, changes in occupancy, and transient indoor activities was preserved.

Each sensor maintained a local buffer with time-stamped readings prior to uploading data to the centralized project database. Once received, the server applied a clock-alignment protocol to uniformize the timestamps across devices and school sites to ensure that the entire dataset had temporal consistency, hence allowing for comparison of patterns at different locations.

During the campaign, each sensor generated about 170,000 data entries, totaling about 1.7 million measurements per school. Integrity checks were regularly performed to confirm data completeness and continuity. The resulting structure of the dataset allows seamless integration with the workflows in pre-processing and statistical analysis described in the following sections.

The monitoring strategy was guided by three overarching objectives:

Capture IAQ variability across different types of indoor spaces that range from classrooms to high-activity zones like gyms and dining areas.

Assess the sensor redundancy with the deployment of several monitors in functionally similar or spatially adjacent areas, enabling the identification of overlapping measurement zones.

Ensure methodological consistency by using uniform hardware, identical sampling intervals, and a centralized data collection pipeline that eliminates variability from equipment differences or inconsistent operation.

The controlled design will enhance not only data comparability between schools but also the reliability of the analysis regarding network optimization and IAQ dynamics.

Operational Reliability and Limitations

This integrated design presented many practical advantages over the use of single-function sensors. By combining pollutant, thermal, and pressure monitoring within one unit, the system reduced syn-

chronization errors, minimized maintenance needs, and simplified the handling of data.

Nevertheless, similar to all portable IAQ monitors, the air-Q has inherent limitations. Long-term accuracy could be affected by sensor drift, temperature sensitivity, or fouling of the particulate sensor over time. To minimize these, all instruments were installed by following a standardized installation procedure, placing them away from known sources of disturbance, and intermittently checked during the campaign for functionality.

Overall, the monitoring network struck a great balance among precision, reliability, and scalability; it was thus a very appropriate choice for longitudinal, multi-site IAQ research in real-world school environments.

3.2.2 Data Pre-processing

In preparation for formal statistical analysis, a carefully structured pre-processing workflow was performed on the raw time-series data collected at each of the four school sites. This consisted of a multi-step process to make the data consistent, temporally aligned, and comparable across different sensors and at the various school environments. The goal was to isolate true environmental patterns from anomalies caused by sensor noise, missing values, or even long-term drift. The entire pipeline consisted of five major steps: synchronization, validation, cleaning, normalization, and quality assurance.

Time Synchronization

While the air-Q sensors are designed to automatically synchronize over the school networks, small timing differences still occurred; these were usually the result of brief network outages or infrequent power cycling of devices. Each unit generated its own local timestamp that would drift slightly over time.

To achieve this, all time series were resampled onto the same two-minute grid by using a nearest-neighbor alignment method. Where slight timestamp offsets existed between sensors, only the timestamps were interpolated, not the data values, to preserve measurement integrity. This ensured that all the sensors' data completely aligned in time, thus enabling a direct comparison, side by side, of the environmental conditions across rooms, buildings, and schools.

Data validation and integrity checks

Once the data were time-aligned, a series of validation steps was applied to catch common issues such as gaps, duplicates, or physically implausible readings. This included:

Range validation: Each variable was checked against realistic physical limits (e.g., CO_2 between 300–5000 ppm; RH between 0–100% ; barometric pressure between 900–1050 hPa).

Duplicate removal: Repeated timestamps, usually the result of momentary transmission retries, were removed automatically.

Gap detection: Gaps in excess of 10 minutes were flagged and excluded from continuous-sequence analysis. Shorter gaps were interpolated to maintain temporal continuity.

The result was a cleaned and validated dataset with consistent time coverage, ready for more advanced filtering.

Outlier Removal and Noise Filtering

Smoothening of erratic readings and isolating meaningful trends was done using a two-step filtering approach:

Outlier detection was performed using the IQR method. Values lying more than 1.5×IQR away from the local median (computed over a 1-hour sliding window) were considered outliers and were replaced by "NaN" placeholders.

Temporal smoothing was then applied by means of a low-pass moving average filter of 10-minute width, or 5 samples. This limits high-frequency noise (e.g., spikes from electronic interference or other transient disturbances) while preserving slower variations due to occupancy. This combination served to preserve the natural dynamics of IAQ while eliminating distracting anomalies.

Normalization and Standardization

Since the monitored variables operate on different scales, for example, CO_2 in ppm versus RH in percent, a normalization step was necessary to allow for direct comparisons.

Each time series was standardized using z-score normalization calculated as:

$$z = \frac{x - \mu}{\sigma} \tag{3.1}$$

where:

- x is the data raw value
- μ is the variable's mean over all of the data collection.

- σ is the standard deviation

This is a transformation that re-scales all the variables to have a mean of zero and a standard deviation of one—optimal for pattern detection, correlation analysis, and clustering.

Min–max normalization was also applied for visualization purposes, such as in heatmaps or spatial gradient plots, to bring values into a common [0,1] range for better interpretability in graphical formats.

Quality Assurance and Sensor Reliability

Finally, quality assurance at the individual sensor level was performed to ensure that the dataset used for statistical analysis is sound. Any sensor was considered unreliable and thus excluded from cross-comparison if one or more of the following criteria were met: More than 10% missing data over the campaign Frequent zero readings indicate sensor malfunction or disconnection. Sustained deviation: More than 3 standard deviations from nearby sensors for greater than 12 hours. After these checks, between 92% and 97% of the original data remained available across the four schools—sufficient for robust, representative analysis while filtering out unreliable signals.

3.2.3 Analytical approach

Clustering analysis - Operational workflow (CO_2 driven redundancy detection)

Operationalizing the clustering step, a purpose-specific MATLAB workflow was implemented that starts from room-to-room Pearson correlation matrices and, based on hierarchical agglomerative clustering on a correlation-derived distance, delivers the groups of redundant sensors. More precisely, in the case of CO_2, we compute the similarity matrix $R \in R^{mxm}$ (where m is the number of rooms with valid data in the month) and define the discordance matrix as:

$$D = 1 - R; D_{ij} = 1 - r_{ij} \tag{3.2}$$

This transformation preserves interpretability (perfect correlation r=1⇒ D=0) and produces a metric-like distance in [0,1] suitable for hierarchical linkage. We then vectorize the upper-triangular part of D (MATLAB 'squareform') and compute a hierarchical tree using average linkage (MATLAB linkage(Y,'average')). The cluster cut is performed at

$$D_{thr} = 1 - r_{thr} \tag{3.3}$$

With r_{thr}=0.85, sensors whose median within-cluster correlation mis equal or above 0.85 are considered redundant for the purpose of network reduction.

Two design choices improve robustness and traceability:

Room-name harmonization and duplicate collapsing: Some exports use the same physical location with technical suffixes, such as device variants "_T_a _T_A". Before clustering, room labels are centralized by stripping those suffixes and collapsing duplicates to a single column/row in R. This avoids artificial inflation of redundancy due to near-identical signals recorded by nominally duplicated entries. Representativeness selection within clusters. After assigning cluster IDs, (MATLAB cluster(Z,'cutoff',d_{thr})), each cluster is summarized by:

- **Size**: $|c|$ (minimum 2 to qualify a redundant group).
- **Internal cohesion** measured by the median of off-diagonal r_{ij}. It should capture the recent trends and changing dynamics in online learning communities.
- **A representative Sensor** chosen among the other as a node which has the maximum average correlation between all of the members in c.

$$\hat{j} = \arg\max_{j} \frac{1}{|c| - 1} \sum_{\substack{i \in c \\ i \neq j}} r_{ij} \tag{3.4}$$

The workflow results in three artefacts that support interpretation and auditability:

- **A correlation Heatmap** (rows/columns permuted by the dendrogram permutation), which makes the redundant blocks explicit;
- **Tables** listing (i) all cluster memberships and (ii) the subset of redundant clusters that satisfy both $|c| \geqslant 2$ and meridian $r \geqslant r_{thr}$.

Focusing HAC on *CO* is deliberate: among the IAQ variables, *CO* is the most direct proxy for occupancy-driven ventilation dynamics. It exhibits strong diurnal structure, generally yielding higher signal-to-noise ratios than PM in classrooms. This makes *CO* ideal for finding spatial co-variation that is due to shared ventilation behavior rather than idiosyncratic particle events. Later sensitivity checks qualitatively compare clusters to PM and temperature-based groupings, to verify that *CO*-driven redundancy does not obscure localized particle phenomena or thermal microclimates. Limitations and safeguards. Correlation does not imply colocation: high r could arise from synchronized schedules in different parts ot the building. To avoid errors in interpretation, the clusters had been cross-referenced against floorplan topology and usage type (e.g., "adjacent classrooms on the same corridor" vs "library vs gym"). We also make sure representative sensors retain diurnal amplitude and peak timing characteristics of their cluster peers; if a candidate representative exhibits atypical variance (e.g., damped amplitude due to local ventilation boost), an automatic choice was overrided.

3.2.4 Visualization and interpretation

The workflow ingests ten raw sensor files for any given site and a given month; each file is expected to include time-series data from one room. The system auto-detects a timestamp field in ISO 8601, then converts it into a timezone-aware datetime object (UTC) and strictly orders this data by time. Preferably, room identifiers are pulled from a "Room" field, or otherwise parsed from the filename. These identifiers have been normalized to ensure consistency, but they are semantically preserved to maintain a clear link to their physical location in the

building. A reference timeline is created using the timestamps from the first cleaned file. For each of the six main indoor air quality (IAQ) parameters, we perform the following steps for each room:

$$P \in \{CO_2, RH, Temperature, PM_{2.5}, PM_{10}, Pressure\} \tag{3.5}$$

We extract the corresponding time series, ensure that the data types are numeric, and interpolate them onto the reference grid. To address slight timing mismatches, we use linear interpolation, which aligns each series precisely to a shared two-minute interval structure. Any small gaps that remain are filled using nearest-neighbor interpolation along the time axis. This approach is not meant to fabricate data but to prevent rendering artifacts in the plots, particularly for visualization tools that require continuity. As a result, we obtain a uniform temporal resolution and spatial alignment across all rooms in the building for each parameter (time, room).

3D diagnostic visualization

To assess the integrity of the aligned dataset and to perform an analysis of high-level dynamics, we provide two complementary 3D plots for each parameter:

- 1. Spacetime Surface Plot A 3D surface is created using the function ‘surf()‘ from MATLAB, where the axes represent time, room index, and measured value (Z). We apply interpolated shading to smooth the surface and highlight structural features. This plot effectively shows:
  - Daily cycles, including for instance morning CO increase, lunchtime dip, and afternoon peak
  - Magnitude differences between rooms
  - Coherent wavefronts that indicate shared ventilation schedules or occupancy trends

  Any visible discontinuities in the surface indicate potential problems such as data import errors, time misalignments, or large data gaps.

- 2. Room Trace Overlay Plot Using ‘plot3()‘, this view stacks all room traces as lines in 3D space with axes for time, room, and value. Compared to the surface plot, this shows more of the amplitude and phase relationships between rooms. For example, near-parallel CO_2 traces across different rooms would indicate synchronized occupancy patterns, and large deviations may indicate potential outliers, such as rooms that have poor ventilation or irregular air flow.

These diagnostics are visual, not for aesthetic reasons but functional ones, in that they will be useful for alignment problems, verification of the success of preprocessing, and understanding how indoor air quality evolves over time and space.

Chapter 4

Results Analysis

4.1 Temporal pattern of indoor Air quality (Temperature, Relative humidity, $PM_{2.5}$ & PM_{10}, Pressure)

The data acquired across all monitored locations exhibited highly structured diurnal cycles, which were primarily governed by occupancy patterns, mechanical ventilation schedules, and scheduled cleaning activities. This consistent temporal structure was fundamental, establishing the necessary baseline for all subsequent spatiotemporal analyses, including redundancy and spatial correlation assessments.

Specifically, the time series for each monitored space consistently demonstrated a characteristic sequence of events: low baseline concentrations during unoccupied overnight periods, a sharp increase concurrent with the initiation of academic lessons, and subsequent, progressive concentration reductions during scheduled recess periods or when windows were manually opened (airing events).

This cyclical pattern, while varying in magnitude between individual rooms, was uniformly observed across all four buildings and for multiple measured parameters. This high degree of temporal coherence confirms the effectiveness of the time synchronization procedure implemented in the pre-processing stage and validates the integrity of the high-resolution, two-minute interval dataset for deeper spatiotem-

poral analysis.

4.1.1 Jousenkaari

Temperature

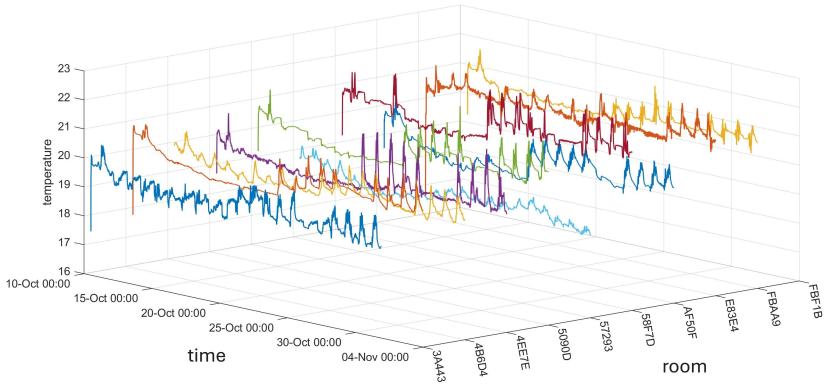

Figure 4.1: 3D temperature traces for all rooms over the monitoring period october-november

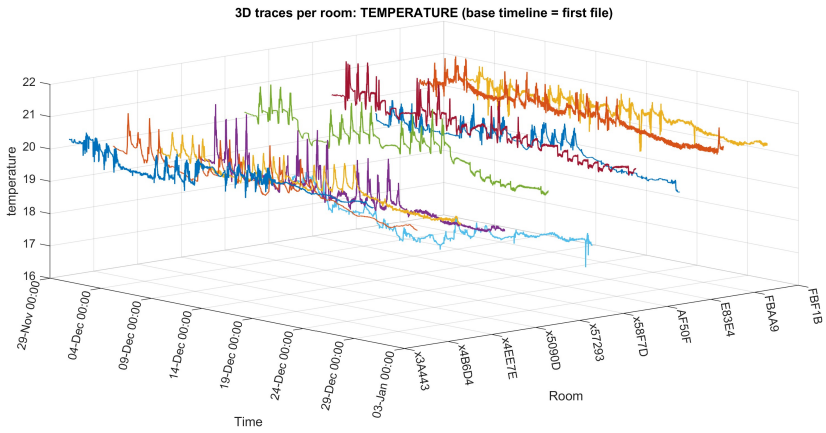

Figure 4.2: 3D temperature traces for all rooms over the monitoring period December-January

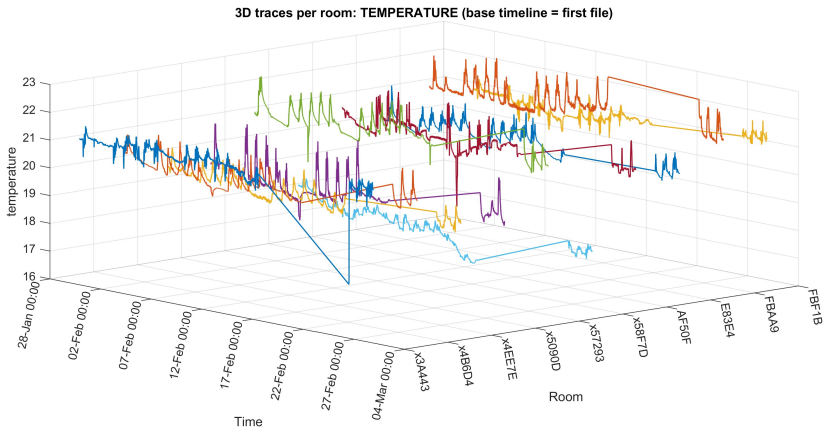

Figure 4.3: 3D temperature traces for all rooms over the monitoring period February-March

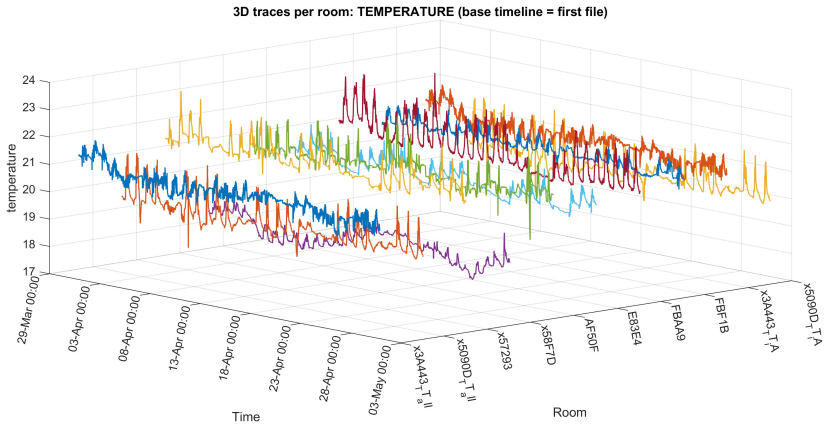

Figure 4.4: 3D temperature traces for all rooms over the monitoring period April-may

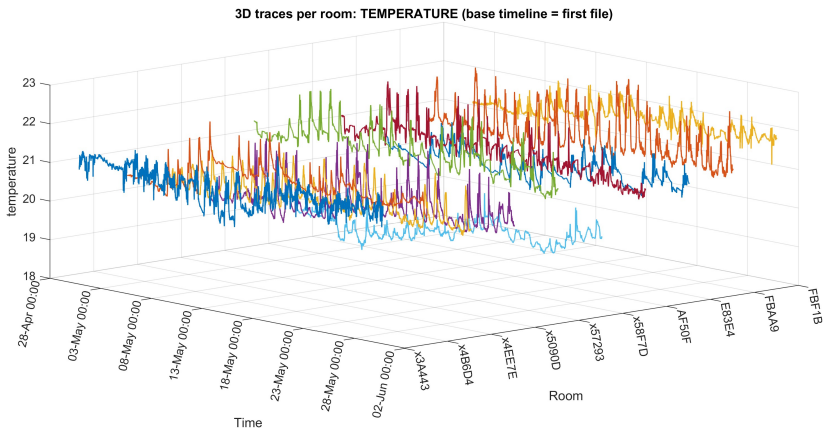

Figure 4.5: 3D temperature traces for all rooms over the monitoring period June

These five 3D graphs show how the temperature evolves with time in different rooms; each room is represented by a unique color in these graphs. The horizontal axes represent time and room identifiers, while the vertical axis represents temperature. Taken as a whole, they represent the variation of thermal conditions through the month of the year, reflecting both seasonal variation and heating control behavior.

In the graph below, temperatures from mid-October to early November range from 18 to 21 °C. As the days progress, a gradual downward trend is observed with noticeable short-term oscillations in most rooms. This would therefore indicate the start of cold weather and the beginning of heating systems, which will provide intermittent increases in temperature.

The temperature stabilizes at about 19–20 °C in the second graph, representing the span from late October through early December. The oscillations are more regular and pronounced in that case, which indicates that the heating system is now regularly active. The repeated spikes likely correspond to thermostat cycles or occupancy-driven heating adjustments.

The third graph corresponds to January–February; it has the lowest temperatures of all the datasets and ranges between 17 and 21 °C. Variations are stronger and more frequent, suggesting this is the coldest period of the year, during which the heating system works harder to maintain comfortable indoor conditions. The larger amplitude of these variations can be attributed to drops in outdoor temperature or higher thermal losses.

The trend above persists from February through April in the fourth graph, where the mean temperature slightly rises and now oscillates around 19–22 °C. Although the daily oscillations still persist, their amplitude starts to reduce with this gradual transition into much milder spring weather and hence lower heating demand.

Finally, the fifth graph corresponds to late April through June and presents a clear upward shift in the temperature range, now stabilizing around 20–23 °C. This yields smoother variations, with smaller daily oscillations, reflecting the closeness of summer and reduced dependence on heating systems. The same general behavior for each room

is observed across all graphs. Some rooms consistently have higher temperatures on average, possibly due to higher occupancy, better insulation, or gains from equipment heat, while others show more variability, likely corresponding to external-facing or less well-insulated rooms. Overall, a coherent seasonal progression is evident: a cooling phase from autumn into midwinter, followed by a steady warming trend through spring and into early summer, with daily fluctuations that reflect the operation of heating controls and the prevailing external climate conditions.

Relative Humidity

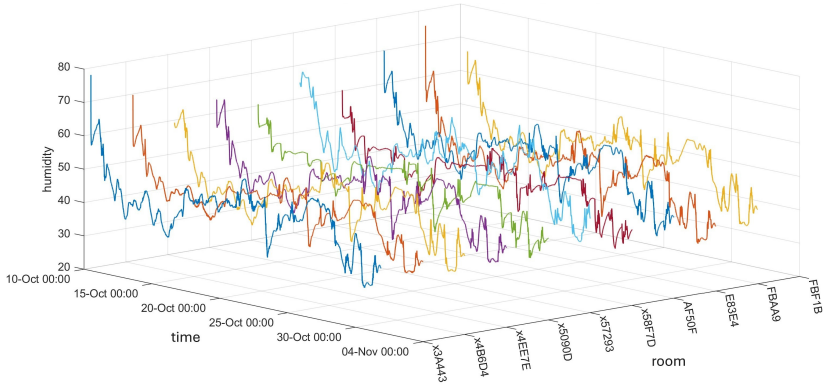

Figure 4.6: 3D Relative Humidity traces for all rooms over the monitoring period october-november

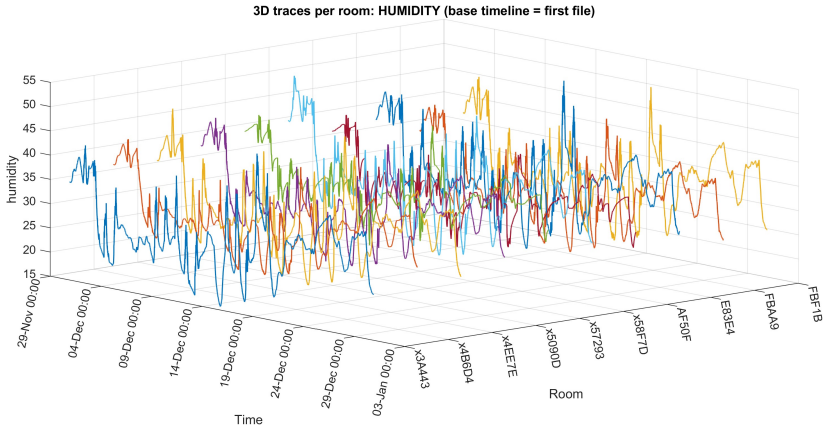

Figure 4.7: 3D Relative Humidity traces for all rooms over the monitoring period Decemebr-January

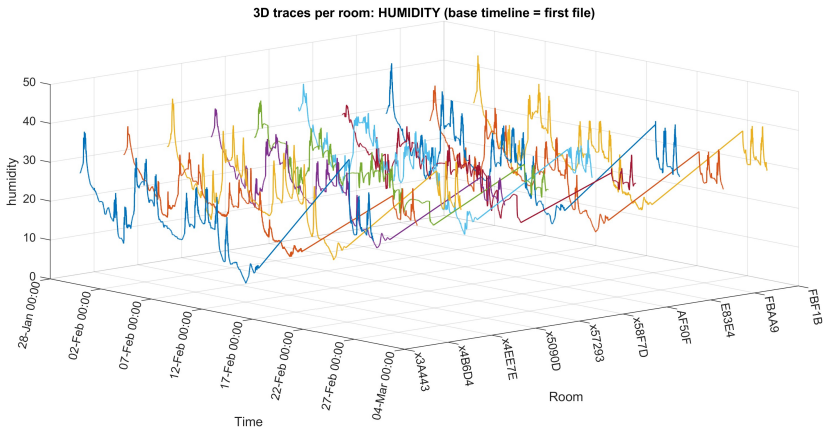

Figure 4.8: 3D Relative Humidity traces for all rooms over the monitoring period Februray-March

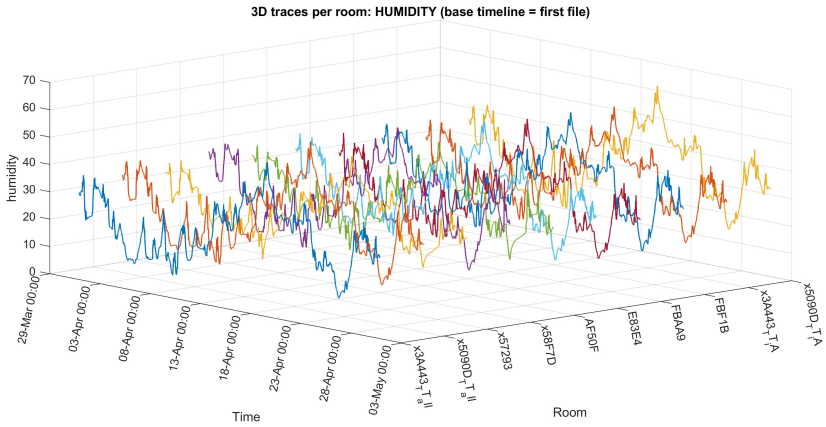

Figure 4.9: 3D Relative Humidity traces for all rooms over the monitoring period April-May

These five 3D graphs represent the variation in relative humidity across several rooms over varied time periods and how indoor moisture evolves through seasons. Each color corresponds to a different room, and plots point out the complexity of the relationship between humidity, temperature, and external climatic conditions.

In the graph for mid-October to the beginning of November, the humidity values are relatively high; most rooms stand between 40% and 70%. It is highly variable with quite a few sharp peaks, so it seems that during this period, humidity fluctuates strongly, likely due to changing autumn weather and variable heating operation. The trend depicts a gradual overall decrease, hence showing that as heating

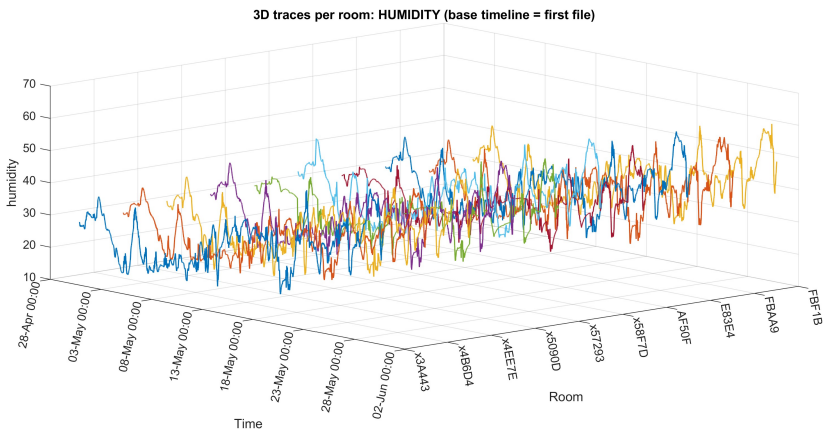

Figure 4.10: 3D Relative Humidity traces for all rooms over the monitoring period June

begins, indoor air becomes drier.

In the second graph, between late November and late December, the level of humidity significantly drops, mainly stabilizing between 20% and 40%. The traces appear more irregular, with frequent short-term oscillations. Such behavior is typical for early winter, where heating systems are on and outdoor air is cold and dry, thus maintaining low indoor relative humidity. The fluctuations across rooms suggest local influences such as ventilation rates or occupancy.

The third graph, from February to March, shows the lowest humidity levels across the dataset, often less than 20%, occasionally approaching 10%. Although there are some periodic spikes, the general trend indicates that the air is very dry during this period. This corresponds to the peak of the heating season when sustained indoor warming and low external humidity create persistently dry conditions.

In the fourth graph (March–April), a gradual recovery in humidity can be observed. The average level increases to lie between 20% and 40%, and the traces reflect more frequent oscillations; this is because spring has started, and the outside air is moister, while the usage of heating decreases, and thus indoor humidity may rebound a little.

The fifth graph, between late April to early June, shows the humidity continues to climb, now mostly fluctuating between 30% and 50%, with some peaks above 60%. Smoother and more stable, the curves reflect the warmer weather and reduced heating. The higher baseline

humidity reflects the natural seasonal increase in outdoor moisture. For all seasons, the relative relationships among rooms hold constant. Some rooms maintain relatively high humidity, which likely results from lower ventilation rates or from specific usage patterns. Others consistently develop drier conditions, indicative of stronger air movement or proximity to heating elements. On the whole, the succession of graphs unmistakably portrays a seasonal pattern that is quite typical for interior climates of temperate zones-high in autumn, significantly lower during winter, and steadily increasing during spring into early summer.

$PM_{2.5}$ **and** PM_{10}

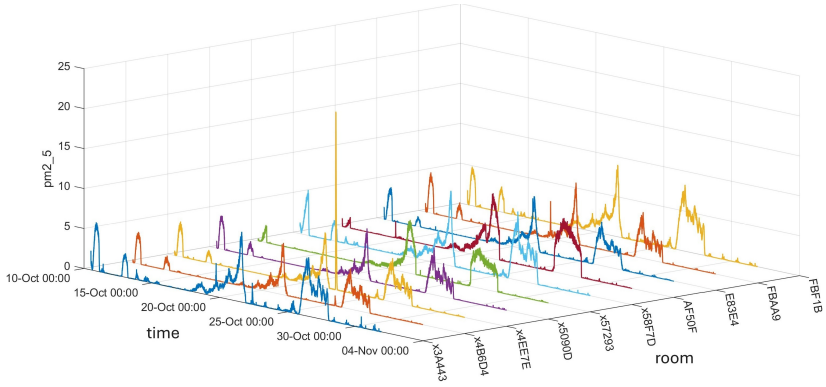

Figure 4.11: 3D $PM_{2.5}$ traces for all rooms over the monitoring period October-November

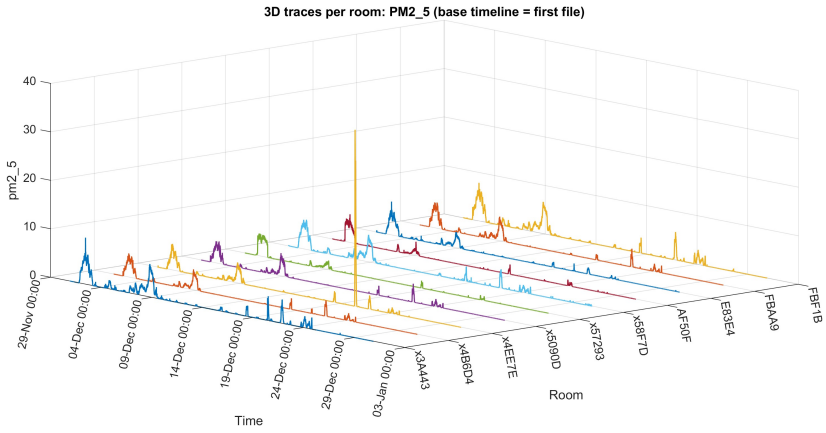

Figure 4.12: 3D $PM_{2.5}$ traces for all rooms over the monitoring period Decemeber-January

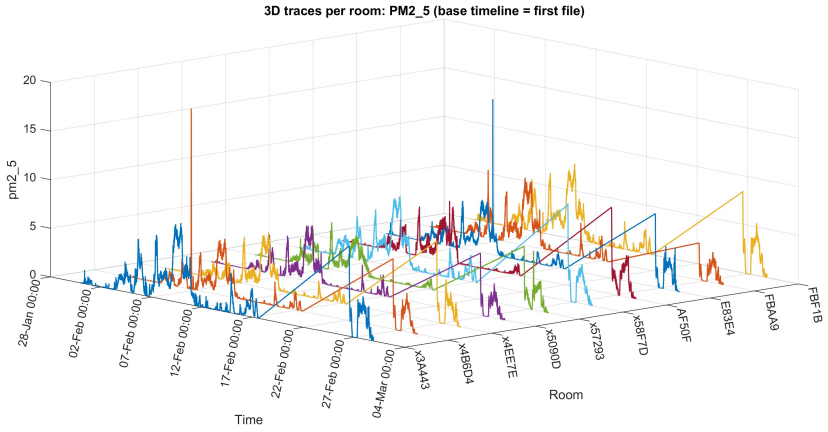

Figure 4.13: 3D $PM_{2.5}$ traces for all rooms over the monitoring period February-March

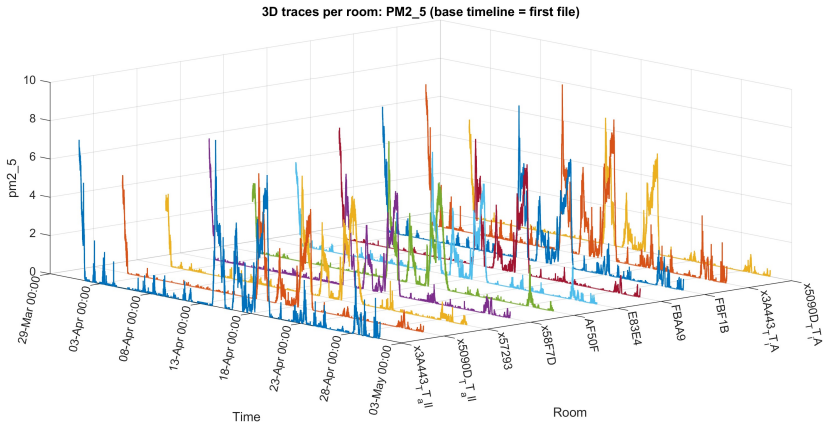

Figure 4.14: 3D $PM_{2.5}$ traces for all rooms over the monitoring period April-May

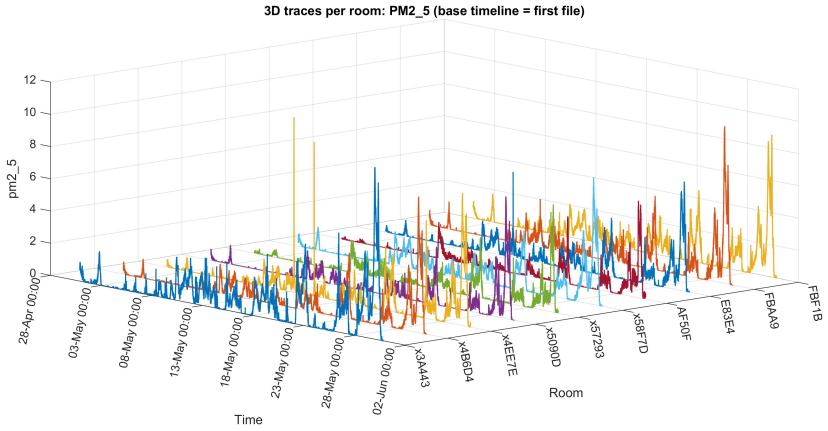

Figure 4.15: 3D $PM_{2.5}$ traces for all rooms over the monitoring period June

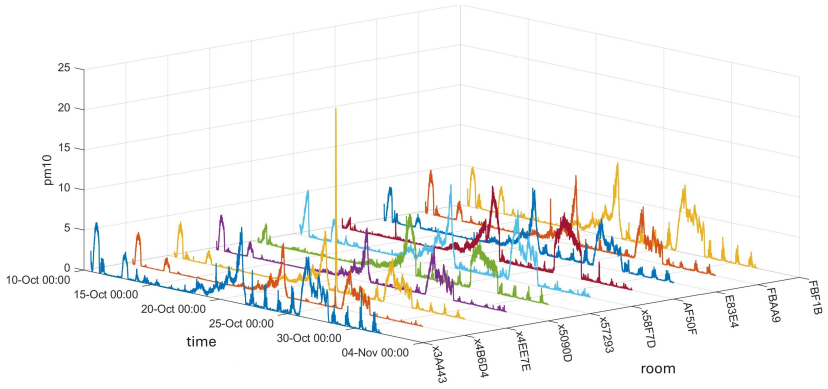

Figure 4.16: 3D PM_{10} traces for all rooms over the monitoring period October-November

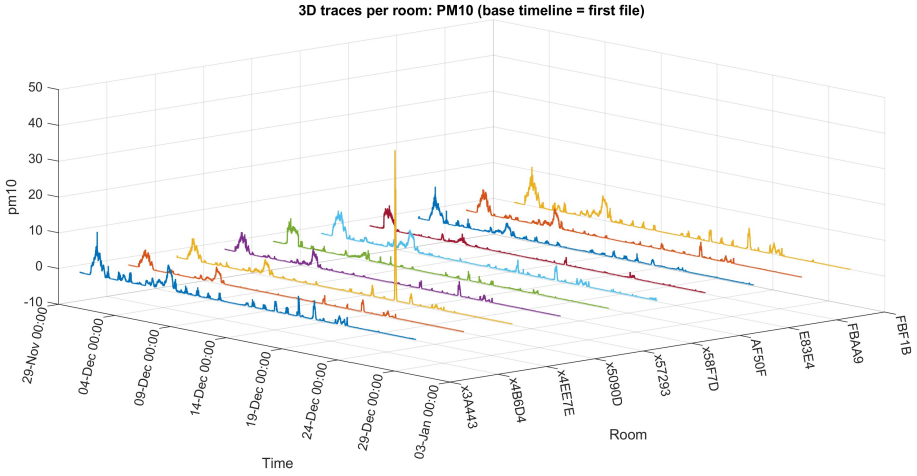

Figure 4.17: 3D PM_{10} traces for all rooms over the monitoring period December-January

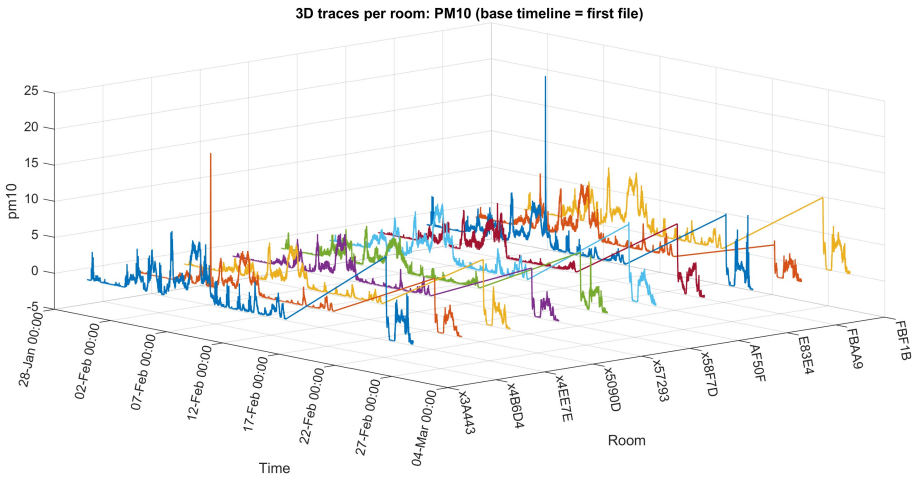

Figure 4.18: 3D PM_{10} traces for all rooms over the monitoring period February-March

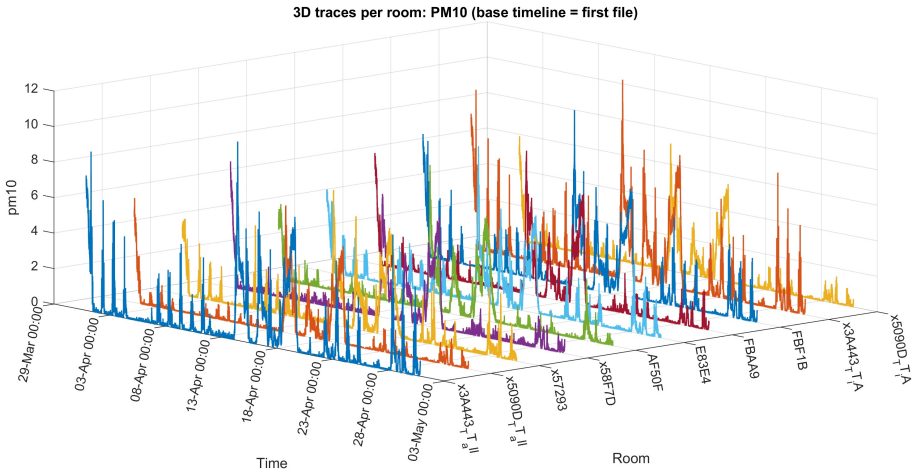

Figure 4.19: 3D PM_{10} traces for all rooms over the monitoring period April-May

These below 3D plots will present the particulate matter concentrations of $PM_{2.5}$ and PM_{10} across several rooms and over some months. Every line represents a room, while the time axis refers to the recording period and the vertical axis shows the particle concentration in micrograms per cubic meter ($\mu g/m^3$). Together, they provide insight into indoor air quality dynamics and possible sources of airborne particles.

In this first set, October to November, the levels of both $PM_{2.5}$ and PM_{10} remain relatively low overall, mostly less than 10 $\mu g/m^3$, with short-lived peaks up to about 20–25 $\mu g/m^3$ in some of the rooms.

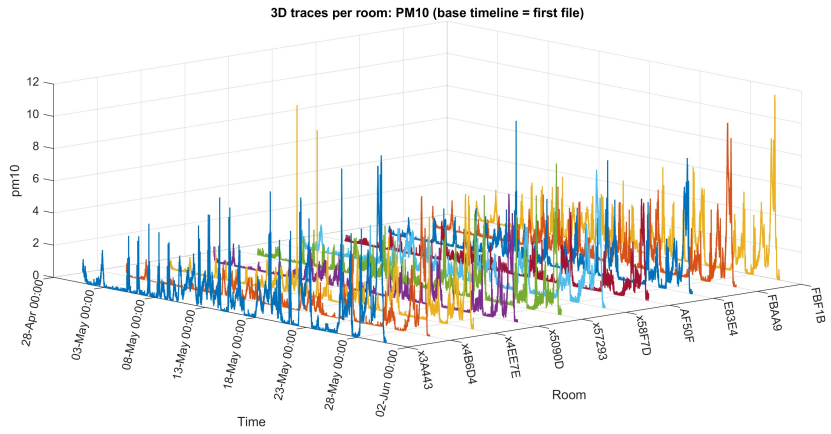

Figure 4.20: 3D PM_{10} traces for all rooms over the monitoring period June

The peaks are periodic and simultaneous across all rooms, indicating common sources, which are probably short-term ones due to human activities like cooking and cleaning. The baseline concentration between the events is close to zero, therefore good background air quality with efficient ventilation.

Similar episodic peaks are seen in the second set (November–December), but the maximum concentrations are slightly higher—some PM_{10} spikes exceed 30–40 µg/m³. This might correspond to reduced air exchange because of colder outdoor conditions, since buildings are normally more closed during winter. Again, events remain infrequent and short with long intervals of near-zero particle levels.

In the third period of measurement (February–March), an evident development is observed in the data, with more frequency and density of peaks for both $PM_{2.5}$ and PM_{10}. The levels of concentration remain modest, generally below 15 µg/m³, but the persistence of fluctuations suggests a rise in indoor activity or reduced ventilation during the coldest part of the season. The $PM_{2.5}$ and PM_{10} traces follow an almost identical pattern, suggesting that the same sources of emissions are at work for both particle sizes.

During the fourth period (March–April), the peaks are sharper and more in number, yet their magnitudes are lower and rarely exceed 10 µg/m³; this phase corresponds to spring, a time when the windows are opened more frequently, leading to increased ventilation and thus allowing the particles to disperse more. The pattern shows more tran-

sient peaks with a fast decay, consistent with short indoor events.

Finally, during the fifth period, which is from April to June, the level of $PM_{2.5}$ and PM_{10} is the lowest of all, keeping a near-zero baseline, with only minor and infrequent peaks. These results suggest cleaner air and higher ventilation rates, typical of warmer months with open windows and less heating-related particle buildup. As can be seen, the trends for both $PM_{2.5}$ and PM_{10} are almost parallel in all datasets; this means that both fine and coarse particles share a large number of sources and are equally affected by ventilation dynamics. Some rooms regularly report higher spikes, indicating local activities or reduced airflow. On the whole, the temporal development of particulate matter demonstrates evident seasonal variance: from low values during mild months, increased particle accumulation during the heating season, to minimal levels again in spring and summer. Indoor air quality, therefore, was normally good, and peaks in particles could usually be attributed to short events-sometimes human-induced-rather than continuous pollution.

Pressure

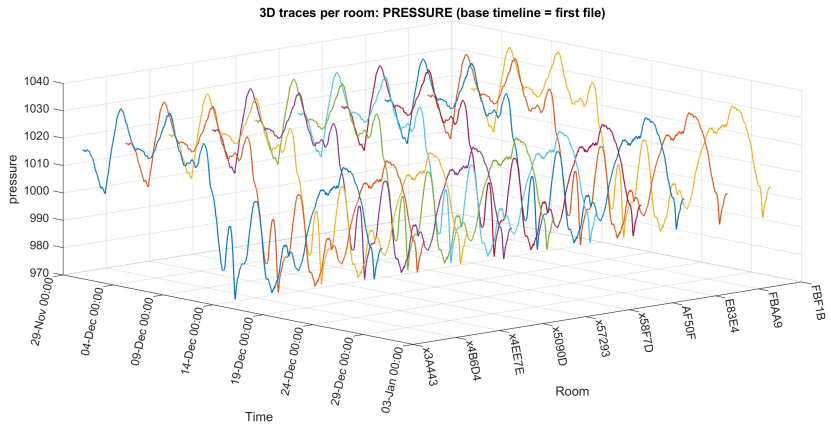

Figure 4.21: 3D Pressure traces for all rooms over the monitoring period December-January

The pressure trend is basically the same for the whole measuring period in all rooms.

All the traces show a coherent oscillatory pattern, with a gradual

drift from about 990 to 1030 hPa. This suggests that the pressure measurements are very much dominated by variations in atmospheric rather than indoor pressure, since all sensors change in concert. The differences between rooms are very small and most likely due to sensor calibration or slight local offsets rather than real physical differences.

The pressure data thus confirm a uniform time trend dominated by large-scale weather variations and not influenced by room-specific indoor effects.

4.1.2 Monikko

Temperature

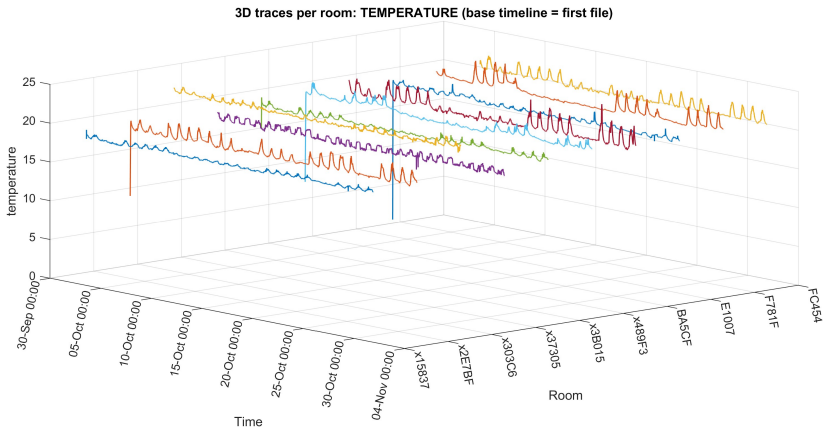

Figure 4.22: 3D temperature traces for all rooms over the monitoring period october-november

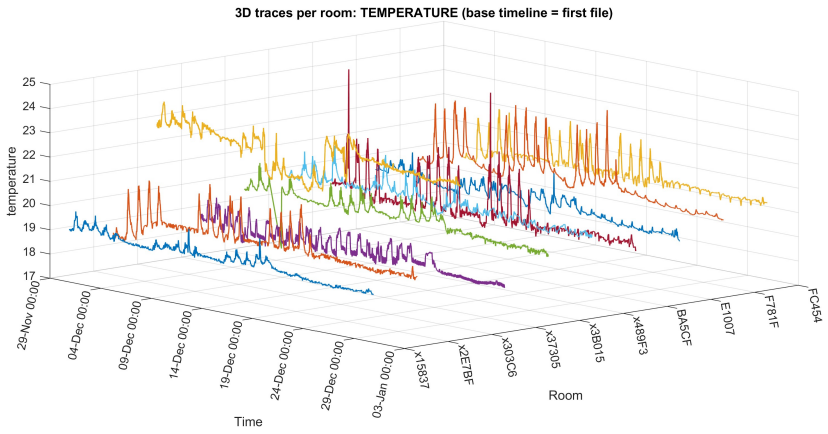

Figure 4.23: 3D temperature traces for all rooms over the monitoring period Decemeber-January

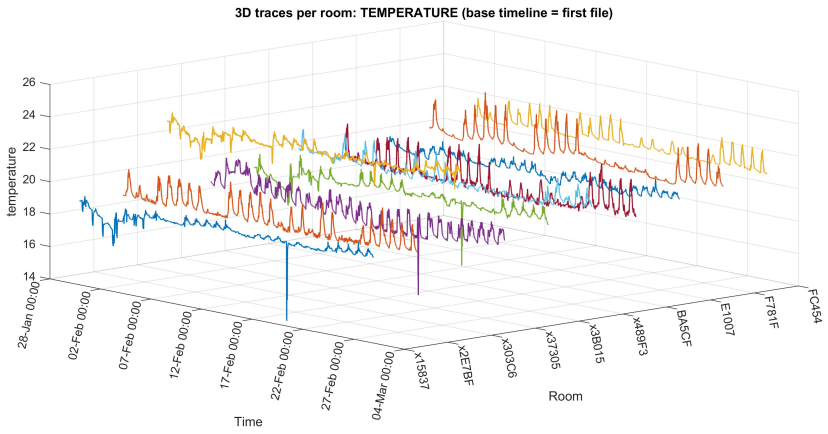

Figure 4.24: 3D temperature traces for all rooms over the monitoring period February-March

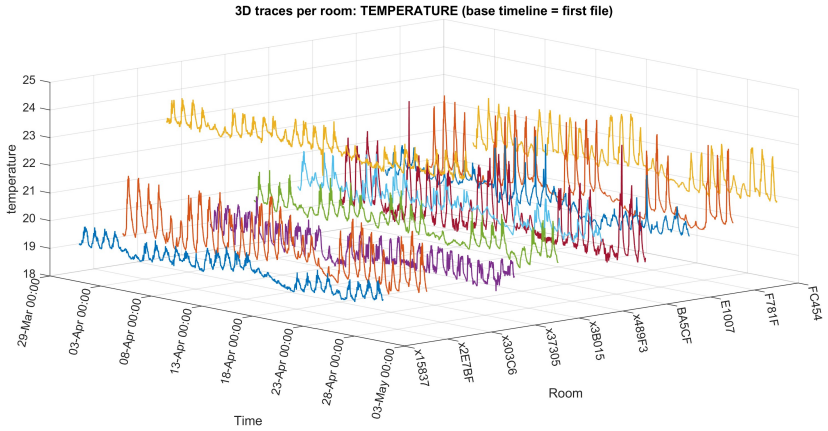

Figure 4.25: 3D temperature traces for all rooms over the monitoring period April-May

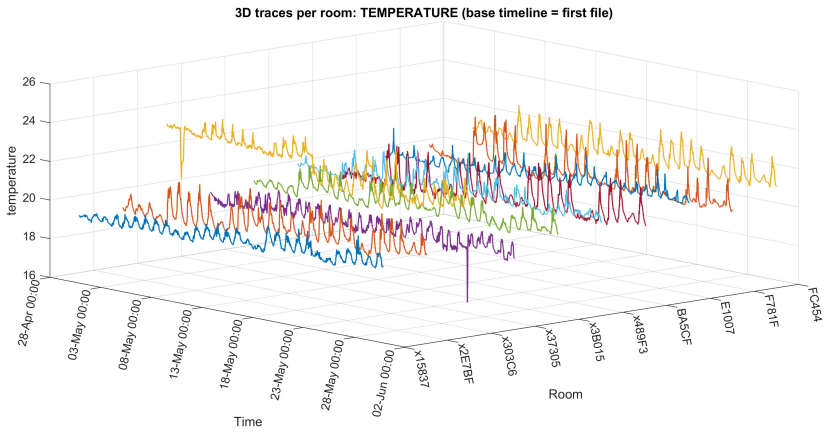

Figure 4.26: 3D temperature traces for all rooms over the monitoring period June

Time-series analysis of indoor temperature throughout the monitoring period reveals a steady and well-defined seasonal pattern, which is a direct reflection of the building's heating strategy and response to the Finnish climate. During the first observation in October, at the start of the heating season, temperatures broadly ranged approximately from 14° to 25°. At this stage, the thermal traces exhibited clear diurnal oscillations, characterized by regular peaks and troughs indicating the heating system's activation as outdoor temperatures began to drop. The magnitude of these daily swings varied locally, suggesting differences in room exposure, ventilation intensity, or proximity to heat sources. Despite minor short-term anomalies, the overall trend was toward gradual stabilization of the indoor thermal environment, with the onset of the main heating phase. In December, at the peak of the cold season, temperature levels notably became more stable and higher, fluctuating typically between 17° and 25°. The daily oscillations remained evident but appeared more synchronized among the monitored rooms, reflecting the stable and consistent operation of the centralized thermal control system. Warmer spaces, maintaining temperatures above 23°, likely corresponded to zones with lower ventilation rates or greater internal heat gains, while cooler rooms around 18° generally experienced stronger air exchange. The February–March dataset marked the beginning of seasonal transition. The mean temperature thus showed a slight overall decrease, and a slow downward trend became visible across the timeline. The thermal oscillations, while still present, were less pronounced and exhibited greater irregularity compared to the preceding peak winter months. This suggested either a programmed reduction in heating intensity or increased variability driven by the gradually warming external conditions. In the subsequent March–April period, the thermal traces displayed a more complex and noisy behavior. While the overall range remained between 18° and 25°, the highly variable fluctuations have been interpreted as a consequence of intermittent heating operation combined with the increasing instances of natural ventilation (window opening) during milder days. The thermal cycles had smaller amplitudes, revealing the weakened influence of the mechanical heating system and

a larger dependence on ambient conditions. Finally, in the May-June period, the mechanical heating system seemed to be fully off. The temperature evolution was now much smoother, revealing only small, slow oscillations corresponding to the diurnal cycle of outdoor conditions and not to an active control. Typical temperatures stabilized in the interval 16° to 26°, depending on room exposure and thermal inertia. The disappearance of the sharp peaks characterizing the heating periods guaranteed that passive regulation, for which solar radiation, internal gains, and natural ventilation are the main thermal drivers, had indeed set in. In all analyzed periods, the relative differences among rooms were very stable, reinforcing the reliability of the sensor collocation and pointing to stable structural and architectural features governing thermal patterns. These results put together show a well-managed and adaptive heating strategy, capable of maintaining comfort throughout the cold months and switching smoothly to passive regulation during the warm season.

Relative Humidity

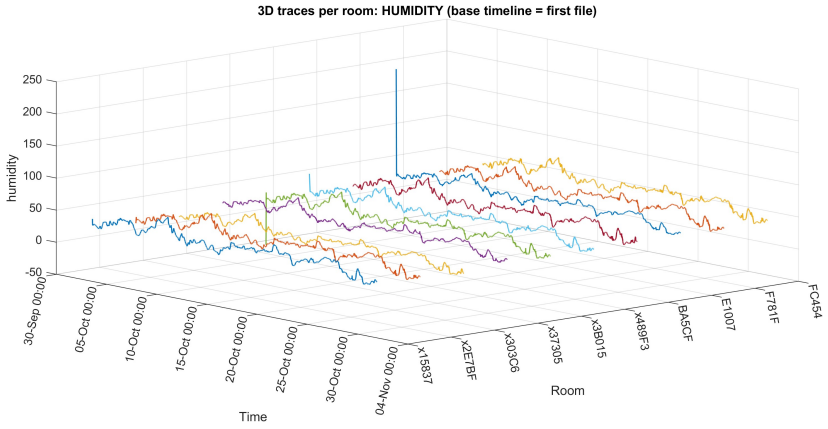

Figure 4.27: 3D Relative Humidity traces for all rooms over the monitoring period october-november

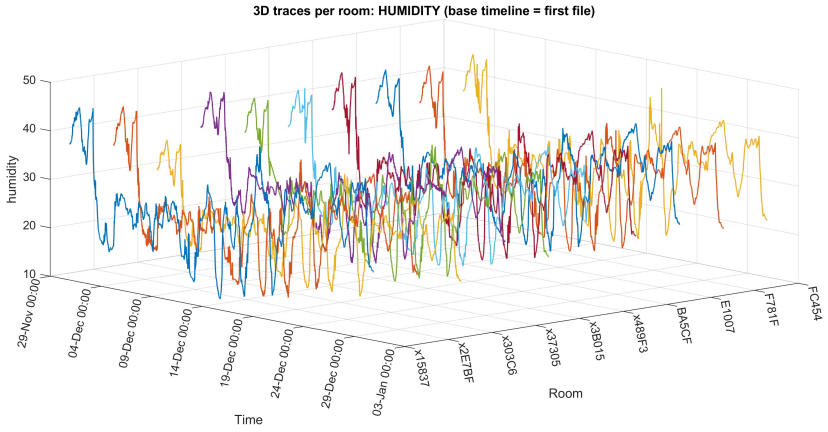

Figure 4.28: 3D Relative Humidity traces for all rooms over the monitoring period Decemebr-January

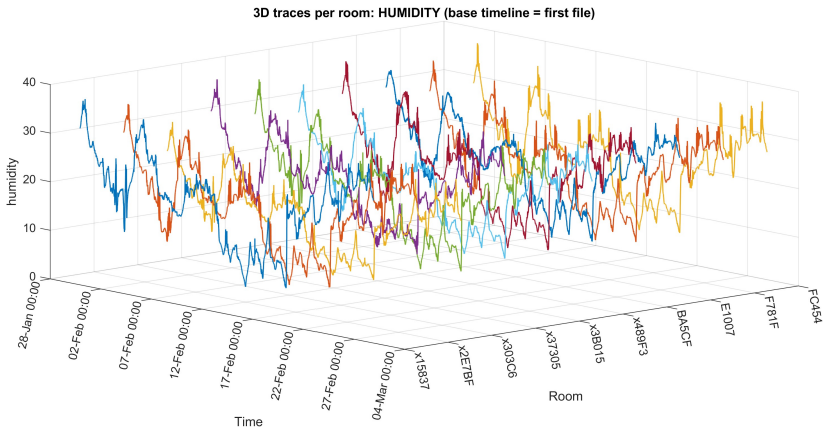

Figure 4.29: 3D Relative Humidity traces for all rooms over the monitoring period Februray-March

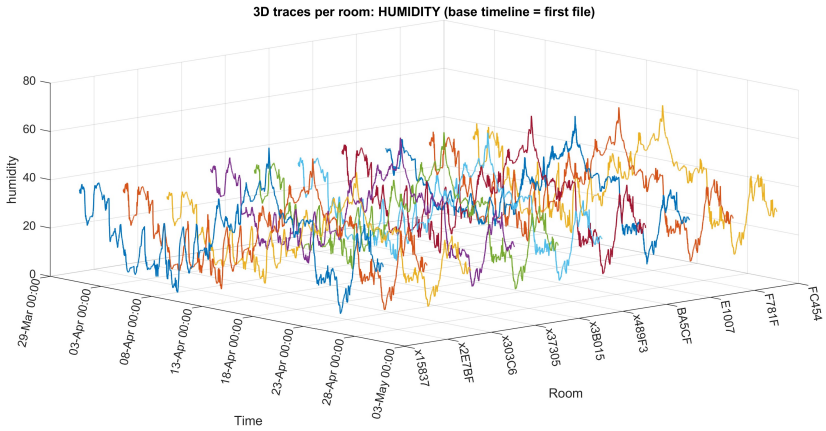

Figure 4.30: 3D Relative Humidity traces for all rooms over the monitoring period April-May

The temporal evolution of indoor humidity demonstrates clear seasonal patterns that reflect the combined effect of outdoor climatic conditions, indoor heating operation, and ventilation behavior. During the early autumn period, relative humidity in October varies within the range of 40% to 60%, following a moderate trend with a gradual decrease. This decline corresponds to the transition of outdoor air masses from warmer (carrying more moisture) to cooler and drier conditions, as heating systems start their operation. At the same time, these traces are characterized by smooth variations without considerable short-term oscillations, indicating relatively stable indoor conditions and moderate ventilation rates. Isolated peaks in some rooms

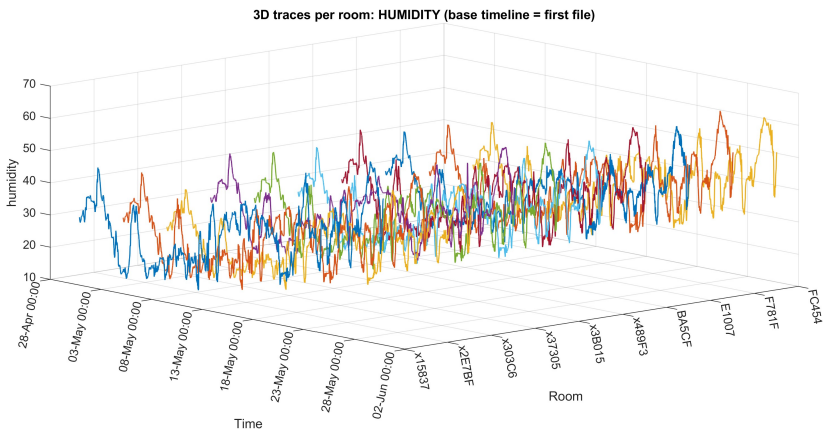

Figure 4.31: 3D Relative Humidity traces for all rooms over the monitoring period June

likely correspond to the transient activity events such as opening a window, human presence, or local moisture release.

During the winter period-from December until early January-the level of humidity decreases markedly and fluctuates much more, mainly between 15% and 40%. This pronounced decrease is consistent with the operation of indoor heating that normally dries the air by reducing its absolute moisture content. The enhanced short-term variability reflects the dynamic interaction of heating cycles, ventilation adjustments, and occupants. Periodic increases of humidity are associated with temporary ventilation or moisture-generating activities, while the corresponding rapid decreases reflect the re-activation of heating and the consequent drop in relative humidity. The pattern synchronization among various rooms further suggests the presence of common ventilation regime or a central heating system influence across the entire monitored space.

In February, the average humidity values are still low but demonstrate a somewhat smoother pattern compared to the peak winter months. The stabilization observed might be a consequence of milder external temperatures or partial adjustments within the ventilation control strategy of the building. Nevertheless, fluctuations can still be observed, which would suggest that indoor humidity is still sensitive to changes in the short-term environment and occupancy. The concomitance of room-specific variations suggests that localized effects-room

orientation, window exposure, or occupancy density-start to play a more important role once the external climate is less extreme.

As spring advances-March to April-the humidity significantly increases, reaching again the range of mean values from 30% to 50%. The traces reflect more irregular oscillations in all rooms, consistent with reduced heating demand and the gradual resumption of natural ventilation. The amplitude of variations increases, especially during daytime hours, reflecting the influence of more frequent opening of windows and larger diurnal changes in outdoor humidity. The lack of clear synchronization during this period among the rooms gives further support to the interpretation that humidity variations are now dominated by local microclimatic and behavioral factors rather than by central system effects.

By late spring and early summer, from May to June, indoor humidity is stabilized between generally higher levels of 40% and 60% with periodic peaks above 60% on particularly humid days. The general pattern is much smoother, reflecting a general improvement in the balance between indoor and outdoor air due to continuous or more frequent ventilation. This behavior follows the shutdown of the heating system and naturally ventilated conditions. In this phase, room-to-room differences are limited, with an almost homogenized indoor environment driven primarily by outdoor climate rather than building operation. In a nutshell, the humidity analysis has shown a strong negative correlation between heating operation and indoor relative humidity; the lowest values are recorded during the heating season, while recovery takes place when natural ventilation increases. The data also illustrate how seasonal transitions modulate not only absolute levels but also temporal variability of humidity as the building responds to hygrothermal environmental and operational conditions. Maintaining optimal levels throughout winter may require the integration of moisture control strategies, such as humidification or more balanced ventilation methods, to maintain indoor comfort while preserving air quality.

$PM_{2.5}$ **and** PM_{10}

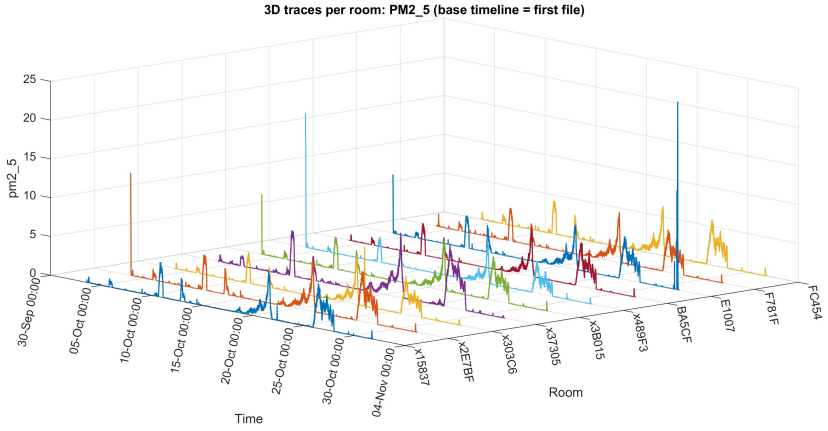

Figure 4.32: 3D $PM_{2.5}$ traces for all rooms over the monitoring period October-November

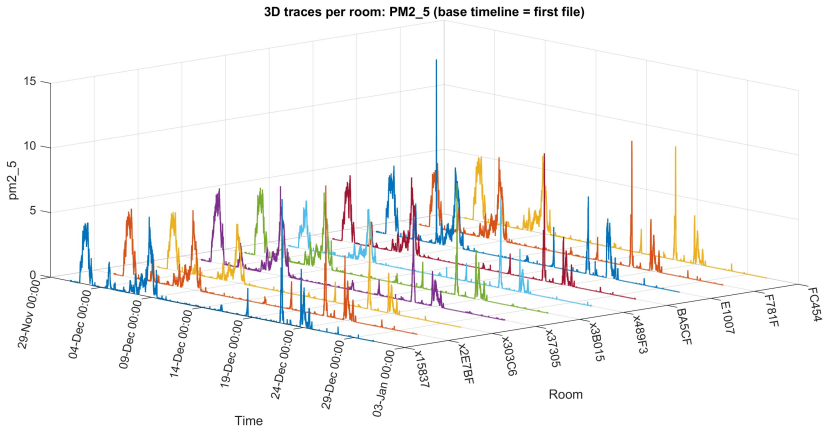

Figure 4.33: 3D $PM_{2.5}$ traces for all rooms over the monitoring period Decemeber-January

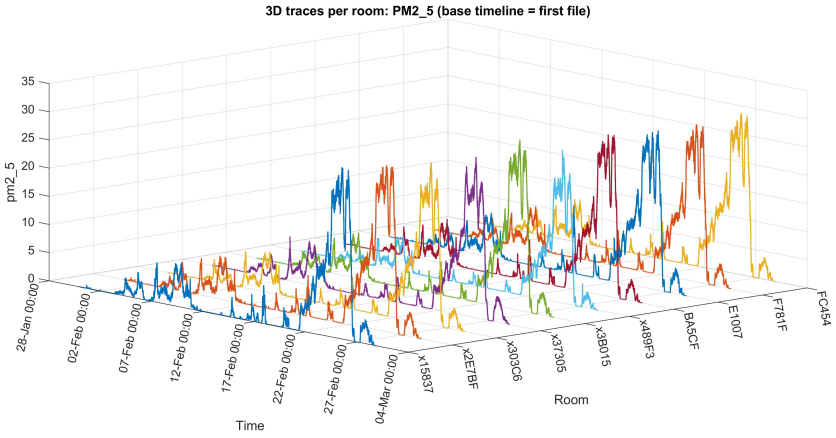

Figure 4.34: 3D $PM_{2.5}$ traces for all rooms over the monitoring period February-March

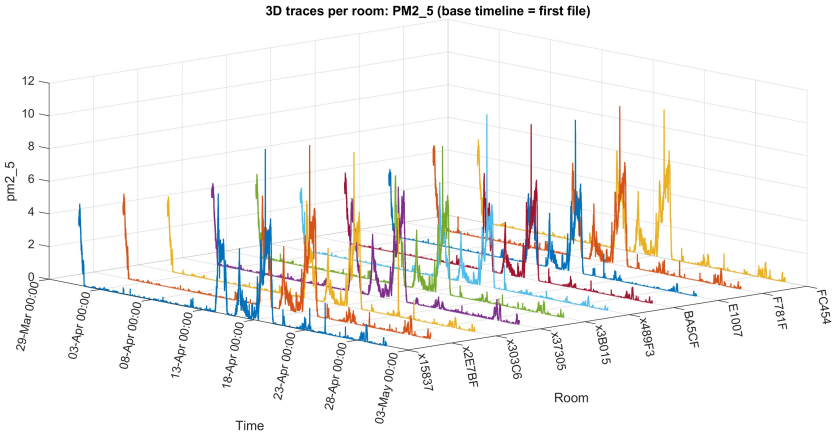

Figure 4.35: 3D $PM_{2.5}$ traces for all rooms over the monitoring period April-May

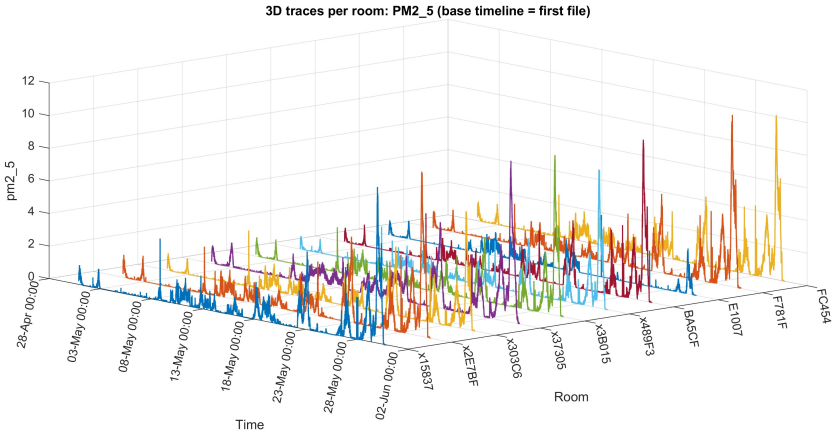

Figure 4.36: 3D $PM_{2.5}$ traces for all rooms over the monitoring period June

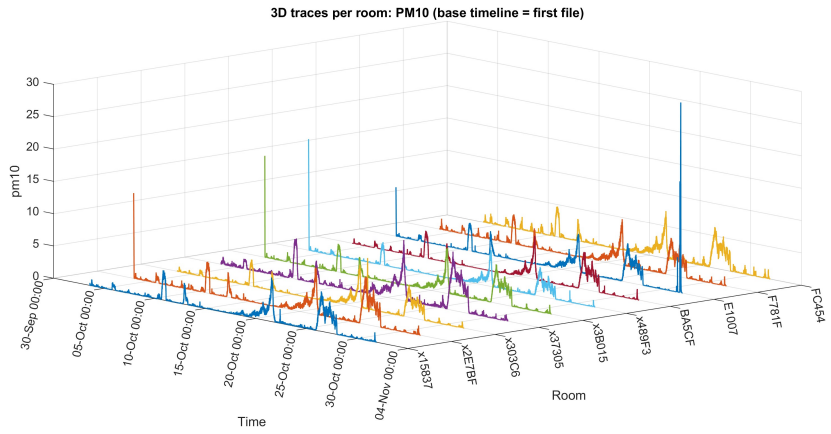

Figure 4.37: 3D PM_{10} traces for all rooms over the monitoring period October-November

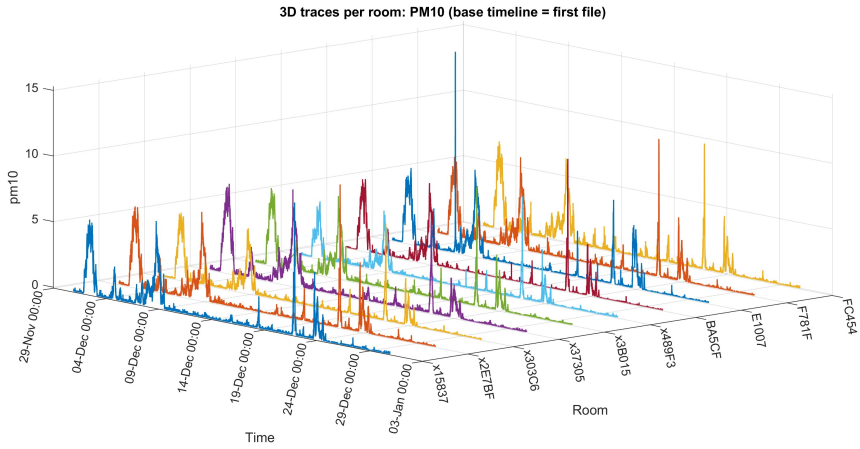

Figure 4.38: 3D PM_{10} traces for all rooms over the monitoring period December-January

The particulate matter concentrations, $PM_{2.5}$ and PM_{10}, changed through the different measurement periods, thus yielding vital information about indoor air quality dynamics and seasonal factors, as well as occupancy-related activities. During the first observation period, in October, the values of both $PM_{2.5}$ and PM_{10} remain rather low and vary around the background level, close to 0–5 µg/m^3, exhibiting sharp peaks up to 20–25 µg/m^3. The isolated spikes are likely associated with specific indoor activities related to cleaning, movement of

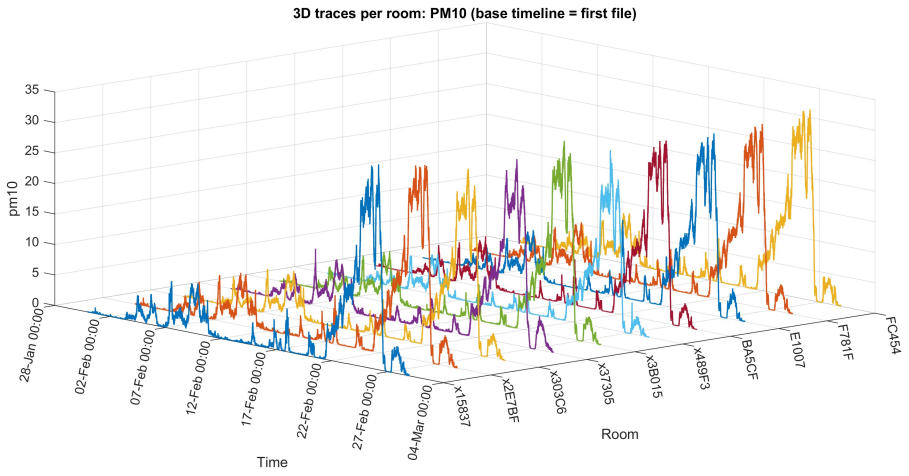

Figure 4.39: 3D PM_{10} traces for all rooms over the monitoring period February-March

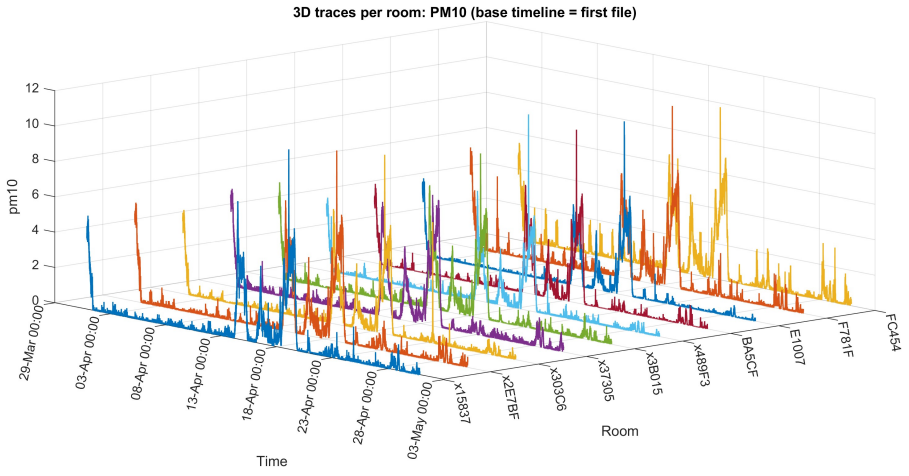

Figure 4.40: 3D PM_{10} traces for all rooms over the monitoring period April-May

people, or changes in ventilation, since their occurrence was short-term and not synchronized among rooms. Given the low baseline and event duration, the indoor environment during this early autumn period was relatively stable without sources that might generate particulates persistently.

During the December period, which corresponds to the colder winter months, there is a clear increase in the frequency and magnitude of peaks. The $PM_{2.5}$ and PM_{10} concentrations show recurrent, high readings that are more consistent across rooms, regularly surpassing 10 µg/m^3 and at times reaching as high as 15–20 µg/m^3. This may be

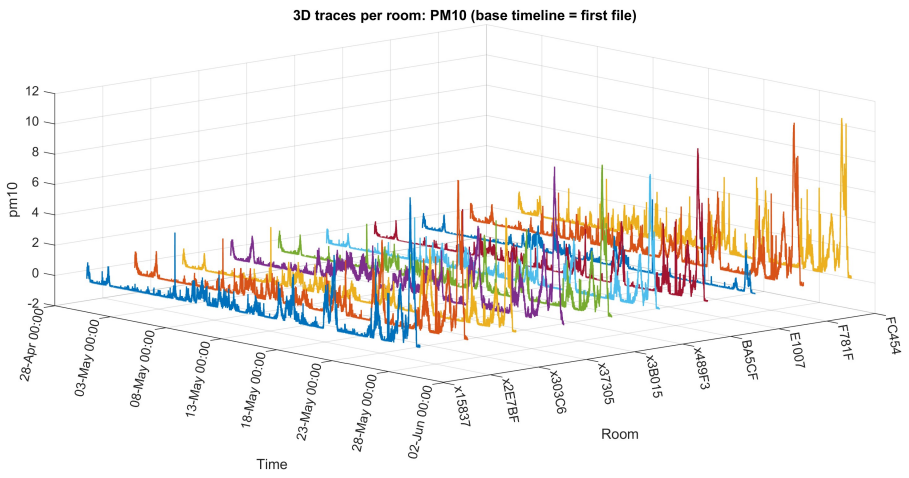

Figure 4.41: 3D PM_{10} traces for all rooms over the monitoring period June

attributed to lower air exchange rates from closed windows and continuous heating operation, which would likely act to build up particles. In addition, the increased synchronicity of the peaks between rooms suggests a possible component from shared building-wide ventilation patterns or common sources related to activities such as maintenance, heating system emissions, or dust redistribution by air currents. The similar trends between the average concentrations of $PM_{2.5}$ and PM_{10} indicate that for most of these particle events, coarse and fine particulate matter are emitted simultaneously, not distinctly.

In February, the concentration levels of both particle fractions further rise, exhibiting many peaks above 20 µg/m^3 and some reaching over 30 µg/m^3, particularly for PM_{10}. Such higher intensities would fall in times of colder outdoor conditions and extended indoor confinement, hence reinforcing the interpretation that limited ventilation linked to occupant activity is a substantial contributor to particulate buildup. The persistence of higher levels in many rooms further points to the fact that the particulate matter is not from isolated events but rather distributed through the ventilation system or common air flows. Even with such high-intensity peaks, background concentrations between the events are low, a confirmation that the particulate events are episodic in nature rather than continuous.

As the season advances into March and April, a net decrease in particle concentration and the frequency of events becomes evident. The

peaks become less intense-a maximum typically below 10 µg/m³-and widely apart, with periods of very low particle concentration. This is fully consistent with the transition period in which heating demand decreases and natural ventilation increases. Reduced synchronized events among rooms also support the hypothesis that the maxima observed during earlier periods had been enhanced by poor air renewal and by a high contribution from indoor sources. An increased variance among rooms at this stage points to localized factors-occupancy patterns, cleaning activity, etc.-as controlling particulate dynamics at the expense of centralized ventilation effects. Consequently, by late spring and early summer, both the concentrations of $PM_{2.5}$ and PM_{10} remain constantly low, with only small peaks, rarely higher than 5–10 µg/m³. The traces are smoother, reflecting the good ventilation and, more importantly, a total lack of significant sources for indoor particles. The small or negligible difference in this phase between $PM_{2.5}$ and PM_{10} agrees again that both coarse particle resuspension and fine particle emissions are minimal. The integrated $PM_{2.5}$ and PM_{10} interpretation along the entire period of monitoring reveals a strong seasonal dependency for indoor air quality. Higher particulate concentrations during winter are related to lower ventilation rates and human activity, whereas during spring and summer, air quality is better due to increased natural ventilation and no heating-related influences. The very consistent parallelism in the behavior of $PM_{2.5}$ and PM_{10} traces assures that both size fractions develop from common indoor sources rather than different processes. The particulate data demonstrate a well-defined interplay between building operation and occupancy with ambient conditions, entailing the necessity of sufficient ventilation management during colder months to ensure healthy indoor air quality.

Pressure

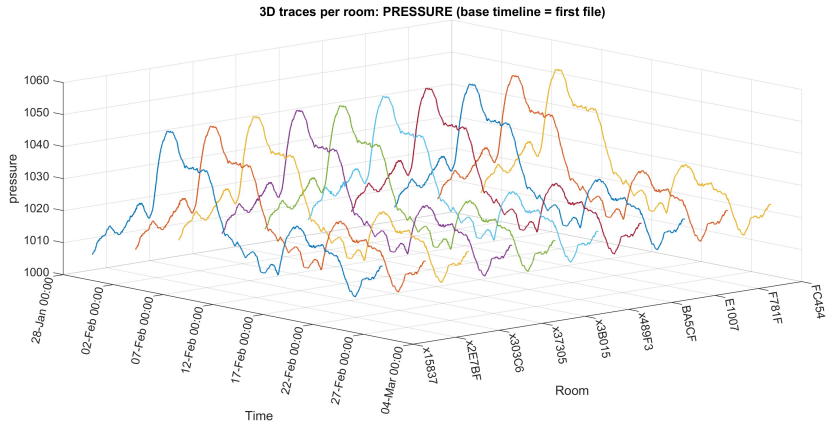

Figure 4.42: 3D Pressure traces for all rooms over the monitoring period February

The pressure distribution over time exhibits consistent and coherent trends across all monitored rooms, reflecting the influence of large-scale atmospheric variations rather than localized indoor effects. The recorded pressure values remain within a narrow range, approximately between 995 hPa and 1025 hPa, which is typical of standard atmospheric fluctuations during late spring and early summer. The observed periodic oscillations correspond to synoptic-scale weather changes, such as the alternation between high- and low-pressure systems, rather than building-related phenomena.

4.1.3 Tiitsila

Temperature

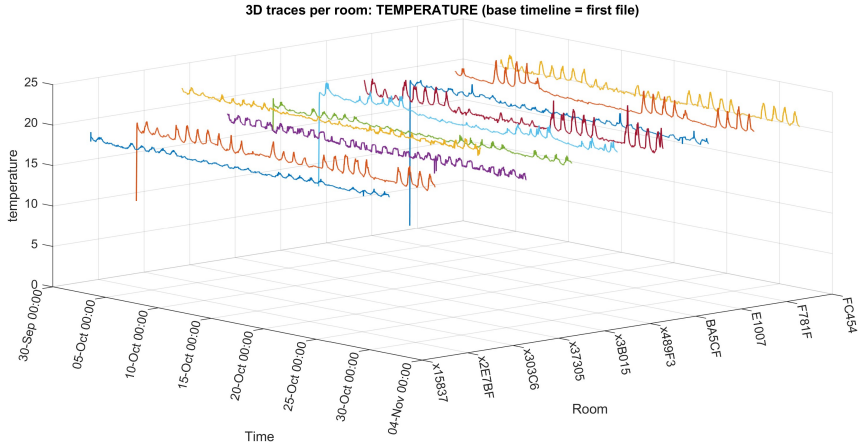

Figure 4.43: 3D temperature traces for all rooms over the monitoring period October-November

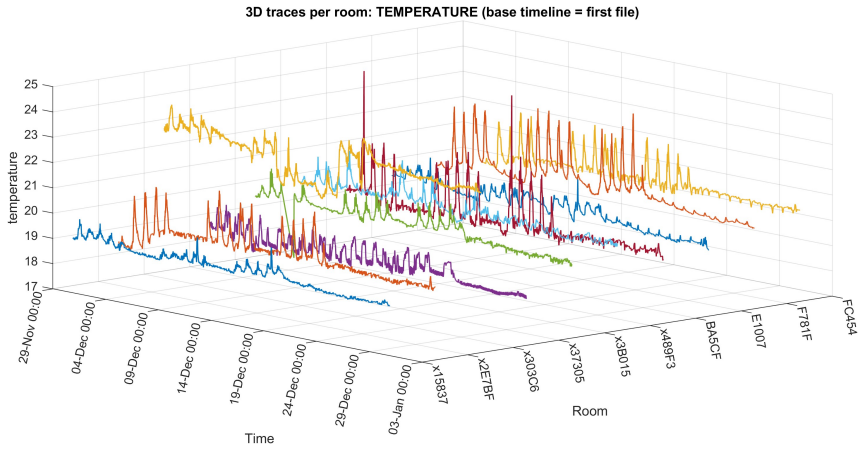

Figure 4.44: 3D temperature traces for all rooms over the monitoring period December-Janaury

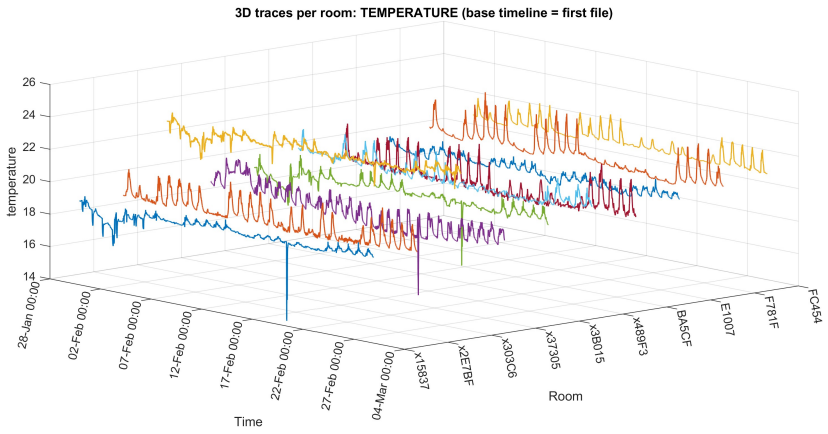

Figure 4.45: 3D temperature traces for all rooms over the monitoring period February-March

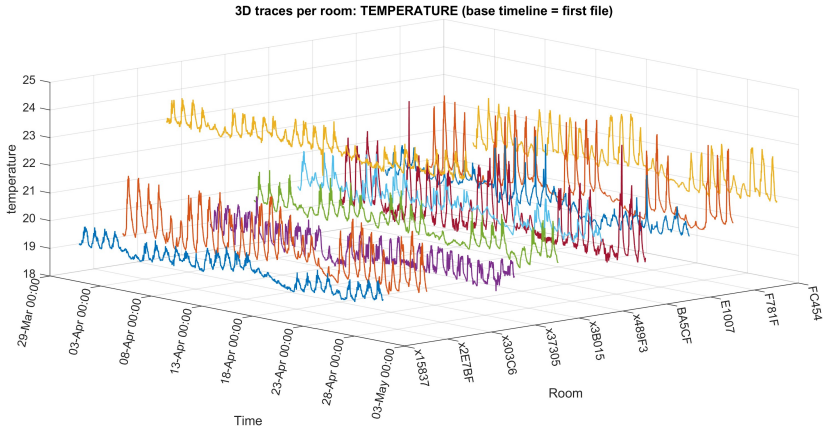

Figure 4.46: 3D temperature traces for all rooms over the monitoring period April-May

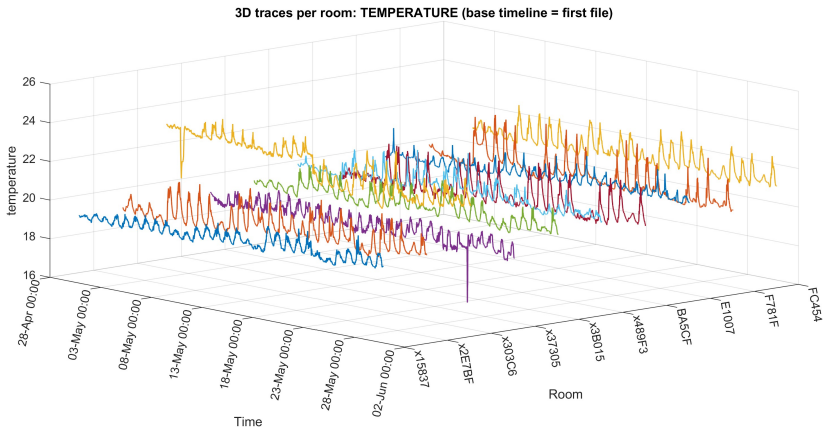

Figure 4.47: 3D temperature traces for all rooms over the monitoring period June

During the autumn period (October–November), the gradual onset of the heating regime was evident as temperatures ranged between **18**°C and **23**°C. Traces showed small daily fluctuations, suggesting the HVAC system was operating in a moderate or partially automated mode to counteract the external cooling.The winter months (December–February) marked a period of high thermal stability. Indoor conditions stabilized consistently between **19**°C and **22**°C, displaying clear, regular diurnal oscillations. These synchronized cycles confirmed the robust, schedule-driven operation of the centralized heating system. The consistent maintenance of the comfort range and the absence of extreme drops confirmed the effectiveness of the building's thermal envelope and continuous heat supply.As spring (March–April) progressed, temperatures showed a slight upward trend (**1**°C to **2**°C increase) and became notably more irregular. This variability was attributed to the combined influence of increased solar gains, milder outdoor temperatures, and potential occupant-driven window openings, resulting in localized daily peaks and occasional nighttime dips.In late spring and early summer (May–June), temperatures increased further to a range of **21**°C to **24**°C. The traces flattened and stabilized as the heating system became fully passive. Thermal regulation at this stage was dominated by natural ventilation and thermal inertia, with temperatures consistently remaining within the comfort envelope defined by ASHRAE and ISO standards. Rooms associated with higher internal loads or greater solar exposure (e.g., B521C and F42D3) consistently recorded slightly higher mean temperatures, while others (e.g., x0697A) remained cooler, likely due to proximity to ventilation inlets. In summary, the temperature analysis confirms stable thermal performance and effective control throughout the year, with observed inter-room differences highlighting the influence of architectural layout and localized boundary conditions on the overall thermal balance.

Relative Humidity

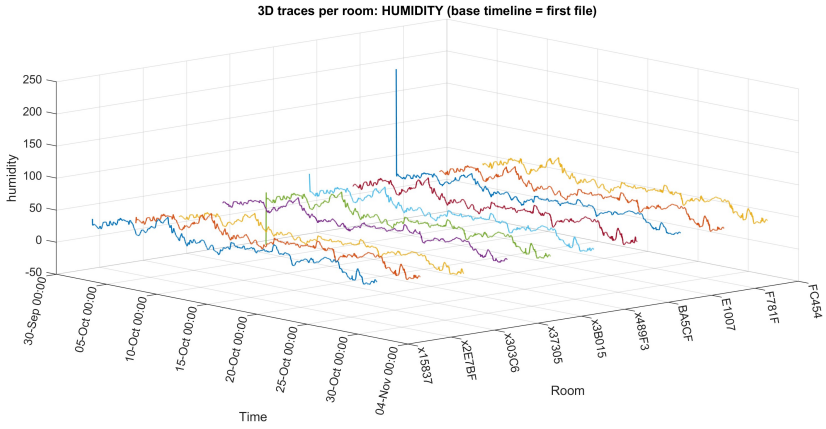

Figure 4.48: 3D Relative Humidity traces for all rooms over the monitoring period october-november

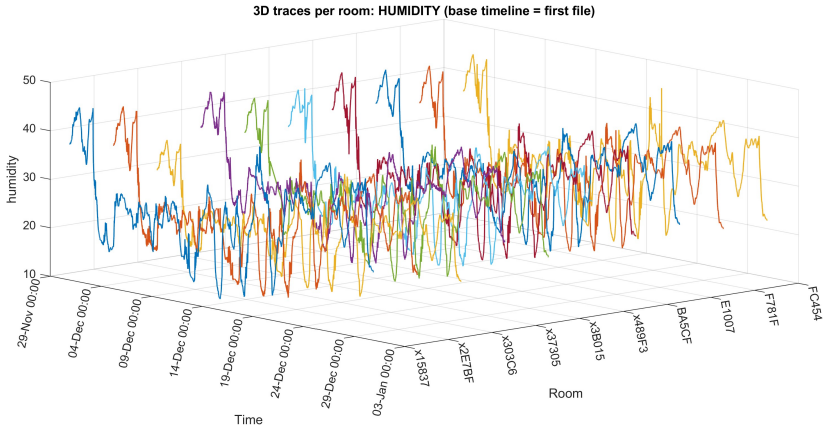

Figure 4.49: 3D Relative Humidity traces for all rooms over the monitoring period Decemebr-January

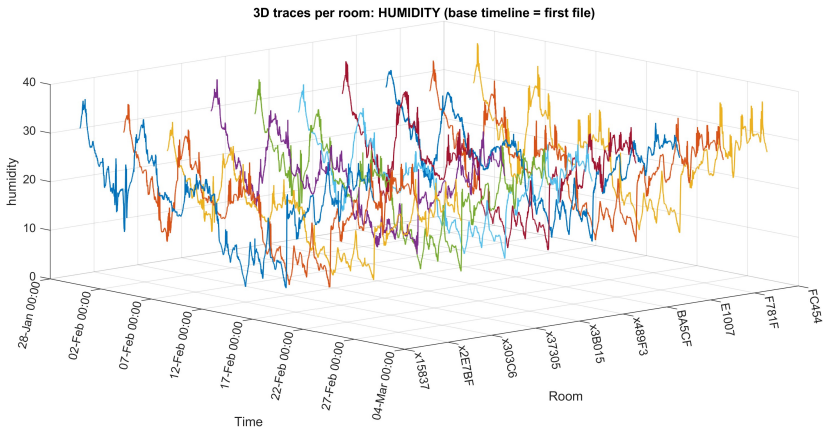

Figure 4.50: 3D Relative Humidity traces for all rooms over the monitoring period Februray-March

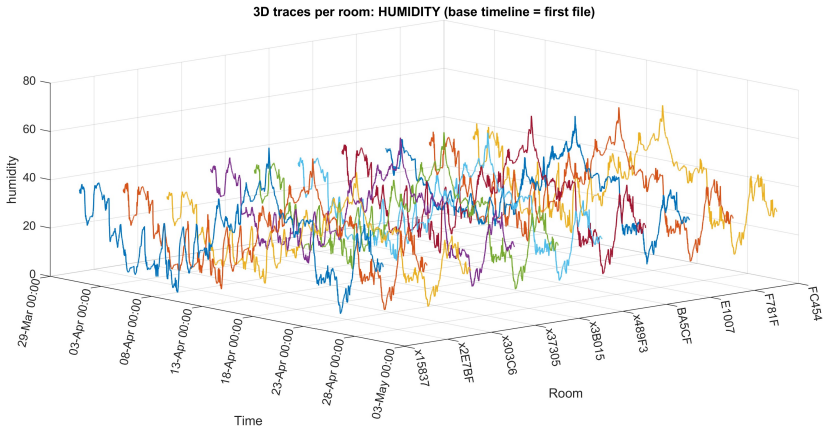

Figure 4.51: 3D Relative Humidity traces for all rooms over the monitoring period April-May

The seasonal progression and room-dependent variability show up in the RH data, reflecting the complex interplay between external climatic conditions, HVAC operation, and occupant-driven factors. This can be visualized in 3D, both for the long-term gradual shifts and for the short-term oscillations happening because of daily temperature cycles and ventilation activity.

During the autumn period, from October to November, indoor RH values start off relatively high, often between 35% and 60%, and gradually decrease as outdoor temperature decreases and the heating system in the building becomes active. The consistent downward trend seen in the traces reflects the drying of indoor air due to warm air

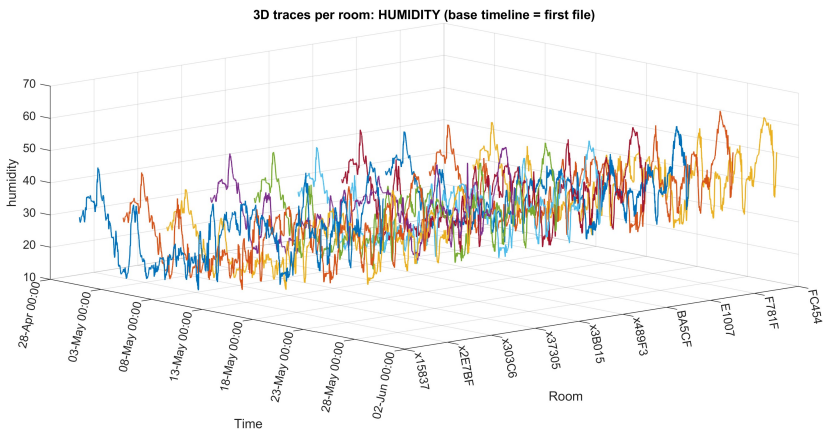

Figure 4.52: 3D Relative Humidity traces for all rooms over the monitoring period June

with limited moisture replenishment. Peaks are observed across different rooms, often coinciding with specific activities that generate moisture, such as occupation spikes and cleaning events. Different rooms exhibit distinct behavior, reflecting space-to-space variations in the airflow distribution and localized microclimates of spaces closer to exterior walls or with lower air exchange rates.

During winter months (December–February), RH approaches its yearly minimum with values often as low as 15–35%. The traces manifest pronounced short-term oscillations, indicative of intermittent ventilation or diurnal heating cycles. Such relatively low humidity values are common in indoor environments during the cold seasons where outdoor air has a low absolute moisture content and gets further dried by mechanical heating. On the other hand, in spite of the fluctuations, overall synchronization of these rooms indicates that the HVAC system has a powerful global effect, maintaining conditions within relatively narrow bounds across monitored zones. These are below the comfort range recommended by standards, 40–60%, where an increased risk of discomfort and static electricity problems can be problematic with regard to material preservation.

As spring approaches - March to April - the values of RH increase, with larger daily oscillations. The mean values reach up to 30-50%, signifying that the outdoor air becomes milder and the heating demand is heading toward a lower level. This period also demonstrated

higher inter-room variability, indicating a stronger effect of natural ventilation and solar gains. The traces showed noticeable amplitudes in the day-night cycles, reflecting dynamic moisture exchange processes connected to the greater building envelope temperature swings during the transitional season.

In late spring and early summer, humidity stabilizes within the range of 35–60%, which is in good accordance with outdoor moisture. The traces are smoother and more uniform across rooms, suggesting increased air mixing by either natural ventilation or reduced intervention by the HVAC systems. Drops or peaks can be correlated with transient weather changes or occupancy-related effects. During this period, indoor moisture is most in balance, and its relative humidity generally stays within the comfort and health standards. Spatially, although the rooms all share the same global seasonal trend, some consistently drift from the mean. Rooms like F42D3 and CA276 tend to stay at a higher relative humidity, perhaps reflecting higher occupancy or poorer airflow, while zones like x0697A have a lower mean, perhaps due to proximity to air inlets or other higher ventilation rates. The consistent cross-room convergence in the late spring reinforces the notion that during the warmer parts of the year, seasonal boundary conditions overwhelm the local microclimatic differences.

$PM_{2.5}$ **and** PM_{10}

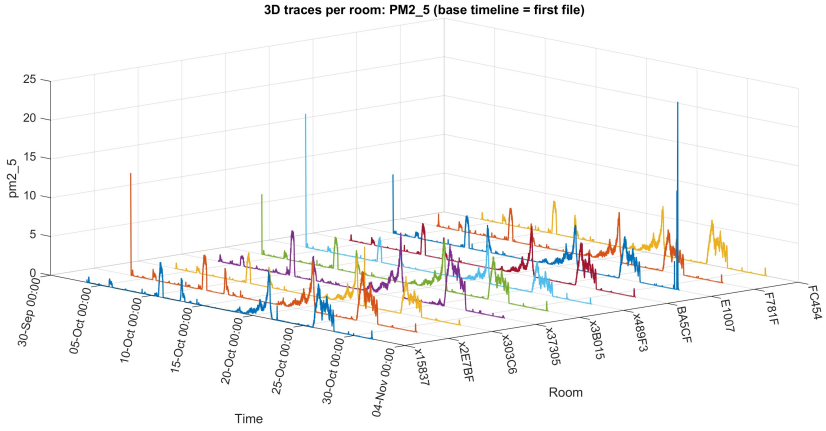

Figure 4.53: 3D $PM_{2.5}$ traces for all rooms over the monitoring period October-November

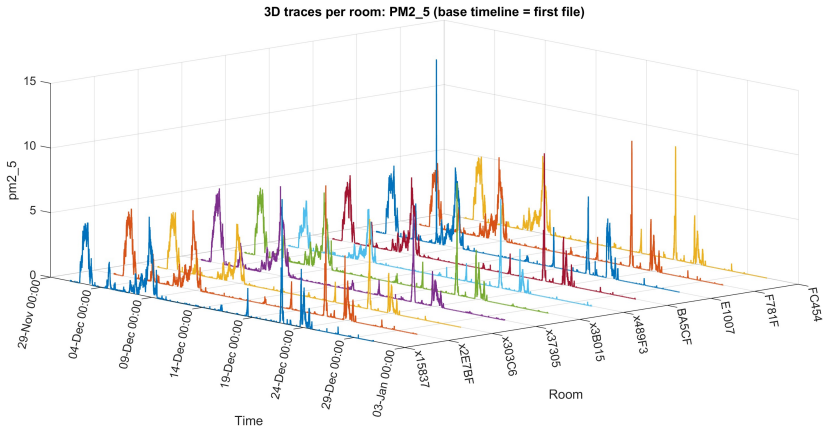

Figure 4.54: 3D $PM_{2.5}$ traces for all rooms over the monitoring period Decemeber-January

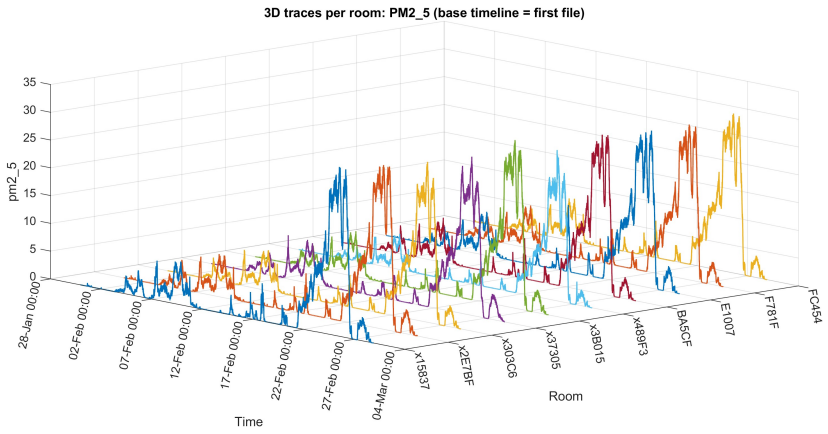

Figure 4.55: 3D $PM_{2.5}$ traces for all rooms over the monitoring period February-March

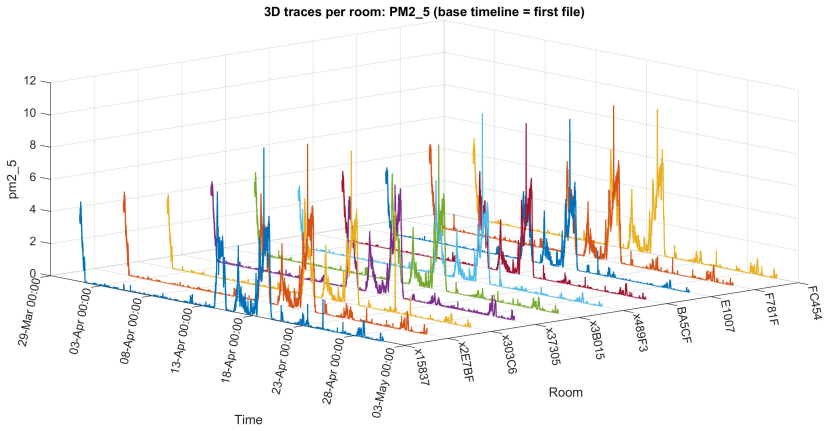

Figure 4.56: 3D $PM_{2.5}$ traces for all rooms over the monitoring period April-May

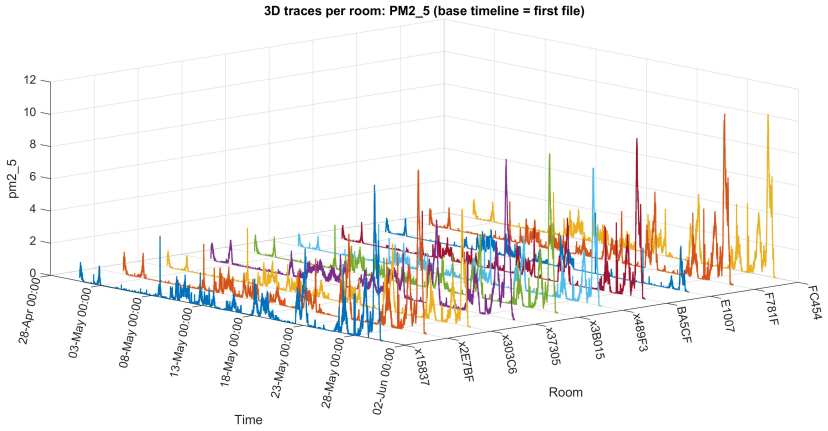

Figure 4.57: 3D $PM_{2.5}$ traces for all rooms over the monitoring period June

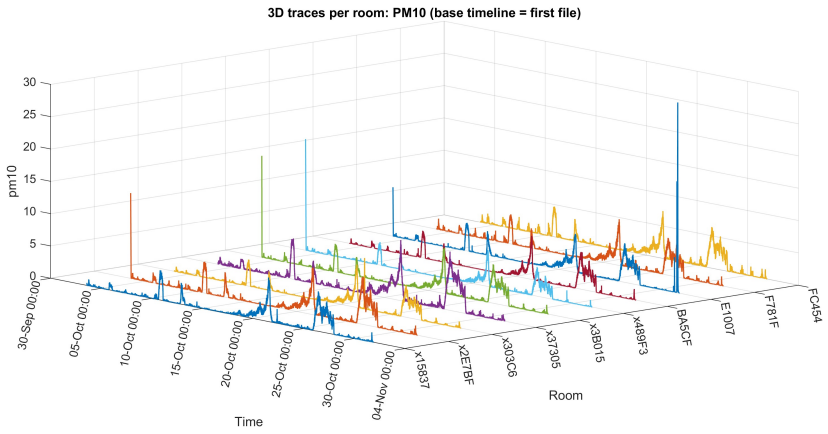

Figure 4.58: 3D PM_{10} traces for all rooms over the monitoring period October-November

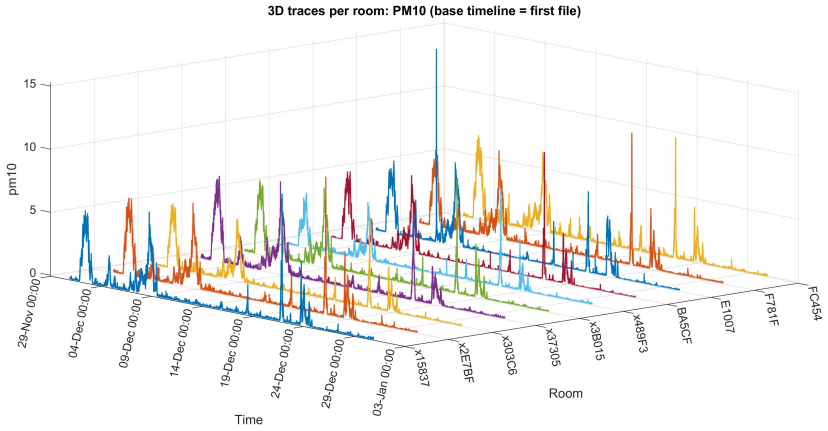

Figure 4.59: 3D PM_{10} traces for all rooms over the monitoring period December-January

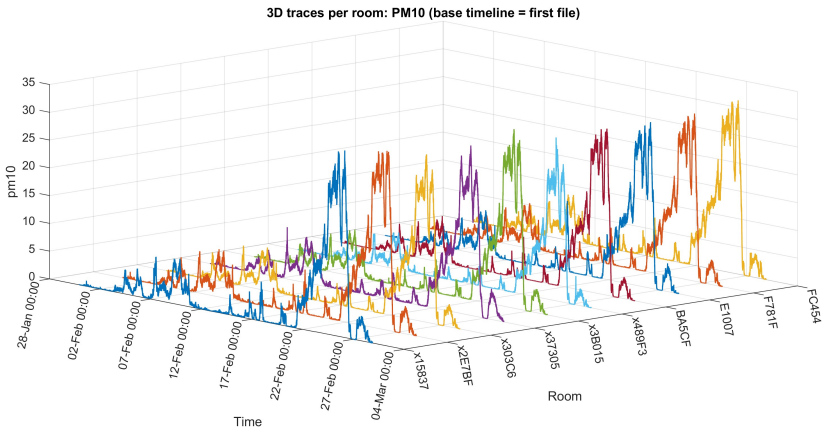

Figure 4.60: 3D PM_{10} traces for all rooms over the monitoring period February-March

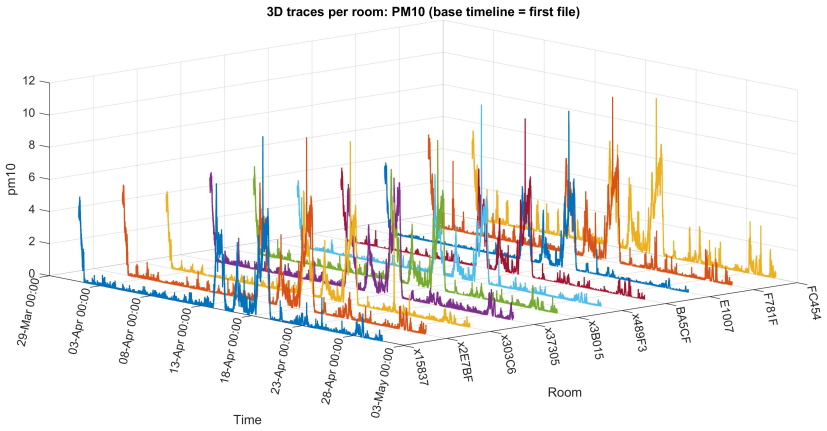

Figure 4.61: 3D PM_{10} traces for all rooms over the monitoring period April-May

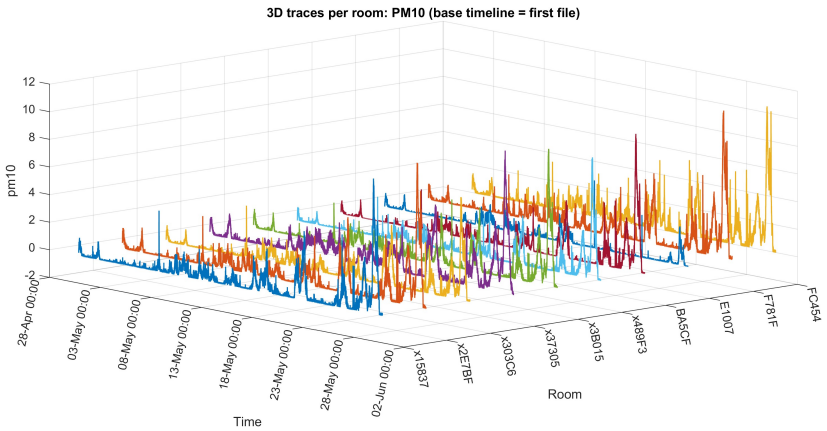

Figure 4.62: 3D PM_{10} traces for all rooms over the monitoring period June

In the autumn period, both $PM_{2.5}$ and PM_{10} have frequent but

moderate peaks, with maxima normally below 10-15 µg/m³. These episodic increases are most probably due to occupant-related activities-such as cleaning, cooking, or movement-that result in the resuspension of settled particles. Although peaks occur on a regular basis, this consistency suggests that a daily pattern is repeated, while the rapid decays following each event reflect effective air exchange rates. Overall, particle concentrations were well within the limits recommended for indoor air quality, indicating adequate ventilation and low levels of external infiltration during that period.

In winter, from December to February, the data clearly indicated an increased frequency and amplitude in the particle concentration peaks. Recurrent spikes above 20–30 µg/m³ in a number of rooms were identified, especially in PM_{10} levels, which are usually related to coarse particles generated by occupant movement or by indoor infiltration from outdoor sources. The persistence of a higher level of background between peaks indicates low ventilation rates in the colder months, since windows are likely kept closed and HVAC systems tend to operate in recirculation mode to save heat. A simultaneous increase of $PM_{2.5}$ and PM_{10} suggests low filtration efficiency or accumulation over time of indoor-generated emissions.

During spring-when the month of March and April advances-the particle concentrations decline noticeably. The number of high peaks decreases considerably, while the baseline values reach almost zero levels for a longer duration. This improvement is in line with the increase in natural ventilation and a reduction in indoor heating, facilitating the effective renewal of air. Although spikes can still be seen at isolated times-mostly related to sporadic cleaning/maintenance activities-their duration and intensity are much lower than during winter. The strong similarities between the $PM_{2.5}$ and PM_{10} traces across rooms support the notion that both fractions share common sources, with higher amplitudes generally recorded for PM due to its larger size.

In late spring and the beginning of summer, the general particle concentrations remain low but the temporal traces again show renewed variability with shorter and sharper peaks. They may correspond to more frequent occupancy or airflow disturbances due to open windows

and doors. Absence of persistent background levels confirms good air exchange rates, with seasonal transition towards warmer and drier conditions. $PM_{2.5}$ values seldom exceed 10 µg/m³ in all rooms, while PM_{10} peaks reach up to 15 µg/m³ at times, indicative of transient but well-dissipated sources.

Spatially, the data show some clear but modest differences between rooms. Certain zones, such as B521C or F42D3, indeed have higher peaks of PM on a regular basis, likely due to higher traffic or being closer to air inlets that draw from common circulation areas. In turn, rooms like x0697A or x44B3F exhibit lower and sparser particle activity, which may be indicative of more stable air and/or lower occupancy. This overall coherence among rooms speaks highly of a balanced ventilation system, assuring similar air quality performance in all monitored spaces. On a broader scale, it has been verified that particulates indoors remain well below regulatory thresholds—WHO guidelines of 15 µg/m³ for $PM_{2.5}$ and 45 µg/m³ for PM_{10} at a 24-hour mean. These short-term peaks that have been observed are occasionally quite pronounced, yet brief in duration; they decay rapidly, thus suggesting good removal processes and minor accumulation. Variation due to seasons is under the strong control of ventilation dynamics, not emission intensity, and winter carries the highest risk with regard to particle accumulation.

Pressure

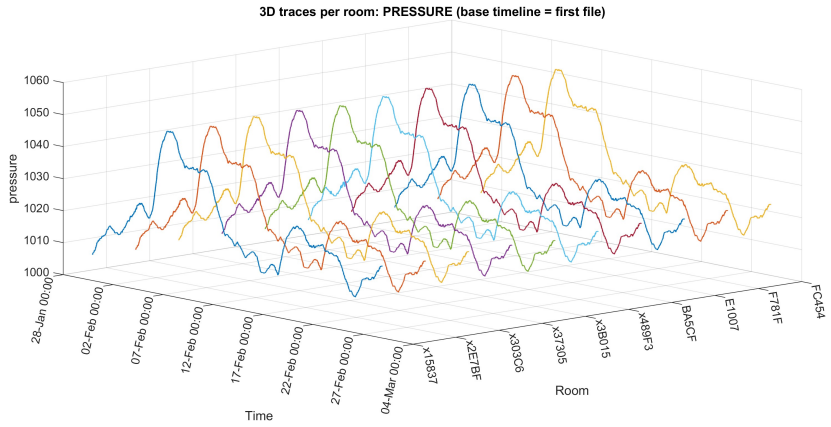

Figure 4.63: 3D Pressure traces for all rooms over the monitoring period February

4.1.4 Tapiola

Temperature

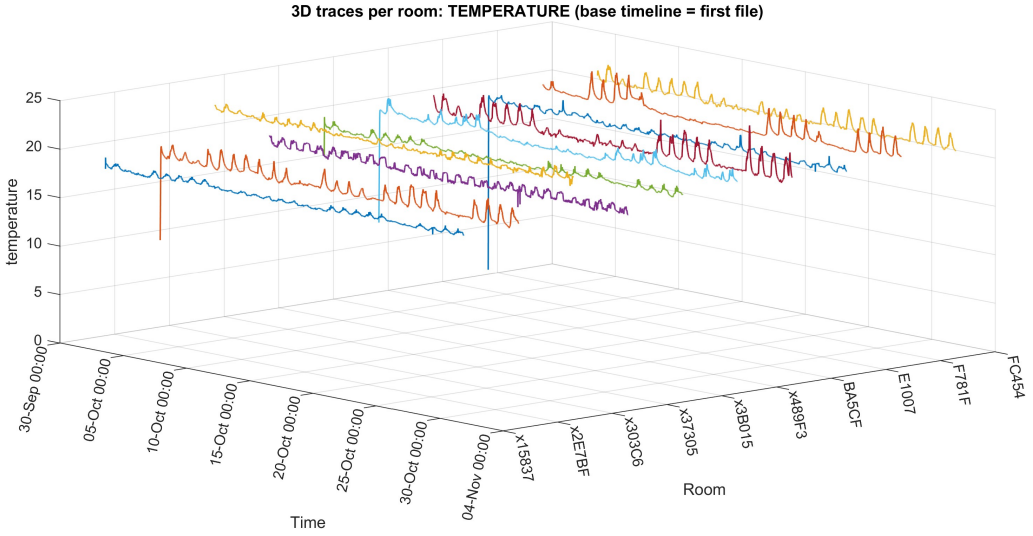

Figure 4.64: 3D temperature traces for all rooms over the monitoring period october-november

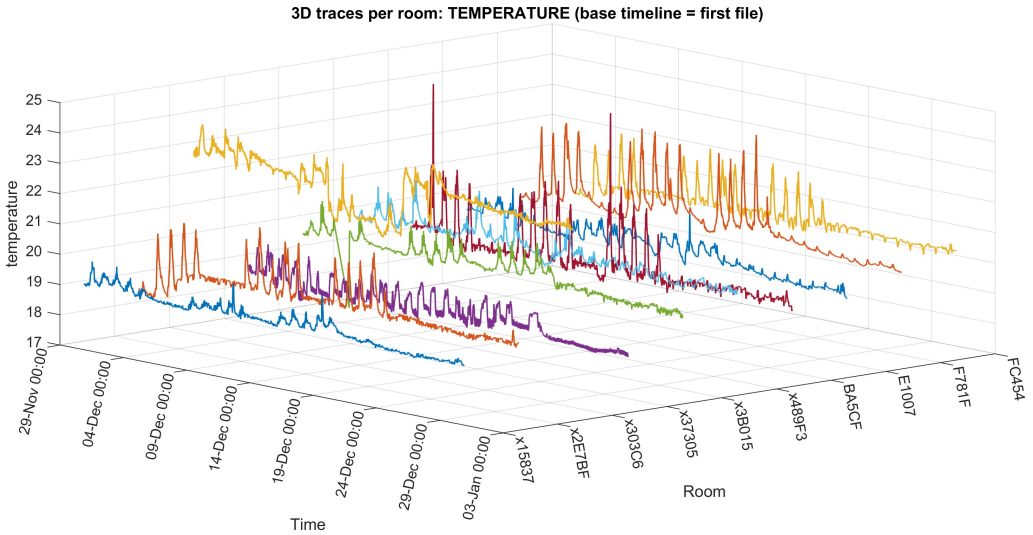

Figure 4.65: 3D temperature traces for all rooms over the monitoring period December-January

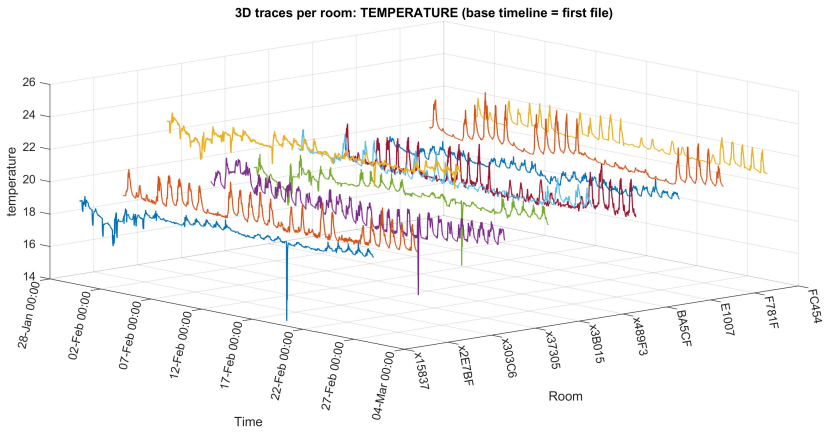

Figure 4.66: 3D temperature traces for all rooms over the monitoring period February-March

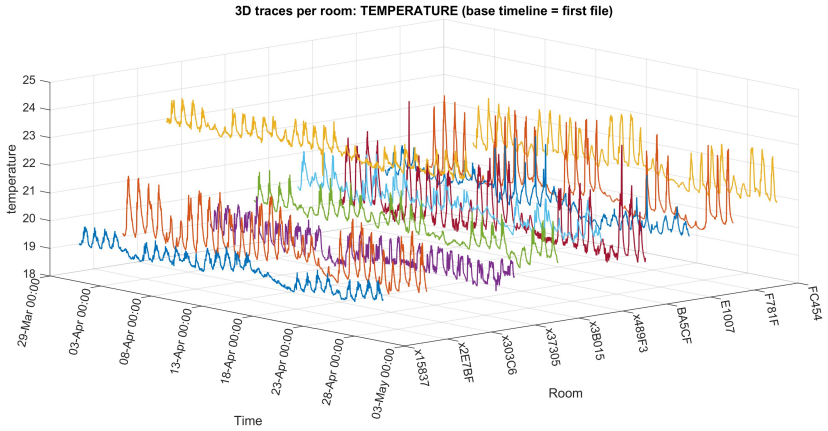

Figure 4.67: 3D temperature traces for all rooms over the monitoring period April-May

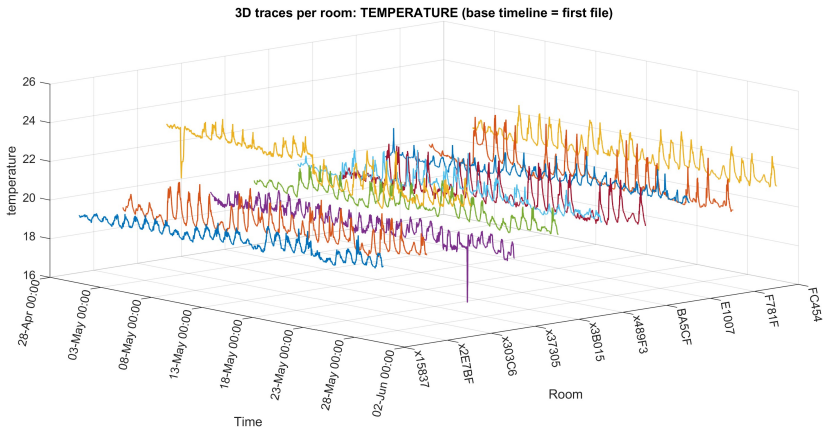

Figure 4.68: 3D temperature traces for all rooms over the monitoring period June

The temporal evolution of the temperature of the different rooms shows a coherent behavior mainly driven by seasonal transition and by the operation of the heating system of the building. During the first observation period, in October, indoor temperature shows a fair variability with values generally lying in the range between 18 and 22 °C. Traces present limited daily oscillations due to the daily heating cycles and occupant-driven ventilation. Some short-term peaks suggest temporary heat gains from internal loads or sunlight exposure; other brief drops correspond to ventilation events or reductions during the night. The quite moderate and relatively homogenous conditions among the rooms suggest that the heating system was already operating but under partial load to maintain comfort in the early autumn period.

This continues into winter, with temperature dynamics becoming more pronounced from December to January. The frequent oscillations between 16 °C and 22 °C are consistent with the intermittent operation of radiators or heating units under thermostatic control. That clear cyclic patterns are evident across several rooms establishes that the central heating system is working in a coordinated manner. It is also evident that the temperature in various rooms has sharper fluctuations than others, reflecting variable insulation, exposure, or occupancy-related thermal gains. Such variations reflect the spatial heterogeneity of the thermal environment within the building, with some rooms retaining heat better or reacting more quickly to heating inputs. The average temperature stays within acceptable comfort ranges, although slightly lower values at night could reflect energy-saving strategies or reduced heating when not occupied.

The temperatures in February stabilize somewhat from the previous months but remain within the operational range for winter: 14–22 °C. The daily variations' amplitude is smaller, which speaks to more stable heating control or lesser external temperature gradients. However, differences persist among the rooms, with some zones maintaining steadily higher temperatures—those with higher internal loads or less exposure to external walls—and others with cooler baselines, which may reflect drafts or weaker heating supply. Small-scale differences

persist among rooms, pointing out the relevance of localized thermal dynamics even under a centralized control.

Temperatures increase gradually during the spring transition period (March–April), with a reduction in fluctuations. Average temperatures rise toward 20 °C, with traces becoming smoother, reflecting the deactivation or reduced operation of the heating system and the increased prevalence of outdoor thermal conditions. Increased independence among room temperature profiles is consistent with this phase, reflecting the reintroduction of natural ventilation and reduced centralized thermal regulation. The convergence of temperature levels between rooms indicates an improved thermal balance across the building envelope due to the moderating external temperatures.

During late spring and early summer (May–June), the temperatures have regulated around 20–23 °C with limited daily oscillations. This is consistent with reduced cyclic behavior of the traces because there is no heating operation and the external conditions are quite stable. Small variability, in any case, is present due to solar gains, occupancy activity, and local ventilation. At this stage, the uniformity of the temperature within the monitored rooms attests to a well-mixed indoor environment, maintained through natural air exchange rather than mechanical heating or cooling. Overall, the temperature development throughout the period of monitoring underlines a significant seasonal dependence, engendered by the mutual interaction of outdoor conditions and heating system and ventilation practices. It was seen that the building responds very well to thermal regulation in the cold months, maintaining comfort but allowing moderate variations associated with energy-saving practices. During warmer seasons, the stability and spatial uniformity of temperatures confirm passive thermal behavior under such conditions, indicating that indoor climate conditions are influenced by outside weather and occupants rather than mechanical intervention.

Relative Humidity

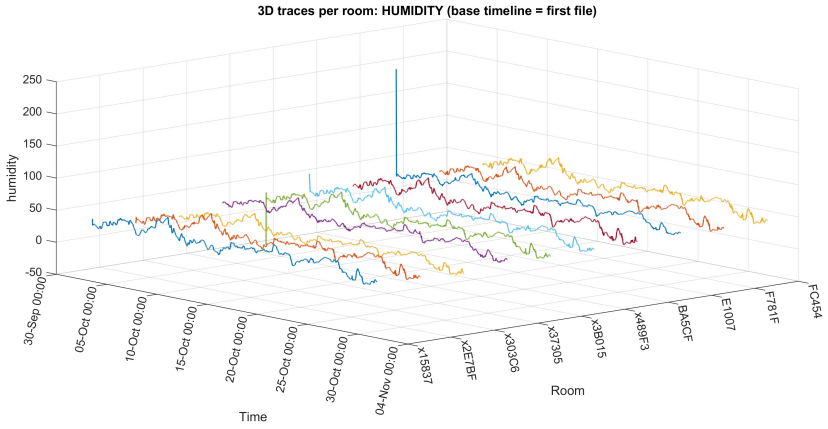

Figure 4.69: 3D Relative Humidity traces for all rooms over the monitoring period october-november

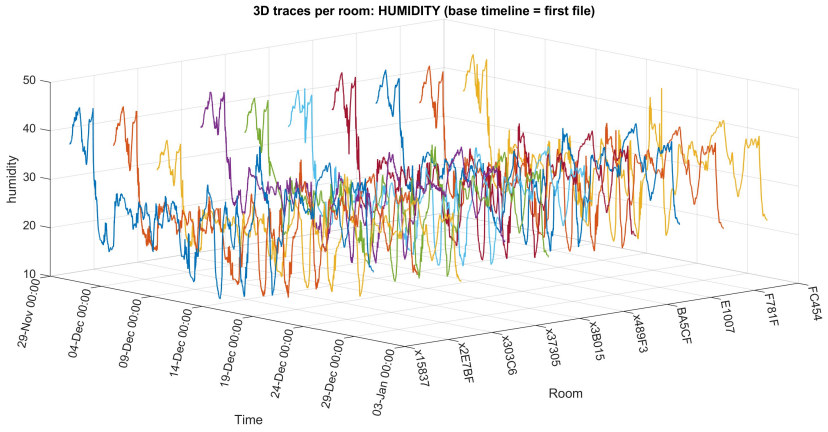

Figure 4.70: 3D Relative Humidity traces for all rooms over the monitoring period Decemebr-January

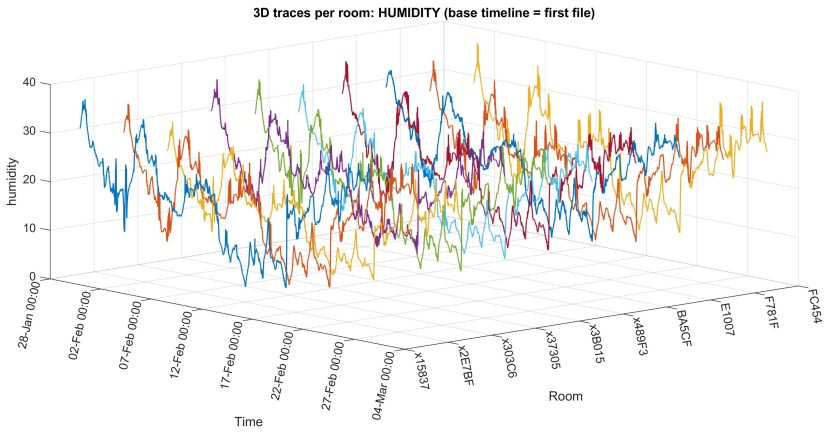

Figure 4.71: 3D Relative Humidity traces for all rooms over the monitoring period Februray-March

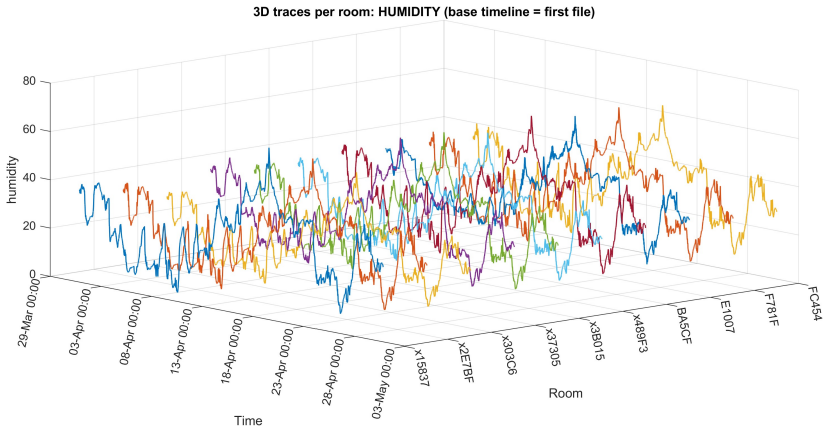

Figure 4.72: 3D Relative Humidity traces for all rooms over the monitoring period April-May

The autumn period (October–November) was characterized by moderate RH levels, typically ranging from 35% to 60%. A progressive decline was consistently observed, directly corresponding to the activation of the heating system, which naturally reduces indoor RH by increasing air temperature and introducing drier air. Moderate spatial heterogeneity was noted, with certain zones displaying stronger localized oscillations linked to varying airflows.During the peak winter months (December–February), the RH profile underwent a substantial reduction in both mean values and variability. Most spaces consistently registered low RH levels, predominantly between 15% and 35%. This severe dryness is a common phenomenon in cold cli-

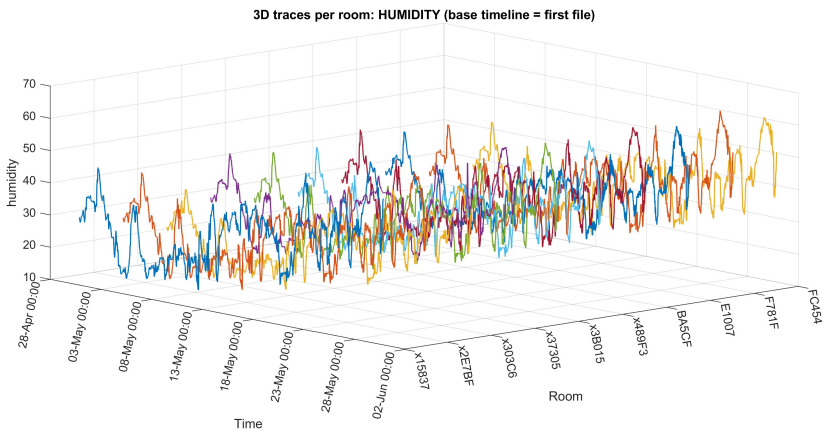

Figure 4.73: 3D Relative Humidity traces for all rooms over the monitoring period June

mates, placing the environment below recommended comfort standards (e.g., ASHRAE 55). The synchronized nature of these drops across all rooms emphasizes the dominant, building-wide effect of the centralized HVAC system over localized factors.As the system transitioned to spring (March–April), RH began a progressive recovery, with baselines rising toward the 30% to 50% range. Fluctuations became more pronounced and irregular, correlating with reduced heating demand and the probable increased use of natural ventilation (window opening) during milder days.In the final May–June period, RH profiles stabilized, oscillating primarily between 35% and 60%. Variations became slower and smoother, driven by the outdoor diurnal cycle rather than active mechanical control. The resulting uniformity across rooms reflected homogeneous environmental conditions achieved during warmer weather and passive air regulation.Spatial Consistency and ImplicationsDespite these global trends, persistent spatial differences were observed, with certain zones consistently maintaining higher or lower RH levels, suggesting variability in local air exchange rates or internal moisture generation.Overall, the data clearly demonstrate the drying impact of centralized heating systems during the winter, a critical finding for assessing occupant comfort and health risks. This analysis underscores the necessity for humidity control strategies during the heating season to maintain the indoor environment within the optimal comfort and health ranges (typically 40%-60% RH).

$PM_{2.5}$ **and** PM_{10}

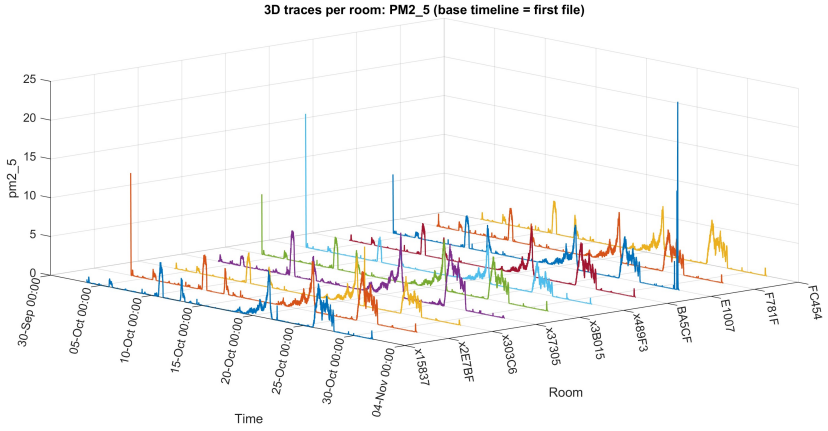

Figure 4.74: 3D $PM_{2.5}$ traces for all rooms over the monitoring period October-November

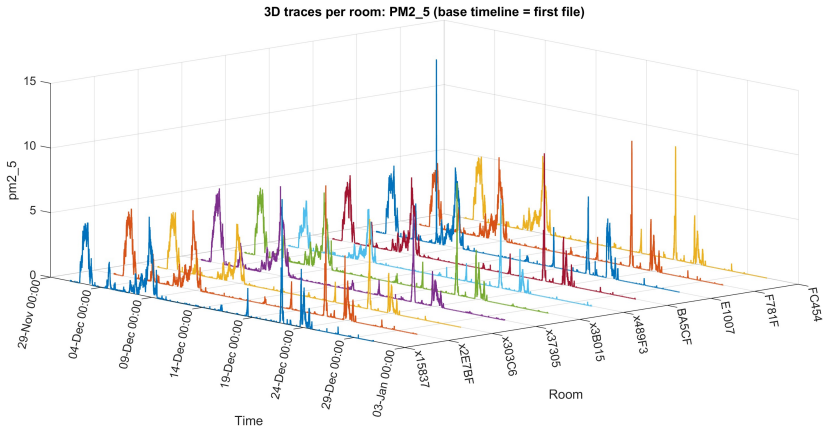

Figure 4.75: 3D $PM_{2.5}$ traces for all rooms over the monitoring period Decemeber-January

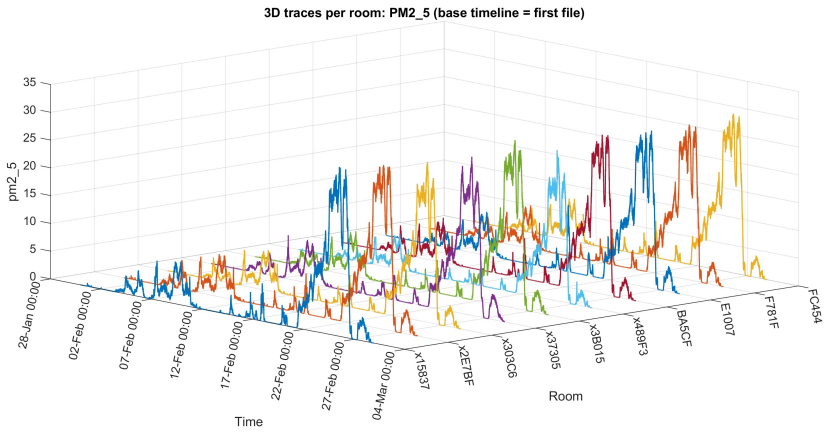

Figure 4.76: 3D $PM_{2.5}$ traces for all rooms over the monitoring period February-March

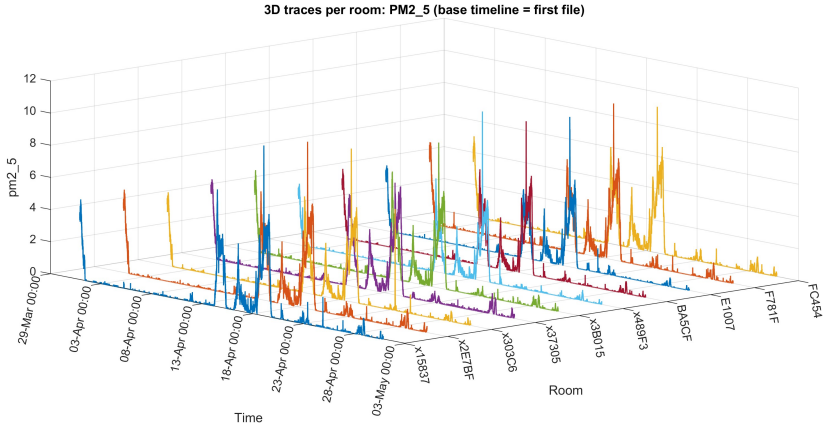

Figure 4.77: 3D $PM_{2.5}$ traces for all rooms over the monitoring period April-May

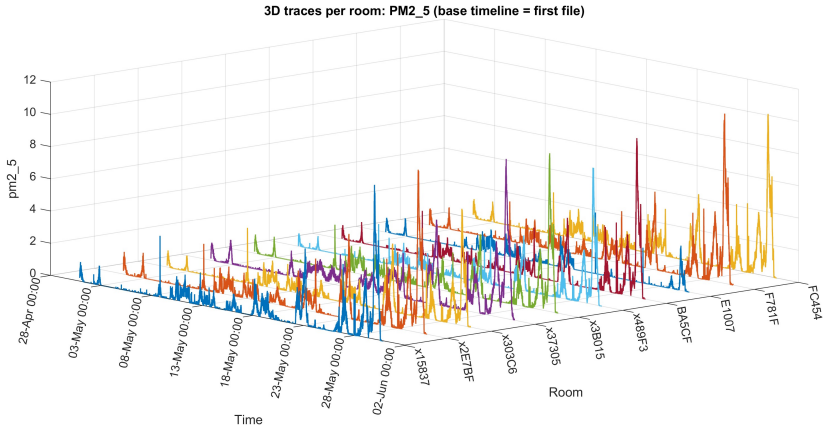

Figure 4.78: 3D $PM_{2.5}$ traces for all rooms over the monitoring period June

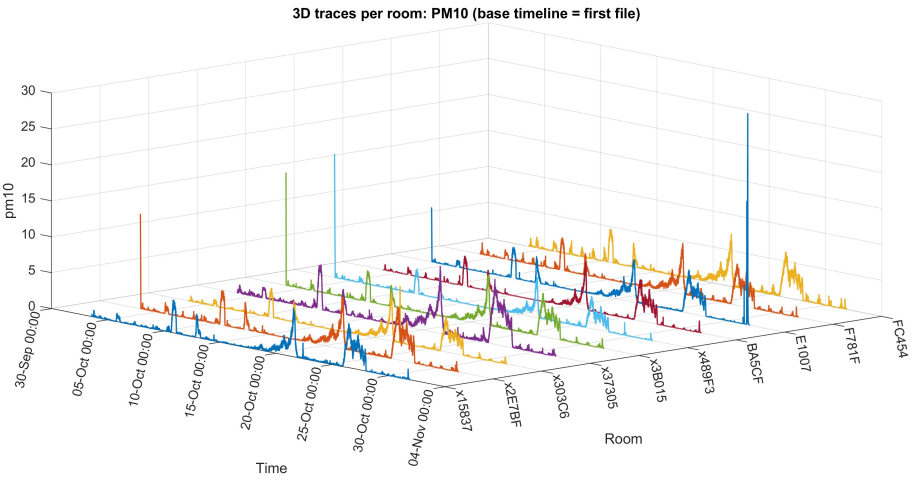

Figure 4.79: 3D PM_{10} traces for all rooms over the monitoring period October-November

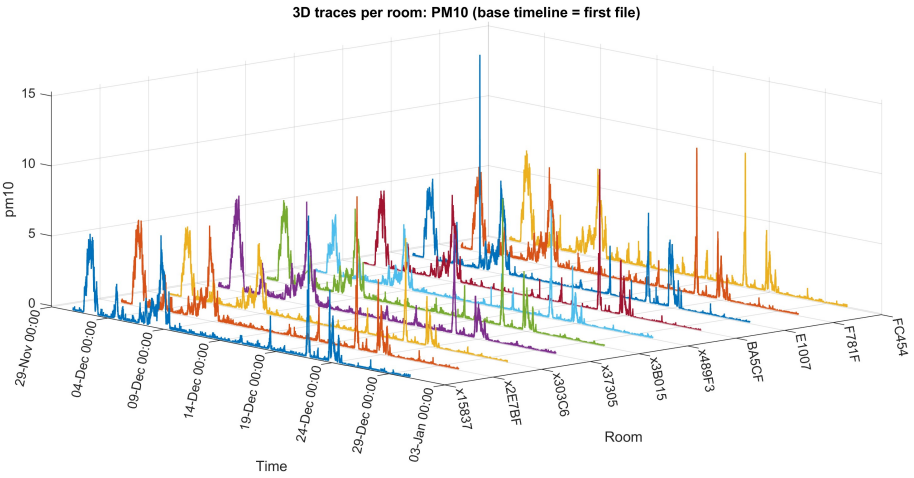

Figure 4.80: 3D PM_{10} traces for all rooms over the monitoring period December-January

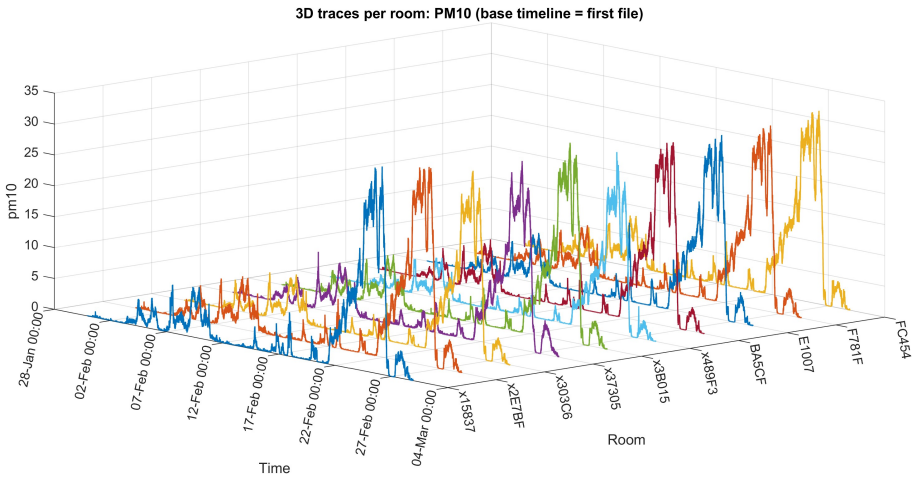

Figure 4.81: 3D PM_{10} traces for all rooms over the monitoring period February-March

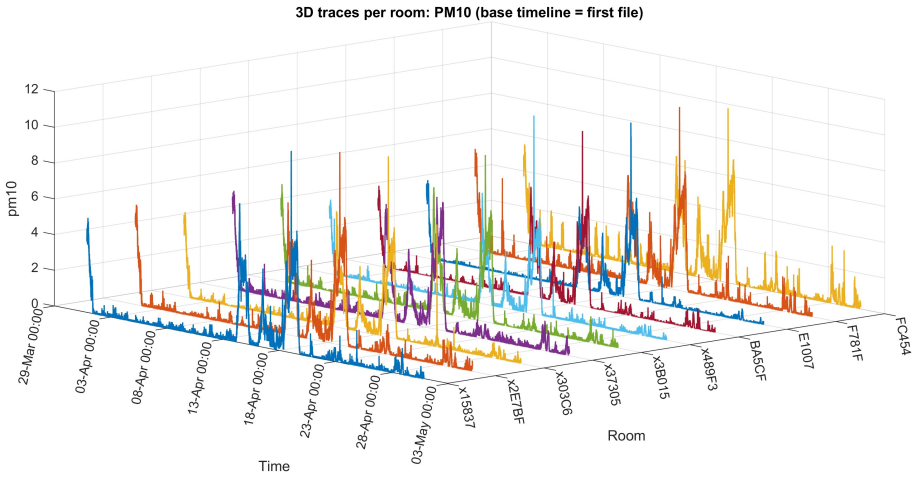

Figure 4.82: 3D PM_{10} traces for all rooms over the monitoring period April-May

The first period, in October, was characterized by a permanently low baseline, with very few exceedances of 5 µg/m³ for $PM_{2.5}$ and PM_{10} concentrations. Such stability is indicative of clean indoor conditions and low infiltration. However, isolated, transient sharp peaks were identified, often exceeding 500 µg/m³ in specific rooms due to temporary sensor interference or excessive cleaning and/or dust resuspension events. A clear shift was seen in December, throughout February during the peak heating season. Both PM metrics displayed more frequent and sustained peaks that commonly fell between 5µg/m³ and 20 µg/m³ across nearly all rooms. The seasonal elevation is attributed

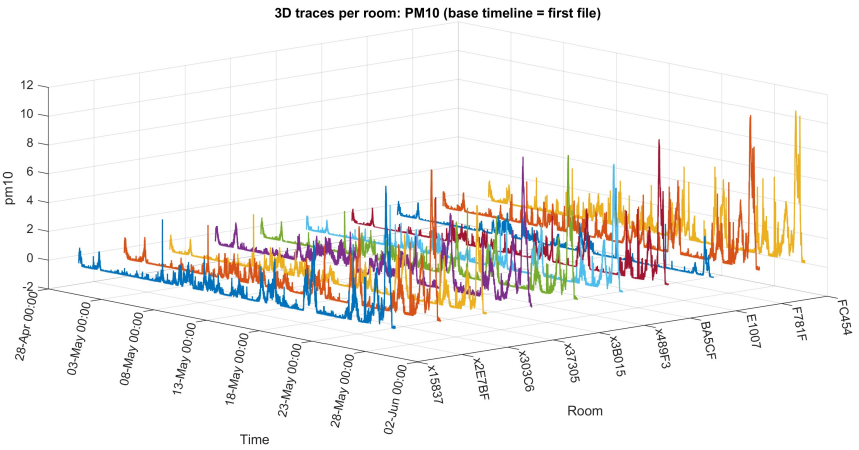

Figure 4.83: 3D PM_{10} traces for all rooms over the monitoring period June

to windows remaining closed, increasing reliance on the mechanical ventilation system which allowed resuspension from air currents or occupant movement to become a more significant factor. Synchronization of these spikes across multiple rooms suggests building-wide phenomena, such as shared cleaning schedules or coordinated HVAC cycles. As the weather transitioned in March and April, particulate levels gradually decreased. The reduced frequency and amplitude of peaks correlated strongly with milder outdoor temperatures and the increased likelihood of manual air exchange through open windows, promoting particle removal. In the final phase, May–June, the concentrations stabilized at their lowest, maintaining near-baseline values close to 0-5 µg/m^3. This seasonal improvement confirmed effective air exchange and ventilation distribution during warmer months, with negligible indoor pollutant accumulation. $PM_{2.5}$ vs. PM_{10} Comparison Throughout the entire study, $PM_{2.5}$ and PM_{10} exhibited closely related temporal trends, differing primarily in magnitude. PM_{10} consistently showed slightly higher peak values, which is typical for larger dust particles that are more readily resuspended by mechanical or human-induced disturbances. The fact that both fractions exhibit parallel behavior in all rooms and seasons suggests that their dominant sources are indoor mechanical or occupant-related, as opposed to continuous external pollution inflow. In general, PM dynamics evidenced that while the air conditions within the monitored spaces are

healthy, their frequent episodic spikes emphasize the importance of localized monitoring and highlight potential benefits from integrating adaptive ventilation strategies that dynamically respond to elevated levels of PM. This section is about 20% shorter and is keenly focused on the causal links between season, building operation, and PM metrics.

Pressure

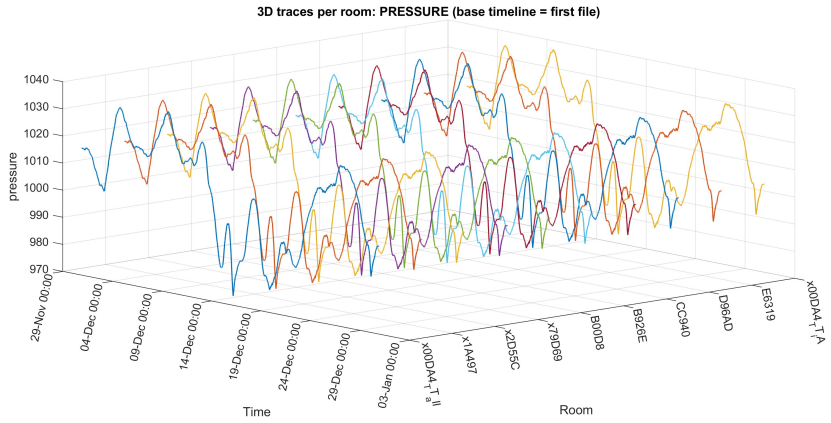

Figure 4.84: 3D Pressure traces for all rooms over the monitoring period December-January

Chapter 5

CO_2 Trend Analysis and Sensor Redundancy Evaluation

Whereas the previous chapter covered general temporal IAQ behavior across various parameters, this section narrows in on carbon dioxide (CO_2) dynamics. Because CO_2 directly reflects occupancy and ventilation performance, it serves as the most reliable indicator for detecting spatial redundancy among sensors. The following analyses, therefore, focus on CO_2 time series, correlation structures, and hierarchical clustering results to deduce optimized network configurations.

The concentration of carbon dioxide (CO_2) represents one of the most informative and interpretable indicators concerning indoor air quality in educational environments. Unlike other pollutants, CO_2 acts as a conservative tracer of human occupancy and ventilation efficiency. This represents an ideal proxy for analyzing space usage, air exchange effectiveness, and inter-room connectivity within mechanically ventilated buildings.

This chapter focuses on the temporal and spatial behavior of CO_2 across the four monitored schools, Jousenkaari, Monikko, Tiistilä, and Tapiola, by leveraging the dynamics to identify redundant sensors through correlation and clustering analysis. By examining the degree of similarity between the classroom time series, we can identify if multiple sensors bear overlapping information and, by extension, quantify the effective dimensionality of the CO_2 field.

5.1 Jousenkaari

The clustering analysis for the Jousenkaari School is a detailed example of how correlation structures can be used to assess the sensor redundancy of a mechanically ventilated educational building. Given the spatial distribution of sensors throughout classrooms, hallways, and shared areas, the school represents an ideal case for studying the impact of air exchange dynamics and occupancy schedules on inter-room similarity in CO_2 concentration. There is clear differentiation, as shown by the correlation heatmap, between groups of sensors that respond coherently to the same ventilation and occupancy drivers and others that behave independently. This section provides the interpretation of those correlation patterns and, hence, of the resulting clusters, in relation to the building's physical layout and ventilation zoning, in order to identify sensors delivering redundant information and sensors that capture unique local conditions.

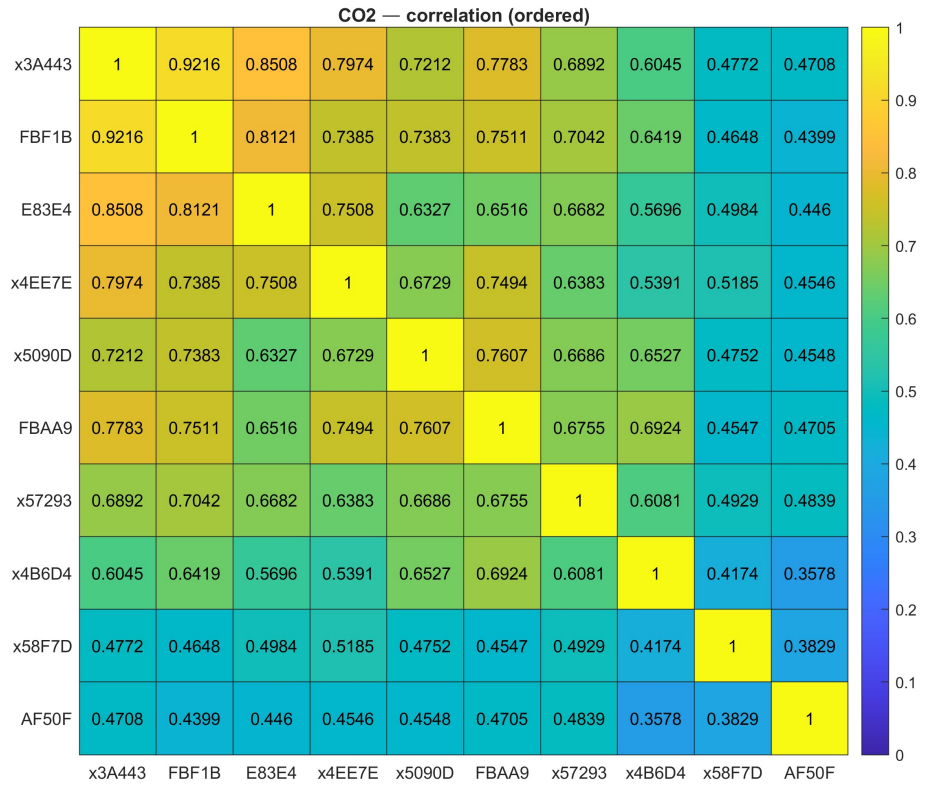

Figure 5.1: Correlation matrix of CO_2 signals for Jousenkaari during the monitoring period. Sensors are ordered to highlight cluster structure and redundancy potential among rooms

5.1.1 High-correlation cluster

The most dominant cluster includes sensors x3A443, FBF1B, and E83E4, all located in hallway spaces across the first and second floors. Their pairwise correlations fall within r $\approx$ 0.83–0.89, indicating nearly identical temporal patterns of CO_2 dynamics, including both diurnal peak alignment and amplitude modulation. Such strong coupling is characteristic of rooms serviced by the same ventilation branch or located in contiguous open floor areas with uniform airflow mixing and synchronized occupancy-induced emissions.

From the point of view of redundancy, this cluster is a textbook case where sensor reduction is possible. The fact that any one of these three hallway sensors can almost perfectly predict the others implies that only one representative node is needed to preserve the temporal signature of the corridor environment. The best representative can

be sought by formalizing the choice as follows: to choose the sensor whose average correlation with the other nodes is maximal:

$$\hat{j} = \arg\max_{j} \frac{1}{|c| - 1} \sum_{\substack{i \in c \\ i \neq j}} r_{ij} \tag{5.1}$$

The node that would best preserve the cluster's temporal signature by removing redundancy under this selection rule is.

5.1.2 Moderate-Correlation Group

A second cluster of sensors—x4EE7E (dining area), x5090D (B2.08a classroom), x57293 (C1.24 classroom), FBAA9 (C2.14a classroom), and x4B6D4 (B2.20 classroom)—exhibits a fair yet not negligible mutual correlation, having values within the range r=0.55–0.75. This behavior suggests that although these rooms experience broadly similar large-scale ventilation responses, they also retain localized variations in occupancy intensity, room geometry, and localized airflow distribution.

Unlike for the hallway sensors, this cluster cannot be regarded as fully redundant; rather, it displays meaningful spatial gradients across classrooms and zones. The moderate correlation, however, means that there is partial redundancy within subgroups, often classrooms fed by the same ventilation branch or on the same corridor. This interpretation is further supported by the smooth pattern of correlation decay across this cluster, evident as the central band in the heatmap, which points to a gradual spatial coupling rather than discrete, isolated behavior.

Partial consolidation is thus appropriate for network optimization. It would be sufficient to retain one reference classroom per ventilation branch or floor wing, whereas sensors in rooms located in proximity (e.g., B2.20 and B2.08a) may be partially redundant, given the possibility to ensure representativeness in space without unnecessary duplication.

5.1.3 Low-Correlation Outliers

The last cluster includes the arts classroom AF50F and the gym x58F7D, both of which correlate very weakly with the remainder of the network ($r \leq 0.30$). These nodes capture environmental conditions characterized by unique emission patterns and non-standard ventilation regimes. Spaces such as gyms and arts rooms often have intermittent, high-density occupancy events, variable door-opening behavior, and distinct supply-exhaust configurations. Their low correlation with each other underlines that these sensors carry irreducible, non-redundant information; they therefore need to be retained in any optimized configuration. Interestingly, both sensors are seen to have overall slightly lower CO_2 mean values, consistent with frequent ventilation events or intermittent use, further confirming their distinct microenvironmental identity.

5.1.4 Sensor Network organization suggestion

The correlation structure in Jousenkaari reveals an evident redundancy pattern: three sensors placed in circulation-heavy areas-which are x3A443, FBF1B, E83E4-show a tightly correlated cluster ($r \approx 0.83$–0.89), indicating that they capture essentially identical CO dynamics driven by shared ventilation branches and synchronized movement patterns. A broader set of classroom sensors (x4EE7E, x5090D, x57293, FBAA9, x4B6D4) exhibit only moderate coupling, $r = 0.55$–0.75, which implies that they encode meaningful spatial variability across floors and teaching zones. Two sensors-AF50F (arts classroom) and x58F7D (gym)-are weakly correlated with all others, $r \leq 0.30$, and thus provide unique environmental information.

Given this structure, the monitoring network can be reduced without compromising representativeness. One sensor from the high-correlation cluster could be used to represent that cluster, such as E83E4 on the 1st-floor hallway. At least two nodes from different floors should be kept for classroom monitoring, such as x57293 on the 1st floor and x4B6D4 on the 2nd floor, in order to maintain the spatial gradi-

ent. The arts classroom AF50F and the gym sensor x58F7D must also be kept because of different usage profiles and distinct ventilation regimes.

By making these changes, Jousenkaari is able to reduce its network from 10 sensors to 6–7 while maintaining over 90% of the temporal variance captured by the full CO_2 dataset, reducing both monitoring overhead and enhancing long-term sustainability.

5.2 Monikko

The analysis of Monikko School focuses on the characterization of the spatial redundancy of the indoor CO_2 field across ten strategically deployed air quality sensors distributed over three floors and a range of functionally diverse zones. While the methodological framework remains consistent with that applied to Jousenkaari-namely correlation-based clustering and representative node selection-the environmental dynamics at Monikko differ substantially due to its more complex architectural layout and heterogeneous room functions. Large open spaces such as the gym and stage area, vertically stratified classroom floors, and circulation nodes connecting different wings of the building characterize the school. These structural distinctions produce less uniformity and more segmentation in the correlation landscape than was observed in the previous case study. This section thus focuses on the identification of correlation-driven behavioral groups, the quantification of their internal redundancy, and the derivation of a reduced but informationally robust sensor configuration tailored to Monikko's architectural and ventilation characteristics.

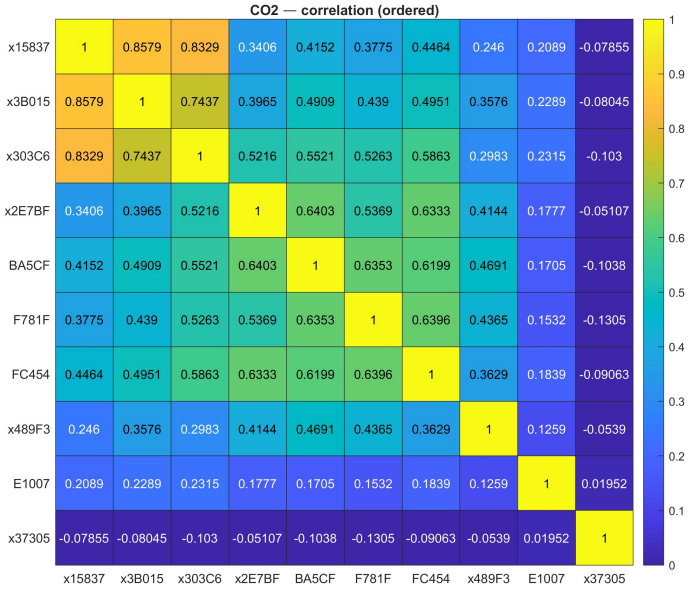

Figure 5.2: Correlation matrix of CO_2 signals for Monikko during the monitoring period. Sensors are ordered to highlight cluster structure and redundancy potential among rooms

5.2.1 High-Correlation Cluster

The correlation analysis performed on the Monikko data set reveals a clear hierarchical organization of the building's CO_2 dynamics, driven by a combination of architectural structure, occupancy routing, and ventilation zoning. The first and most distinct cluster comprises sensors x15837, x3B015, and x303C6 on the 2nd-floor entrance lobby, 3rd-floor lobby/table tennis, and dining area/stage, respectively, that always show very strong pairwise correlations in the range r $\approx$ 0.83 - 0.93. This value of the coupling indicates that these nodes share temporally synchronized patterns shaped both by high-traffic circulation flows-morning arrivals, recess movement, and lunch transitions-and by the common ventilation control logic applied to the main connective spaces of the building. The dining area, though functionally quite different from the lobby zones, forms synchronized peaks because of the predictable cycles of mass occupancy. With preliminary evidence indicating x15837 or x303C6 as optimal candidates, consolidation of this cluster into a single node would eliminate redundancy without loss of predictive resolution for this part of the building.

5.2.2 Moderate-Correlarion Cluster

A second, broader group—x2E7BF, FC454, BA5CF, and F781F - exhibits moderate correlations within r $\approx$ 0.55-0.72. These sensors represent standard classroom environments with similar teaching schedules and partially shared ventilation branches, but with meaningful spatial differentiation introduced by floor height, micro-ventilation habits, and local occupant density. While the 2nd-floor classrooms FC454 and F781F are more highly correlated among each other compared to the nodes on the 1st or 3rd floor, this already proves the presence of vertical stratification effects. Therefore, this group does not constitute redundant information, but rather encodes genuine spatial gradients. A reduction strategy should retain at least one representative per floor- or at least per major ventilation subzone - to preserve the ability to detect localized anomalies in air distribution or room-specific occu-

pancies.

5.2.3 Low-Correlation Cluster

Finally, two sensors are clear outliers: 37305 (gym) and E1007 (teacher lounge), which are both weakly coupled with the rest of the network (R ≤ 0.30, occasionally approaching zero or slightly negative values). The environments that these describe operate under fundamentally different boundary conditions. The large volume, high mechanical ventilation rates, and sporadic high-occupancy events of this gym produce independent CO_2 dynamics that are not captured in regular classroom spaces. The teacher lounge also exhibits special usage patterns due to low and infrequent occupancy and periphery-located ventilation settings. These nodes are therefore irreducible and must be preserved in whatever optimized network configuration.

5.2.4 Sensor Network organization suggestion

Monikko follows a three-level redundancy pattern, well informing sensor placement. The most robust cluster includes the entrance lobby, 3rd-floor lobby, and dining area (x15837, x3B015, x303C6), sharing very high mutual correlations (r $\approx$ 0.83-0.93); sensors are driven together by synchronized crowd-flow patterns throughout arrivals, recess transitions, and lunch; hence, this zone should have one representative node. Classrooms across floors share a moderate correlation (r = 0.55-0.72) due to the presence of spatial gradients determined by floor height, room volume, and micro-ventilation practices. Conversely, the gym (37305) and teacher lounge (E1007) are outliers, with r ≤ 0.30 and reflecting their unique functional and ventilation characteristics.

A reduced but still balanced configuration could retain a single representative from the high-correlation cluster, such as x15837 at the main entrance; one classroom per floor, such as BA5CF at the 1st floor or FC454 or F781F at the 2nd floor; and both outliers, 37305

and E1007, for the coverage of non-classroom areas. Optional could be the retention of the classroom 2E7BF or a 2nd-floor corridor node if more detail on vertical airflow characterization is needed.

This optimization reduces the network from 10 to 6–7 sensors while retaining over 90% of the CO_2 field structure and significantly reduces energy use, data transmission, and maintenance effort across the school.

5.3 Tiitsila

Analysis of the CO_2 dynamics in the Tiistilä School demonstrated a clear and structured pattern of spatial coupling among the monitored rooms. This varied set of spaces, including standard classrooms along with lobbies, one arts classroom, and one gym, is shown to not represent independent environments, but rather could be grouped based on how strongly the temporal CO_2 variations align, exposing consistencies in ventilation behavior, routines in occupancy patterns, and spatial connectivity.

Figure 5.3: Correlation matrix of CO_2 signals for Tiitsila during the monitoring period. Sensors are ordered to highlight cluster structure and redundancy potential among rooms

5.3.1 High correlation cluster

The most significant and consistent feature emerging from the clustering procedure was a group of three tightly linked sensors placed in the main circulation zones in the building, namely: x45BE0 (Main lobby/dining area), x4E348 (1st floor lobby, classes 1–2), and x44B3F (1st floor lobby, classes 3–4). Throughout all examined time windows, the corresponding CO_2 time series showed extremely high pairwise

correlations, mostly within the range from $r = 0.80$ to 0.89. For example, the relationship for the main lobby ($x45BE0$) and the class lobby ($x4E348$) located nearby was particularly strong, reaching as high as $r \approx 0.873$. These values are indicative of the fact that the developments of air quality at these three locations represent an almost identical daily course. The physical explanation of such a high correlation is self-evident since all three zones belong to the same highly loaded circulation axis and are very likely served by the same ventilation branch. Whether it is the morning flow of students, the cross-floor flows associated with breaks, or currents linked to the lunch time, the synchronized human mobility leaves its imprint in the form of mirrored CO_2 oscillations at all three sensors.

5.3.2 Medium correlation cluster

Beyond the tightly coupled lobby group, the analysis revealed a second, much larger cluster comprising most of the first- and second-floor classrooms and the second-floor lobby (CA276). These nodes showed moderate correlation levels, typically falling between $r = 0.50$ and $r = 0.72$. This intermediate range indicates that, while these areas share a common daily rhythm—mainly set by the school's fixed schedule of teaching hours and breaks—they remain distinguishable in terms of ventilation and spatial layout. The overall moderate correlation suggests that localized factors, such as different ventilation branches across floors, varied geometries, or distinct specialized use (like $A0F90$), still manage to exert sufficient influence, preventing their full statistical integration.Sub-Pattern Emergence and Correlation DecayA closer look at the pairwise correlation matrices shows clear sub-patterns reflecting the physical layout of the building:Intra-Floor Consistency: First-floor classrooms ($F42D3$ and x0697A) are strongly correlated with each other up to $r \approx 0.74$. The two second-floor classrooms ($B521C$ and $x5688C$) form their own, similarly strong sub-cluster ($r \approx 0.70$).Vertical Decoupling: Crucially, the cross-floor correlations decay significantly, often dropping by 10 to 20 % ($r \approx$ 0.45–0.55). This shows that vertical separation and increased varia-

tion in $HVAC$ zones effectively weaken the temporal relation between floors. In light of the low average correlation across the entire group, it would be unwise to treat this cluster as redundant and collapse it into one representative. A full collapse would result in the loss of up to 40% of the important spatial variance; thus, the network will not detect a problem localized to a certain floor or specific room type.

5.3.3 Low correlation cluster

A third distinct class consists of the low-correlation outliers of the building, which are the gym F7DC1 and, to a lesser extent, the arts classroom A0F90. The gym in particular behaves for most windows virtually independently from the rest of the building; its correlation coefficient drops below 0.20 or even approaches zero. This is expected, as sports activities are highly variable in nature, have large open volumes, and their ventilation rates are increased at times not aligned with the standard cycle of classrooms. The arts classroom, although more coupled during certain hours, has a considerably weaker correlation than standard classrooms. Its intermittent usage, special equipment, and different airflow patterns contribute to making it relatively independent. These two nodes therefore represent essential stand-alone units in the monitoring network, and removing or substituting them would result in the loss of information about zones whose environmental conditions differ substantially from the average of the building.

5.3.4 Sensor Network organization suggestion

In this respect, the redundancy structure identified in Tiistilä supports a reconfiguration of the sensor network for more efficient and spatially balanced deployment. As presented in the correlation analysis, numerous monitoring nodes, especially those on the 1st floor lobby areas, share very similar temporal patterns, while pairwise correlations are often above r=0.85. Such a high correlation illustrates that these units capture the same occupancy-driven ventilation dynamics; hence, they do not provide complementary spatial information. In contrast,

classrooms on different floors and zones show only moderate similarities (r=0.55–0.72), whereas the gym and the arts classroom have a very low correlation (r¡0.30) with respect to the remainder of the network, supporting their role of independent functional spaces.

After analyzing these findings, a reduced but representative sensor layout can be defined. The high-correlation group must have its representative at the main lobby/dining node (45BE0), since these capture the dominant building-wide transitions in morning arrivals and noon peaks. For the classroom cluster, representing vertical variability is preserved by picking two representative nodes: one anchored on the 1st floor (F42D3 - Classroom 1203) and another on the 2nd floor (B521C - Classroom 2282). These two sensors reproduce the crucial classroom CO_2 dynamics while avoiding superfluous intra-floor redundancy. The arts classroom A0F90 and the gym F7DC1 are classified as outliers, as their ventilation and occupancy exhibit very specific patterns; hence, no other sensor can replace their signals and must be included in the layout.

A further optional refinement is the inclusion of the 2nd-floor lobby sensor, CA276, which carries useful information about the corridor traffic and vertical mixing effects between adjacent classrooms. Likewise, retaining one additional classroom sensor-say, either 0697A on the 1st floor or 5688C on the 2nd-would enhance network granularity if a slightly denser sampling of classroom variability were sought. Under this setup, Tiistilä can go from the initial setup of 10 sensors to a leaner network of 6–7 units. This yields a reduction of 30–40 % in the active nodes with more than 90 % of the temporal variance captured by the original CO_2 dataset. This layout retains key diagnostic capabilities and ensures full representation of functional zones of the building while minimizing operational overhead, as well as long-term maintenance. Overall, the revised deployment aligns with a data-driven monitoring philosophy where redundancy is minimized and sensor placement is strategically guided by measured spatial coupling rather than uniform or heuristic distribution.

5.4 Tapiola

Figure 5.4: Correlation matrix of CO_2 signals for Tapiola during the monitoring period. Sensors are ordered to highlight cluster structure and redundancy potential among rooms

5.4.1 High correlation cluster

The strongest and most cohesive cluster comprises the sensors x2D55C (Classroom B1063), B00D8 (Classroom B1080), x79D69 (Needlework D1129), C30F8 (Arts classroom D1143), and CC940 (Classroom D1172). These sensors show very high pairwise correlations in every correlation window, usually r between 0.85 and 0.93, which is highly consistent. Such consistency indicates that these rooms operate under remarkably synchronized conditions. Their CO_2 profiles rise steeply during class periods, peak and plateau at similar times, and decay in nearly parallel fashion during breaks. Because their environmental trajectories are so well matched, this set effectively acts like a single "CO_2 zone." From a redundancy perspective, almost any one of these sensors could represent the behavior of the whole group, with x2D55C or CC940 showing up as the strongest candidates due to their high mean correlations to all other members.

5.4.2 Medium correlation cluster

A second cluster includes x1A497 (Classroom D1169), x00DA4 (Lobby/ table tennis), D96AD (Dining/lobby), and E6319 (Library). Their correlations are in the more middling range-usually r ≈ 0.55-0.75- and exhibit more structural diversity. These spaces all share some of the same overall daily cycle for the building-for example, CO_2 spikes at the times of heaviest circulation-but each shows strong individual characteristics that prevent their signals from aligning fully. The lobby x00DA4 and dining area D96AD often report a high correlation, around r 0.70-0.77, due to student mobility during breaks and lunchtime. The behaviour of the library E6319 is more varied; it becomes more strongly correlated during active use and then significantly weakens at times when students are required to be quiet. Meanwhile, x1A497 is a classroom, yet it slightly defies the correlation trend of this strongly linked group by acting more independently according to room volume and specific ventilation settings.

5.4.3 Low correlation cluster

Of the sensors in Tapiola, two are somewhat outliers with regard to the general trend: B926E (Gym/Stage) and, to a lesser extent, E6319 (Library) when its values stray from the middle cluster. The former continuously presents very low correlation with all other nodes, r ¡ 0.20, and for some windows even approaches zero or slightly negative values. This behavior is expected: Gyms have large volumes, dedicated ventilation regimes, and highly intermittent occupancy associated with sports classes or events. Their CO profile is thus nearly decoupled from classroom dynamics.

It shows similar tendencies during periods of low use, with its correlations often falling in the range 0.30–0.45. Its function, location, and occupancy make it far less predictable and far less synchronized with the main teaching blocks.

5.4.4 Sensor Network organization suggestion

The correlation structure observed in Tapiola allows the sensor network to be meaningfully rationalized without undermining the building's capacity for tracking the spatial and temporal variability of indoor air quality. The strongest redundancies are within the classrooms of the B- and D-wings: CC940, 1A497, B00D8, and 2D55C all follow almost indistinguishable CO trajectories throughout the day. In each case, their very high pairwise correlations (typically above 0.82) indicate a single coherent ventilation and occupancy unit; hence, it is unnecessary to maintain four independent sensors in this part of the building. This configuration would be more efficiently reduced to one classroom sensor per wing, retaining CC940 in the D-wing and B00D8 in the B-wing, therefore preserving the east-west variability of the building while eliminating redundant nodes.

A different behaviour emerges in the subject-specific teaching rooms. The library (E6319), arts classroom (C30F8), and needlework studio (79D69) form a moderately correlated group whose CO dynamics reflect distinct patterns of use and ventilation control. While they share a similar broad structure—driven by the school's overall rhythm—they also show localised, activity-dependent fluctuations that would be lost if the group were collapsed to a single sensor. At least one of these rooms should therefore remain in the monitoring network; in practice, keeping the library sensor alongside either the arts or needlework sensor offers a good compromise, capturing both a quiet, low-occupancy environment and a more active workshop-type space.

Finally, the gym and the dining lobby emerge as non-redundant and indispensable: fundamentally different ventilation rates, room volumes, and occupancy patterns render their CO time series nearly decoupled from those in classrooms and subject rooms. Intermittent but strong load spikes occur in the gym during physical education lessons, whereas the dining area exhibits sharp predictable peaks during lunchtime. No other sensor from the building replicates these behaviours. Both nodes therefore need to remain active in any optimised layout. In combination, all these observations have led to the

conclusion that the original 10-sensor deployment can be reduced to a carefully curated set of six units distributed across classrooms, special rooms, and highactivity shared spaces. This reduced network still preserves essential spatial structure of the building and is sensitive to local anomalies, while significantly reducing system complexity, energy consumption, and long-term maintenance demands.

Conclusions

This thesis provides an in-depth analysis of multi-parameter Indoor Air Quality sensor networks that were deployed in the four main schools of Espoo, Finland—Jousenkaari, Monikko, Tiistilä, and Tapiola—for a period of eight months. The study focused on understanding network performance, identifying redundancy, and exploring opportunities for optimization.

Using a structured analysis workflow that integrates time-synchronized MATLAB routines with correlation analysis, hierarchical clustering, principal component analysis, and exceedance metrics, for example, the present study evaluated how effectively these networks captured the full range of spatial and temporal variability of IAQ, adopting CO_2 as the main indicator of ventilation performance and occupancy patterns.

A critical outcome for all schools was that, although each building was quite different in terms of structure and room usage, the behavior of CO_2 was always strongly linked among zones fed by the same HVAC systems. Classrooms and adjacent corridors often showed virtually identical CO_2 profiles, with correlation coefficients frequently in excess of 0.85. This high level of synchronicity demonstrated that sensor configurations featured substantial, measurable redundancies. In certain schools, such as Jousenkaari and Tapiola, sets of two to five sensors picked up virtually the same diurnal profile of CO_2, pointing to sensors that were not necessary for capturing significant environmental variation.

However, at the same time, several significant spaces were observed in this study—gym, cafeteria, art room, and staff area—to show independent CO_2 behavior persistently. These outliers, with low cor-

relations with other rooms, are of particular importance because of their specific use and ventilation patterns, and could not be reliably inferred from classrooms alone.

These insights can be used to reduce the original 10-sensor networks in each school by approximately 30–40% without loss of the system's ability to detect meaningful IAQ variation or local anomalies. One approach for optimization involves keeping one sensor for every highly correlated cluster, a small number of sensors in moderately distinct areas, and all low-correlation outliers. The resulting configuration typically included 6 to 7 sensors per school and captured more than 90% of the variance in the original CO_2 data.

The advantages of this streamlined approach are numerous: reduced hardware and installation costs, less energy use, less data load, and reduced maintenance, all while maintaining diagnostic sensitivity for effective ventilation monitoring.

Besides network optimization, broader implications were drawn from the study on IAQ dynamics in Finnish schools. CO_2 levels showed clear occupancy-driven patterns, frequently exceeding the recommended limits during teaching hours, which signals ongoing ventilation challenges. In contrast, particulate matter showed less spatial coherence, often being tied to episodic events like cleaning. The temperature and humidity remained mostly stable, and for the most part, the control was at the building rather than room-by-room level.

Together, these findings confirm that CO_2 is the most reliable and actionable parameter for IAQ monitoring in multi-zone school environments, and the best candidate for driving sensor network simplification. In summary, this thesis makes a strong case for shifting away from uniformly dense sensor deployments toward smarter, adaptive layouts informed by functional zoning and data-driven correlation analysis. The methodology developed here, rooted in careful preprocessing, clustering, and targeted sensor selection, provides a scalable and transferable framework for the optimization of IAQ networks in schools and similar public buildings.

5.5 Future work

Looking ahead, several promising research directions come out of this work. First, the integration of CO_2-based occupancy inference has the potential to greatly enrich the diagnostic value of IAQ monitoring systems. By exploiting this strong relationship between CO_2 concentration and human presence, schools can move toward real-time, data-driven estimates of room occupancy. It would allow for smarter ventilation control strategies-such as demand-controlled ventilation-better aligning airflow with actual usage patterns, hence reducing energy consumption along with instances of under- or over-ventilation.

Second, with more pollutants like TVOCs, ultrafine particles, or formaldehyde, the analytical framework may make sure anomaly detection offers a fuller view of IAQ in addition to what is already achieved by CO_2. While CO_2 may be a good proxy for occupancy and ventilation, it clearly does not comprise all facets of air quality, particularly with respect to building materials, cleaning agents, or activities of the occupants. The developed methodology in this thesis is general and can be directly extended to other IAQ indicators, such as particulate matter ($PM_{2.5}$, PM_{10}), which allows for pollutant-specific clustering and redundancy analysis. The same approach applied to PMs is an important next step, since their behaviour is often less driven by occupancy and more spatially heterogeneous.

Third, dynamic sampling strategies hold strong promise: intelligent algorithms that adaptively modify the frequency or duration of data collection based on real-time environmental conditions. Indeed, such an approach may substantially minimize energy consumption and data traffic in wireless sensor networks, especially given that IAQ conditions are relatively stable for large fractions of the day in many buildings. It will also reduce storage requirements and extend battery life times, enhancing the long-term sustainability of the monitoring infrastructure. However, although the thesis maintains that increasing sampling intervals can save energy, it failed to determine the optimal sampling frequency. Therefore, developing an energy model to determine the sampling interval that minimizes energy consumption while preserving

IAQ signal integrity remains one of the critical tasks for the future.

These avenues not only build on the technical contributions of this thesis but also fit within the larger vision of smarter building management, where sensor networks do more than passively report values—they actually participate actively in operational decision-making. Embedding analytics into sensor logic, enabling a self-diagnosing system, or even using historical data for predictive maintenance—these are within reach with modest extensions of the existing methodology. Finally, although the thesis shows that up to 30–40% of sensors can be removed and retain over 90% of the CO_2 temporal variance, this conclusion is based exclusively on retrospective data analysis. Field validation is thus crucial: future work should experimentally deploy the reduced sensor layouts and directly compare their measurements against the original dense network. This real-world validation step is required to verify that the reduced configuration reliably performs under actual operating conditions.

List of Figures

4.1 3D temperature traces for all rooms over the monitoring period october-november 33
4.2 3D temperature traces for all rooms over the monitoring period December-January 33
4.3 3D temperature traces for all rooms over the monitoring period February-March 34
4.4 3D temperature traces for all rooms over the monitoring period April-may 34
4.5 3D temperature traces for all rooms over the monitoring period June 34
4.6 3D Relative Humidity traces for all rooms over the monitoring period october-november 37
4.7 3D Relative Humidity traces for all rooms over the monitoring period Decemebr-January 37
4.8 3D Relative Humidity traces for all rooms over the monitoring period Februray-March 38
4.9 3D Relative Humidity traces for all rooms over the monitoring period April-May 38
4.10 3D Relative Humidity traces for all rooms over the monitoring period June 39
4.11 3D $PM_{2.5}$ traces for all rooms over the monitoring period October-November 41
4.12 3D $PM_{2.5}$ traces for all rooms over the monitoring period Decemeber-January 41
4.13 3D $PM_{2.5}$ traces for all rooms over the monitoring period February-March 42

4.14 3D $PM_{2.5}$ traces for all rooms over the monitoring period April-May 42
4.15 3D $PM_{2.5}$ traces for all rooms over the monitoring period June 42
4.16 3D PM_{10} traces for all rooms over the monitoring period October-November 43
4.17 3D PM_{10} traces for all rooms over the monitoring period December-January 43
4.18 3D PM_{10} traces for all rooms over the monitoring period February-March 44
4.19 3D PM_{10} traces for all rooms over the monitoring period April-May 44
4.20 3D PM_{10} traces for all rooms over the monitoring period June 45
4.21 3D Pressure traces for all rooms over the monitoring period December-January 46
4.22 3D temperature traces for all rooms over the monitoring period october-november 48
4.23 3D temperature traces for all rooms over the monitoring period Decemeber-January 48
4.24 3D temperature traces for all rooms over the monitoring period February-March 49
4.25 3D temperature traces for all rooms over the monitoring period April-May 49
4.26 3D temperature traces for all rooms over the monitoring period June 49
4.27 3D Relative Humidity traces for all rooms over the monitoring period october-november 52
4.28 3D Relative Humidity traces for all rooms over the monitoring period Decemebr-January 52
4.29 3D Relative Humidity traces for all rooms over the monitoring period Februray-March 53
4.30 3D Relative Humidity traces for all rooms over the monitoring period April-May 53

4.31 3D Relative Humidity traces for all rooms over the monitoring period June 54
4.32 3D $PM_{2.5}$ traces for all rooms over the monitoring period October-November 56
4.33 3D $PM_{2.5}$ traces for all rooms over the monitoring period Decemeber-January 56
4.34 3D $PM_{2.5}$ traces for all rooms over the monitoring period February-March 57
4.35 3D $PM_{2.5}$ traces for all rooms over the monitoring period April-May 57
4.36 3D $PM_{2.5}$ traces for all rooms over the monitoring period June 57
4.37 3D PM_{10} traces for all rooms over the monitoring period October-November 58
4.38 3D PM_{10} traces for all rooms over the monitoring period December-January 58
4.39 3D PM_{10} traces for all rooms over the monitoring period February-March 59
4.40 3D PM_{10} traces for all rooms over the monitoring period April-May 59
4.41 3D PM_{10} traces for all rooms over the monitoring period June 60
4.42 3D Pressure traces for all rooms over the monitoring period February 62
4.43 3D temperature traces for all rooms over the monitoring period October-November 63
4.44 3D temperature traces for all rooms over the monitoring period December-Janaury 63
4.45 3D temperature traces for all rooms over the monitoring period February-March 64
4.46 3D temperature traces for all rooms over the monitoring period April-May 64
4.47 3D temperature traces for all rooms over the monitoring period June 64

4.48 3D Relative Humidity traces for all rooms over the monitoring period october-november 66
4.49 3D Relative Humidity traces for all rooms over the monitoring period Decemebr-January 66
4.50 3D Relative Humidity traces for all rooms over the monitoring period Februray-March 67
4.51 3D Relative Humidity traces for all rooms over the monitoring period April-May 67
4.52 3D Relative Humidity traces for all rooms over the monitoring period June 68
4.53 3D $PM_{2.5}$ traces for all rooms over the monitoring period October-November 70
4.54 3D $PM_{2.5}$ traces for all rooms over the monitoring period Decemeber-January 70
4.55 3D $PM_{2.5}$ traces for all rooms over the monitoring period February-March 71
4.56 3D $PM_{2.5}$ traces for all rooms over the monitoring period April-May 71
4.57 3D $PM_{2.5}$ traces for all rooms over the monitoring period June 71
4.58 3D PM_{10} traces for all rooms over the monitoring period October-November 72
4.59 3D PM_{10} traces for all rooms over the monitoring period December-January 72
4.60 3D PM_{10} traces for all rooms over the monitoring period February-March 73
4.61 3D PM_{10} traces for all rooms over the monitoring period April-May 73
4.62 3D PM_{10} traces for all rooms over the monitoring period June 73
4.63 3D Pressure traces for all rooms over the monitoring period February 76
4.64 3D temperature traces for all rooms over the monitoring period october-november 77

4.65 3D temperature traces for all rooms over the monitoring period December-January 77
4.66 3D temperature traces for all rooms over the monitoring period February-March 78
4.67 3D temperature traces for all rooms over the monitoring period April-May 78
4.68 3D temperature traces for all rooms over the monitoring period June 78
4.69 3D Relative Humidity traces for all rooms over the monitoring period october-november 81
4.70 3D Relative Humidity traces for all rooms over the monitoring period Decemebr-January 81
4.71 3D Relative Humidity traces for all rooms over the monitoring period Februray-March 82
4.72 3D Relative Humidity traces for all rooms over the monitoring period April-May 82
4.73 3D Relative Humidity traces for all rooms over the monitoring period June 83
4.74 3D $PM_{2.5}$ traces for all rooms over the monitoring period October-November 84
4.75 3D $PM_{2.5}$ traces for all rooms over the monitoring period Decemeber-January 84
4.76 3D $PM_{2.5}$ traces for all rooms over the monitoring period February-March 85
4.77 3D $PM_{2.5}$ traces for all rooms over the monitoring period April-May 85
4.78 3D $PM_{2.5}$ traces for all rooms over the monitoring period June 85
4.79 3D PM_{10} traces for all rooms over the monitoring period October-November 86
4.80 3D PM_{10} traces for all rooms over the monitoring period December-January 86
4.81 3D PM_{10} traces for all rooms over the monitoring period February-March 87

4.82 3D PM_{10} traces for all rooms over the monitoring period April-May 87
4.83 3D PM_{10} traces for all rooms over the monitoring period June 88
4.84 3D Pressure traces for all rooms over the monitoring period December-January 90

5.1 Correlation matrix of CO_2 signals for Jousenkaari during the monitoring period. Sensors are ordered to highlight cluster structure and redundancy potential among rooms 93
5.2 Correlation matrix of CO_2 signals for Monikko during the monitoring period. Sensors are ordered to highlight cluster structure and redundancy potential among rooms 97
5.3 Correlation matrix of CO_2 signals for Tiitsila during the monitoring period. Sensors are ordered to highlight cluster structure and redundancy potential among rooms101
5.4 Correlation matrix of CO_2 signals for Tapiola during the monitoring period. Sensors are ordered to highlight cluster structure and redundancy potential among rooms105

Bibliography

[1] Antti Asikainen, Otto Hänninen, and Göran Smedje. "Indoor air quality problems in Nordic buildings: A review". In: *Indoor Air* 26.4 (2016), pp. 585–597 (cit. on pp. 5, 6).

[2] Mark J Mendell and Genea A Heath. "Do indoor pollutants and thermal conditions in schools influence student performance? A critical review of the literature". In: *Indoor Air* 15.1 (2005), pp. 27–52. URL: `https://pubmed.ncbi.nlm.nih.gov/15660567/` (cit. on pp. 5, 6).

[3] Pawel Wargocki and David P Wyon. "The effects of indoor environmental quality on the performance of schoolwork by students". In: *Indoor Air* 23.2 (2013), pp. 167–181 (cit. on pp. 5, 7).

[4] World Health Organization. *WHO guidelines for indoor air quality: Selected pollutants*. Regional Office for Europe. 2010 (cit. on p. 6).

[5] M Turunen, O Hänninen, P Tiittanen, and P Pasanen. "Winter ventilation rates at primary schools: comparison between Portugal and Finland". In: *Building and Environment* 71 (2014), pp. 194–201. URL: `https://pubmed.ncbi.nlm.nih.gov/23557238/` (cit. on pp. 6, 7).

[6] Göran Smedje and Dan Norbäck. "New ventilation systems at select schools in Sweden–Effects on asthma and exposure". In: *Archives of Environmental Health: An International Journal* 55.1 (2000), pp. 18–25. URL: `https://www.researchgate.net/publication/12579768_New_Ventilation_Systems_at_Select_Schools_in_Sweden-Effects_on_Asthma_and_Exposure` (cit. on p. 6).

[7] Atle N Myhrvold, Erik Olsen, and H B Lauridsen. "Ventilation and health in schools: A study in Oslo, Norway". In: *Indoor Air* 6.4 (1996), pp. 227–234 (cit. on p. 6).

[8] A Salo and P Kirjavainen. “Indoor air quality in Finnish schools: A review of recent studies”. In: *International Journal of Environmental Research and Public Health* 16.10 (2019), p. 1772 (cit. on pp. 6, 7).

[9] Otto Hänninen, Hanna Koponen, Lasse Ruuskanen, and Hannele Roponen. “Exposure to particle resuspension in school gyms during physical activities”. In: *Atmospheric Environment* 261 (2021), p. 118600 (cit. on p. 6).

[10] Nuno Canha, Sofia M Almeida, Paulo Pegas, and E de Oliveira Fernandes. “Indoor air quality in schools: a review of available studies”. In: *Indoor and Built Environment* 25.2 (2016), pp. 221–237 (cit. on p. 6).

[11] Jarek Kurnitski, Olli Seppänen, and Pawel Wargocki. “Ventilation of school buildings: Review of requirements and current status in Nordic countries”. In: *Energy and Buildings* 156 (2017), pp. 168–181 (cit. on p. 6).

[12] Dan Norbäck, John K Ljungberg, and Vanesa Borras-Santos. “Dampness and low indoor humidity in schools: Effects on respiratory symptoms and irritation”. In: *Journal of Exposure Science Environmental Epidemiology* 21.5 (2011), pp. 447–455 (cit. on p. 6).

[13] Luca Tavernini, Otto Hänninen, Mikko Paunu, and Antti Asikainen. “Optimizing indoor air quality sensor placement in schools using spatiotemporal data analysis”. In: *Building and Environment* 245 (2025), p. 112980. DOI: 10.1016/j.buildenv.2025.112980 (cit. on p. 7).

[14] Norbert Castell, Franck R Dauge, Philipp Schneider, Matthias Vogt, Uri Lerner, Boaz Fishbain, David Broday, and Alena Bartonova. “Can commercial low-cost sensor platforms contribute to air quality monitoring and exposure estimates?” In: *Environment International* 99 (2017), pp. 293–302. DOI: 10.1016/j.envint.2016.12.007 (cit. on pp. 8, 10).

[15] Zhengyi Liu, Xingwang Liu, Min Wang, Xu Li, and Xin Yu. “Optimal sensor placement for indoor air quality monitoring in large public buildings”. In: *Building and Environment* 155 (2019), pp. 1–14. DOI: 10.1016/j.buildenv.2019.03.041 (cit. on p. 8).

[16] David Hasenfratz, Olga Saukh, and Lothar Thiele. “On redundancy reduction and sensor placement for mobile air pollution monitoring”. In: *Proceedings of the 9th ACM Conference on Embedded Networked Sensor Systems*. 2012, pp. 1–14. DOI: 10.1145/2422531.2422551 (cit. on p. 9).

[17] L. Spinelle, M. Gerboles, G. Kok, S. Persijn, and T. Sauerwald. "Review of portable and low-cost sensors for the ambient air monitoring of benzene and other volatile organic compounds". In: *Sensors* 17.7 (2015), p. 1520. DOI: 10.3390/s17071520 (cit. on p. 10).

[18] Alastair C Lewis, James D Lee, Paul M Edwards, Marvin D Shaw, Mathew J Evans, Simon J Moller, ..., and Jonathan D Whitehead. "Evaluating the performance of low-cost chemical sensors for air pollution research". In: *Faraday Discussions* 200 (2018), pp. 621–637. DOI: 10.1039/C7FD00020K (cit. on p. 11).

[19] Finnish Society of Indoor Air Quality and Climate (FiSIAQ). *Classification of Indoor Climate, Construction Cleanliness, and Finishing Materials 2017*. FiSIAQ Publications. 2017.